

Poles At Infinity in On-shell Diagrams

Taro V. Brown,^a Umut Oktem,^a Jaroslav Trnka^{a,b}

^a*Center for Quantum Mathematics and Physics (QMAP) and Department of Physics,
University of California, Davis, California, USA*

^b*Institute of Particle and Nuclear Physics, Charles University, Prague, Czech Republic*

E-mail: tvbrown@ucdavis.edu, ucoktem@ucdavis.edu, trnka@ucdavis.edu

ABSTRACT: In this paper we study on-shell diagrams in $\mathcal{N}<4$ supersymmetric Yang-Mills (SYM) theory. These are on-shell gauge invariant objects which appear as cuts of loop integrands in the context of generalized unitarity and serve as building blocks for amplitudes in recursion relations. In the dual formulation, they are associated with cells of the positive Grassmannian $G_+(k, n)$ and the on-shell functions can be reproduced as canonical differential forms. While for the case of the $\mathcal{N}=4$ maximally supersymmetric Yang-Mills theory all poles in on-shell diagrams correspond to IR poles when the momentum flows in edges are zero, for $\mathcal{N}<4$ SYM theories there are new UV poles when the loop momenta go to infinity. These poles originate from the prefactor of the canonical dlog form and do not correspond to erasing edges in on-shell diagrams. We show that they can be interpreted as a diagrammatic operation which involves pinching a loop and performing a “non-planar twist” on external legs, which gives rise to a non-planar on-shell diagram. Our result provides an important clue on the role of poles at infinite momenta in on-shell scattering amplitudes, and the relation to non-planar on-shell functions.

Contents

1	Introduction	1
2	Fundamentals of on-shell diagrams	5
2.1	Building on-shell diagrams	6
2.2	Dual formulation	7
2.3	On-shell diagrams for $\mathcal{N}=4$ SYM theory	11
3	UV poles in one-loop graphs	13
3.1	First $\mathcal{N}=3$ examples	13
3.2	Two-loop pentabox diagram	16
3.3	MHV one-loop diagrams	20
3.4	Arbitrary n -gons and helicities	22
4	All planar diagrams	28
4.1	Localization of UV poles in planar diagrams	28
4.2	Three-loop example	30
4.3	Non-planarity from the UV pole	33
4.4	UV poles and modified GRTs	35
5	Higher order poles at infinity	40
5.1	UV pole as a residue	41
5.2	Infinity operator	43
5.3	General on-shell diagram	48
6	Non-planar diagrams	50
7	Conclusion and Outlook	53

1 Introduction

Modern on-shell methods for scattering amplitudes are based on a simple idea of building amplitudes from on-shell gauge invariant objects (see [1–6] for recent reviews). At tree-level, this idea is materialized in the form of on-shell recursion relations where the n -point tree-level amplitude is built recursively from the lower point (on-shell) amplitudes. The primary example is the Britto-Cachazo-Feng-Witten (BCFW) recursion relations [7, 8] where we shift external momenta of two external legs. There are also generalizations to multi-line shifts [9–11], as well as theories with special soft limits [12–15]. At loop level, unitarity methods allow us to write the amplitude as a linear combination of basis integrals with gauge-invariant on-shell prefactors [16–25]. These prefactors are calculated using *cuts of*

the *loop integrand*, where we set propagators to be on-shell and the loop integrand factorizes into simpler objects. The basic cut is the *unitarity cut* where two propagators from one loop are set to zero. This procedure can be iterated further and when the maximal number of propagators are cut, we talk about *maximal cuts*.

(1.1)

In these diagrams both internal and external lines are on-shell, and the result is given by the product of tree-level amplitudes in the corners. In theories with fundamental 3-point amplitudes we can proceed further and express tree-level amplitudes in the corners using BCFW recursion relations. In the end, we get *on-shell diagrams* [26–39] which are on-shell gauge invariant objects. Each diagram is defined as a product of on-shell 3-point amplitudes (all lines, external and internal, are on-shell) integrated over momenta and Grassmann variables of internal legs,

$$= \prod_k \int d^{\mathcal{N}} \tilde{\eta}_k \int \frac{d^2 \lambda_k d^2 \tilde{\lambda}_k}{\text{GL}(1)} \left(\prod_j A_3^{(j)} \right) \quad (1.2)$$

where \mathcal{N} is the number of supersymmetries. On-shell diagrams play multiple roles, such as giving us the kinematical solutions for cuts of loop integrands and reproducing the associated on-shell functions on these cuts, but a subset of them also play a role as building blocks in the recursion relations for tree-level amplitudes or loop integrands. For example, the same diagram represents a maximal cut of 3-loop 6-point MHV amplitude or a term in the BCFW construction of the 6-point MHV tree-level amplitude,

(1.3)

In $\mathcal{N}=4$ SYM theory this diagram evaluates to the Parke-Taylor factor,

$$\Omega = \frac{\delta^4(\lambda \cdot \tilde{\lambda}) \delta^4(\lambda \cdot \tilde{\eta})}{\langle 12 \rangle \langle 23 \rangle \langle 34 \rangle \langle 45 \rangle \langle 56 \rangle \langle 61 \rangle}. \quad (1.4)$$

On-shell diagrams are fascinating objects and are tightly connected to the geometric formulations for on-shell scattering amplitudes using the positive Grassmannian and the Amplituhedron [40–46], which have been successfully used to obtain various explicit results including certain all-loop order quantities [29, 47–60]. In particular, each planar diagram, known in the math literature as a plabic graph [61], is associated with a specific cell in the positive Grassmannian $G_+(k, n)$ represented by the matrix C . The matrix C is parametrized by the variables α_i which are associated with edges (or faces) of the graph. In physics, the on-shell function in $\mathcal{N}=4$ SYM theory is reproduced by a canonical dlog form [26] in all α_i and delta functions which solve for α_i in terms of kinematical variables,

$$\Omega = \int \frac{d\alpha_1}{\alpha_1} \frac{d\alpha_2}{\alpha_2} \dots \frac{d\alpha_m}{\alpha_m} \delta(C \cdot \tilde{\lambda}) \delta(C^\perp \cdot \lambda) \delta(C \cdot \tilde{\eta}). \quad (1.5)$$

The kinematical poles in the on-shell function are related to the poles in the edge variables. One particular parametrization of the on-shell diagram (1.3) is

$$\begin{aligned} \alpha_1 &= \frac{\langle 23 \rangle}{\langle 13 \rangle}, & \alpha_2 &= \frac{\langle 12 \rangle}{\langle 13 \rangle}, \\ \alpha_3 &= \frac{\langle 46 \rangle}{\langle 36 \rangle}, & \alpha_4 &= \frac{\langle 34 \rangle}{\langle 36 \rangle}, \\ \alpha_5 &= \frac{\langle 36 \rangle}{\langle 13 \rangle}, & \alpha_6 &= \frac{\langle 16 \rangle}{\langle 36 \rangle}, \\ \alpha_7 &= \frac{\langle 56 \rangle}{\langle 46 \rangle}, & \alpha_8 &= \frac{\langle 45 \rangle}{\langle 46 \rangle}. \end{aligned} \quad (1.6)$$

and the formula (1.5) reproduces (1.4). The kinematical poles in Ω correspond to poles in edge variables α_j . In fact, taking a residue on the pole $\alpha_j=0$ erases a corresponding edge and produces a lower-loop on-shell diagram. Its on-shell function is equal to the residue of the original on-shell diagram on the kinematical pole. For example, in the diagram (1.6) the condition $\alpha_7=0$ sets the momentum flow in a corresponding edge to zero and forces $\langle 56 \rangle = 0$. The result is a lower-loop on-shell diagram where external legs 5, 6 are attached to the same white vertex.

$\xrightarrow{\alpha_7=0}$

(1.7)

All poles in the on-shell function for $\mathcal{N}=4$ SYM are located deep in the IR region where the internal momenta are set to zero. For $\mathcal{N}<4$ there is an additional Jacobian factor in the Grassmannian form (1.5) which introduces new types of poles other than $\alpha_j=0$ [26]. These poles are in the UV where the loop momenta go to infinity. Nothing is known about these

poles, i.e. what the precise locations in the loop momentum space are (other than being at infinity), what type of kinematical conditions they impose on external momenta, and what the residues of on-shell diagrams on these poles are. Obviously, these poles also naturally arise when calculating the on-shell diagrams from the definition (1.2) but the Grassmannian picture nicely divides the well-understood IR poles (located at $\alpha_j=0$) from these new UV poles, which we also refer to as *poles at infinity*.

The nature of these UV poles is a very important conceptual question, and we address it in the context of on-shell diagrams which properties are inherited from the properties of scattering amplitudes. In fact, the behavior on the IR poles, such as erasing edges in on-shell diagrams, taking residues on $\alpha_j=0$ etc., is just a consequence of perturbative unitarity for scattering amplitudes. However, the unitarity of the S-matrix does not predict what exactly happens with amplitudes (tree-level amplitudes and loop integrands) on UV poles when the loop momenta go to infinity (either external momenta or loop momenta) in a certain direction. The behavior on UV poles might be also tied to symmetries or special properties, for example the complete absence of any poles at infinity in planar $\mathcal{N}=4$ SYM is a consequence of the dual conformal symmetry [62, 63]. The same property has been also conjectured to hold for the non-planar sector of the same theory [64–71], pointing to a possibility of a hidden symmetry in the full theory. The surprising behavior at infinity has also been observed in gravitational theories. This includes the improved $1/z^2$ scaling under BCFW shift [72–74], enhanced cancelations on certain cuts [35, 69, 75, 76] or observed enhanced UV cancelations in higher loop amplitudes [75–79]. This is also likely related to surprisingly simple formulas for tree-level amplitudes [80–87] or other special properties of gravity such as color-kinematics duality [88–90].

This naturally raises a question of a uniform framework to analyze amplitudes at infinite momenta, and search for implications of the *unitarity at infinity* for the perturbative S-matrix. In this paper, we will make a modest step in this direction, and give a partial answer to this question in the context of planar on-shell diagrams in Yang-Mills theory. We will show where the poles at infinity are located in the kinematical space and what the kinematical constraints we have to impose to approach them are. The residue at infinity is then a diagrammatic operation on an on-shell diagram which we call a *non-planar twist*. The residue on this pole of a planar diagram is a lower-loop *non-planar diagram*. For $\mathcal{N}=3$ SYM all poles are simple while for $\mathcal{N}<3$ SYM we have multiple poles and the residue corresponds to a derivative operator acting on the lower-loop twisted on-shell diagram.

The paper is organized as follows: In section 2, we review the basic facts about on-shell diagrams. In section 3, we study the poles at infinity in one-loop on-shell diagrams for $\mathcal{N}=3$ SYM and show that the imposed kinematical condition produces a simple tree-level factorization. In section 4, we show that in planar diagrams all poles at infinity are localized in one-loop subgraphs and we discuss their embedding into a higher-loop on-shell diagrams. We also show a number of examples and discuss Global Residue Theorems which relate UV poles to IR poles. In section 5, we generalize our procedure to $\mathcal{N}<3$ SYM and discuss the multiple poles at infinity. In section 6, we show that in non-planar diagrams the situation is more complicated as one kinematical condition can send multiple loop momenta to infinity. We end with conclusion and outlook in section 7.

2 Fundamentals of on-shell diagrams

On-shell diagrams are gauge invariant objects built from basic tree-level amplitudes. They appear in the context of tree-level recursion relations as building blocks for the amplitude, and in the context of generalized unitarity as coefficients of basis integrals. Most invariantly, they represent *cuts of loop integrand* and provide important gauge-invariant data about the scattering amplitudes. In the theories with elementary three-point amplitudes they are built from two types of vertices, black and white, which represent two solutions of the massless on-shell 3-point kinematics

$$p_1^2 = p_2^2 = p_3^2 = 0, \quad p_1 + p_2 + p_3 = 0. \quad (2.1)$$

Using the spinor helicity variables $p_{a\dot{a}}^\mu = \sigma_{a\dot{a}}^\mu \lambda^a \tilde{\lambda}^{\dot{a}}$ the conditions on p_1, p_2, p_3 turn into collinearity of λ s or $\tilde{\lambda}$ s,

$$\text{MHV: } \tilde{\lambda}_1 \propto \tilde{\lambda}_2 \propto \tilde{\lambda}_3 \quad \text{and} \quad \overline{\text{MHV}}: \lambda_1 \propto \lambda_2 \propto \lambda_3, \quad (2.2)$$

This highly restrictive kinematics fully fixes the form of the three-point amplitude for any external helicities. For the maximally $\mathcal{N}=4$ supersymmetric Yang-Mills theory we get two elementary 3-point MHV and $\overline{\text{MHV}}$ amplitudes,

$$\begin{aligned} \text{MHV vertex (black circle)} &= \frac{\delta^4(P) \delta^8(Q)}{\langle 12 \rangle \langle 23 \rangle \langle 31 \rangle}, \\ \overline{\text{MHV vertex (white circle)}} &= \frac{\delta^4(P) \delta^4(\tilde{Q})}{[12][23][31]}, \end{aligned} \quad (2.3)$$

where $\langle ij \rangle = \epsilon_{\alpha\beta} \lambda_i^\alpha \lambda_j^\beta$, $[ij] = \epsilon_{\dot{\alpha}\dot{\beta}} \tilde{\lambda}_i^{\dot{\alpha}} \tilde{\lambda}_j^{\dot{\beta}}$. Following the notation of [26, 35] we have denoted

$$\begin{aligned} P \equiv \lambda \cdot \tilde{\lambda} &= \lambda_1 \tilde{\lambda}_1 + \lambda_2 \tilde{\lambda}_2 + \lambda_3 \tilde{\lambda}_3, \quad Q \equiv \lambda \cdot \tilde{\eta} = \lambda_1 \tilde{\eta}_1 + \lambda_2 \tilde{\eta}_2 + \lambda_3 \tilde{\eta}_3, \\ \tilde{Q} &= [12] \tilde{\eta}_3 + [23] \tilde{\eta}_1 + [31] \tilde{\eta}_2, \end{aligned} \quad (2.4)$$

the momenta and supermomenta. The shorthand notation stands for $\lambda \cdot \tilde{\lambda} = \sum_{a=1}^n \lambda_a \tilde{\lambda}_a$, $\lambda \cdot \tilde{\eta} = \sum_{a=1}^n \lambda_a \tilde{\eta}_a$, where the sum goes over all external on-shell particles (we suppressed the SU(4) index I in these formulas). Note that $\tilde{\eta}$ are the fermionic variables in the expansion of the $\mathcal{N} = 4$ superfield Φ .

$$\Phi(\tilde{\eta}) = g^+ + \tilde{\eta}^I \tilde{g}_I + \frac{1}{2!} \tilde{\eta}^I \tilde{\eta}^J \phi_{IJ} + \frac{1}{3!} \epsilon_{IJKL} \tilde{\eta}^I \tilde{\eta}^J \tilde{\eta}^K \tilde{g}^L + \frac{1}{4!} \epsilon_{IJKL} \tilde{\eta}^I \tilde{\eta}^J \tilde{\eta}^K \tilde{\eta}^L g^-. \quad (2.5)$$

If we have less than maximal supersymmetry, we need to indicate the helicities $h = \pm 1$ of external particles. The elementary 3-point amplitudes in $\mathcal{N} < 4$ SYM theory are then

$$\begin{aligned} \text{MHV vertex (black circle)} &= \frac{\langle 23 \rangle^{4-\mathcal{N}} \delta^4(P) \delta^{2\mathcal{N}}(Q)}{\langle 12 \rangle \langle 23 \rangle \langle 31 \rangle}, \\ \overline{\text{MHV vertex (white circle)}} &= \frac{[23]^{4-\mathcal{N}} \delta^4(P) \delta^{\mathcal{N}}(\tilde{Q})}{[12][23][31]}. \end{aligned}$$

This includes the pure $\mathcal{N}=0$ Yang-Mills case. Note that the helicity flow (arrow) denotes the helicity assignment (negative helicity for incoming and positive helicity for outgoing), hence we can freely drop the \pm labels on external legs.

2.1 Building on-shell diagrams

On-shell diagrams are given by the product of three-point amplitudes, multiplied by a Jacobian that stems from eliminating λ 's and η 's of internal on-shell legs in the momentum and super-momentum conservation delta functions. The final result depends on external kinematic data and possibly on free unfixed parameters.

Putting an internal edge on-shell gives one constraint equation, from which we can solve for the internal momenta in terms of the external kinematic data. Denoting the difference between the number of constraints and the internal degrees of freedom by n_δ , we get three distinct cases. $n_\delta = 0$ where we can express all internal momenta in terms of external data, $n_\delta > 0$ which places additional conditions on the external data, and $n_\delta < 0$ which leaves us with unsolved parameters that the amplitude will depend on. The simplest example of $n_\delta = 0$, is the four-point one-loop box diagram,

$$\begin{aligned} \ell_1 &= \frac{\langle 23 \rangle}{\langle 13 \rangle} \lambda_1 \tilde{\lambda}_2, & \ell_3 &= \frac{\langle 14 \rangle}{\langle 13 \rangle} \lambda_3 \tilde{\lambda}_4, \\ \ell_2 &= \frac{\langle 12 \rangle}{\langle 13 \rangle} \lambda_3 \tilde{\lambda}_2, & \ell_4 &= \frac{\langle 34 \rangle}{\langle 13 \rangle} \lambda_1 \tilde{\lambda}_4. \end{aligned} \tag{2.6}$$

You can see that each vertex imposes collinearity conditions on λ or $\tilde{\lambda}$. For example, the holomorphic part of momentum ℓ_2 is given by the λ_3 spinor (from the upper right white vertex) and the anti-holomorphic part is given by the $\tilde{\lambda}_2$ spinor (from the upper left black vertex). This itself solves for 3 of 4 on-shell conditions on internal on-shell propagators, $\ell_1^2 = \ell_2^2 = \ell_3^2 = 0$. The constraint from the final propagator $\ell_4^2 = 0$ fixes the overall constant in ℓ_2 to be $\langle 12 \rangle / \langle 13 \rangle$. In $\mathcal{N}=4$ SYM theory we do not need to specify helicities of internal and external legs. For $\mathcal{N}<4$ SYM theory we have to specify them (or equivalently helicity flows denoted by arrows) to fully define an on-shell diagram. Solutions for internal momenta are the same regardless of the number of supersymmetries or theory (it can also be gravity on-shell diagrams or other). However, the actual on-shell function associated with the on-shell diagram is sensitive to these details. In particular, the on-shell function in $\mathcal{N}=4$ SYM for (2.6) is

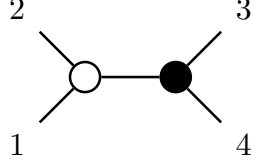
$$\begin{aligned} \Omega &= \int d^4 \tilde{\eta}_1 \dots d^4 \tilde{\eta}_4 \int \frac{d^2 \lambda_{\ell_1} d^2 \tilde{\lambda}_{\ell_1}}{\text{GL}(1)} \dots \frac{d^2 \lambda_{\ell_4} d^2 \tilde{\lambda}_{\ell_4}}{\text{GL}(1)} \\ &\times \left\{ A_3(1, \ell_1, \ell_4) A_3(2, \ell_1, \ell_2) A_3(3, \ell_2, \ell_3) A_3(4, \ell_3, \ell_4) \right\} = \frac{\delta^4(P) \delta^8(\mathcal{Q})}{\langle 12 \rangle \langle 23 \rangle \langle 34 \rangle \langle 41 \rangle}. \end{aligned} \tag{2.7}$$

All integrals are evaluated on the delta functions using

$$\int dx f(x) \delta(x - x_0) = f(x_0) \tag{2.8}$$

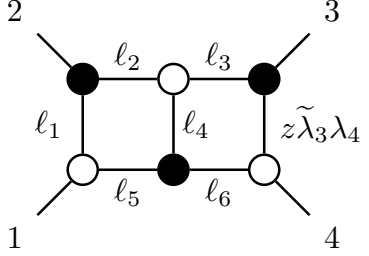
(see [26] for more details). All poles in the on-shell function correspond to sending one of the internal momenta of the diagram to zero as evident from (2.6). Taking the residue on

this pole erases an edge and the result corresponds to a new on-shell diagram. For example, sending $\langle 12 \rangle = 0$ implies $\ell_2 = 0$ and we get



$$= \frac{\delta(\langle 12 \rangle) \delta^4(P) \delta^8(Q)}{\langle 23 \rangle \langle 34 \rangle \langle 41 \rangle}. \quad (2.9)$$

This diagram is an example of $n_\delta > 0$ where the extra constraint on the external kinematics $\langle 12 \rangle = 0$ is evident from the delta function $\delta(\langle 12 \rangle)$ in the on-shell form (2.9). The condition on external kinematics can be also seen directly in the diagram where legs 1, 2 meet in the same white vertex. At the same time, legs 3, 4 meet in the same black vertex which imposes $[34] = 0$ – which is indeed a consequence of $\langle 12 \rangle = 0$ for four-point kinematics. The simplest example of an on-shell diagram with $n_\delta < 0$, is the four-point double-box diagram,



$$\begin{aligned} \ell_1 &= \frac{\langle 23 \rangle + z \langle 24 \rangle}{\langle 13 \rangle + z \langle 14 \rangle} \lambda_1 \tilde{\lambda}_2, & \ell_2 &= \frac{\langle 12 \rangle}{\langle 13 \rangle + z \langle 14 \rangle} \hat{\lambda}_3 \tilde{\lambda}_2, & \ell_3 &= \hat{\lambda}_3 \tilde{\lambda}_3, \\ \ell_4 &= \frac{\langle 14 \rangle}{\langle 13 \rangle + z \langle 14 \rangle} \hat{\lambda}_3 \tilde{\lambda}_4, & \ell_5 &= \frac{\langle 34 \rangle}{\langle 13 \rangle + z \langle 14 \rangle} \lambda_1 \tilde{\lambda}_4, & \ell_6 &= \lambda_4 \hat{\lambda}_4. \end{aligned} \quad (2.10)$$

where $\hat{\lambda}_4 = \tilde{\lambda}_4 + z \tilde{\lambda}_3$ and $\hat{\lambda}_3 = \lambda_3 - z \lambda_4$. This diagram can be thought as a heptacut of the two-loop four-point amplitude in the $\mathcal{N}=4$ SYM theory, with z being the last parameter in ℓ_1, ℓ_2 not localized by on-shell conditions from the cut. Alternatively, we can also interpret the diagram as a BCFW shift of the one-loop four-point amplitude (on legs 3, 4) with z being the BCFW shift parameter. The on-shell function is given by

$$\Omega = \int \frac{dz \delta^4(P) \delta^8(Q)}{z \langle 12 \rangle (\langle 23 \rangle + z \langle 24 \rangle) \langle 34 \rangle \langle 41 \rangle}. \quad (2.11)$$

Each pole corresponds to erasing an edge in the diagram but not all edges are erasable (hence we have five poles rather than seven). The residue on the pole $z = 0$ corresponds the diagram (2.6) already encountered.

2.2 Dual formulation

In addition to calculating on-shell diagrams by treating them as the amalgamation of three-point amplitudes, there is a dual formulation where they can be viewed as differential forms on the positive Grassmannian space. To understand this picture better, let's consider the momentum conservation equation, namely:

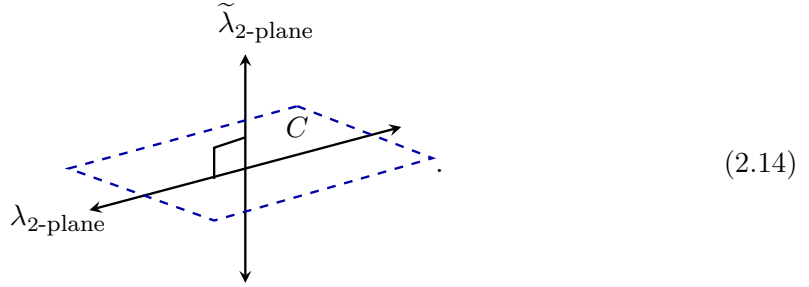
$$\delta^4(P) = \delta^4(\lambda \cdot \tilde{\lambda}) = \delta^4(\lambda_1 \tilde{\lambda}_1 + \dots + \lambda_n \tilde{\lambda}_n). \quad (2.12)$$

While this is a quadratic constraint, there is a way to re-write this condition in terms of two linear conditions for the λ 's and the $\tilde{\lambda}$'s separately. To do so, we introduce a k -plane

in n -dimensions represented by a $(k \times n)$ -matrix (modded out by $GL(k)$ since such row operations leave the k -plane invariant). The space of such planes is denoted $G(k, n)$ and is known as the Grassmannian. We will call the $(k \times n)$ matrix we use to represent a point in the Grassmannian space the C -matrix. Then we can re-write the momentum conservation equation geometrically as follows:

$$\delta(C \cdot Z) = \delta^{((n-k) \times 2)}(C^\perp \cdot \lambda) \delta^{(k \times 2)}(C \cdot \tilde{\lambda}) \delta^{(k \times \mathcal{N})}(C \cdot \tilde{\eta}), \quad (2.13)$$

where C^\perp is an orthogonal complement to C satisfying $C^\perp \cdot C = 0$. We can think about this geometrically in the n -dimensional “particle space” [91]. In this space λ and $\tilde{\lambda}$ are 2-planes which are orthogonal to each other (2.12). We define a k -dimensional plane C which contains λ and is orthogonal to $\tilde{\lambda}$,



The C matrix is then used to linearize the momentum conservation but conditions (2.13) are in fact stronger, $C \cdot \tilde{\lambda} = C^\perp \cdot \lambda = 0$ impose $2n$ conditions on the parameters of C . This reproduces four conditions from the momentum conservation and leaves us with additional $2n-4$ additional conditions. Depending on the exact dimensionality of the C -matrix, we can be left with some free parameters in C (matrix is not completely fixed) or oppositely in order to satisfy (2.13) we need to impose additional conditions on external kinematics. Note that the last delta function in (2.13) involves fermionic variables $\tilde{\eta}$ and it does not impose any conditions on C – we should just think about it as a polynomial in $\tilde{\eta}$.

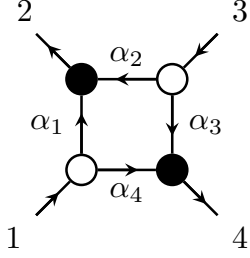
Each on-shell diagram provides a particular parametrization of the C -matrix using edge variables α_i , or face variables f_i . For planar diagrams, if the variables are real and take definite signs, all the main $(k \times k)$ minors are positive, and the C matrix represents a cell in the *positive Grassmannian* $G_+(k, n)$. The connection between cells in positive Grassmannian and plabic graphs (name used in the math literature) was found by Postnikov in [61], and later the connection to physics and scattering amplitudes was discovered in [26]. Here, we just shortly review the key ingredients.

For a given on-shell diagram, we choose an *orientation* by assigning arrows to all edges such that each black vertex has two incoming and one outgoing leg, while each white vertex has one incoming and two outgoing edges. Then we assign edge variables to all edges, fixing in each vertex one variable to one. It does not matter how we exactly choose the position of edge variables (fixing the $GL(1)$ redundancy) but in each vertex there should be at least one edge with an edge variable. The diagram has k sources, external legs with incoming arrows, and $n-k$ sinks, external legs with outgoing arrows. Then the element of the $(k \times n)$

matrix is given by the following prescription:

$$C_{\alpha a} = \sum_{\Gamma_{\alpha \rightarrow a}} \prod_j \alpha_j. \quad (2.15)$$

For each path from a source α to a sink a we take a product of all edge variables along the path and sum over all paths. The element $C_{\alpha\alpha} = 1$ while $C_{\alpha\alpha'} = 0$ for the path between two different sources. For a simple, one-loop four-point box diagram we have



$$\Rightarrow C = \begin{pmatrix} 1 & \alpha_1 & 0 & \alpha_4 \\ 0 & \alpha_2 & 1 & \alpha_3 \end{pmatrix}, \quad C^\perp = \begin{pmatrix} -\alpha_1 & 1 & -\alpha_2 & 0 \\ -\alpha_4 & 0 & -\alpha_3 & 1 \end{pmatrix}. \quad (2.16)$$

Fixing the signs of edge variables to be

$$\alpha_1 > 0, \alpha_2 > 0, \alpha_3 > 0, \alpha_4 < 0, \quad (2.17)$$

guarantees that all (2×2) minors are positive and the C -matrix represents a top cell of $G_+(2, 4)$. The on-shell function associated with the same on-shell diagram in $\mathcal{N} = 4$ SYM theory is given by

$$\Omega = \int \prod_i \frac{d\alpha_i}{\alpha_i} \delta(C \cdot Z), \quad (2.18)$$

where we are instructed to solve for the α_i variables from the delta functions which fix them as functions of external kinematics. For our example, the delta-function constraint on C^\perp gives the following equations

$$\delta^4(C^\perp \cdot \lambda) = \delta^2(-\alpha_1 \lambda_1 + \lambda_2 - \alpha_3 \lambda_3) \delta^2(-\alpha_4 \lambda_1 - \alpha_2 \lambda_3 + \lambda_4), \quad (2.19)$$

which after contracting with λ_1 and λ_3 turns into 4 equations $\prod_i^4 \delta(E_i)$, that can then be rewritten as

$$J_\delta \times \langle 13 \rangle^2 \times \delta\left(\alpha_2 - \frac{\langle 12 \rangle}{\langle 13 \rangle}\right) \delta\left(\alpha_1 - \frac{\langle 23 \rangle}{\langle 13 \rangle}\right) \delta\left(\alpha_3 - \frac{\langle 14 \rangle}{\langle 13 \rangle}\right) \delta\left(\alpha_4 - \frac{\langle 43 \rangle}{\langle 13 \rangle}\right). \quad (2.20)$$

Here $J_\delta \equiv \left| \frac{\partial E_i}{\partial \alpha_j} \right|^{-1} = \frac{1}{\langle 13 \rangle^4}$ is the Jacobian that stems from solving the four δ -function equations, and the factor $\langle 13 \rangle^2$ stems from the contraction with λ_1 and λ_3 . Plugging the solutions for the edge-variables into the other δ -function, one finds:

$$\begin{aligned} \delta^4(C \cdot \tilde{\lambda}) &= \delta^2\left(\tilde{\lambda}_1 + \frac{\langle 23 \rangle}{\langle 13 \rangle} \tilde{\lambda}_2 + \frac{\langle 43 \rangle}{\langle 13 \rangle} \tilde{\lambda}_4\right) \delta^2\left(\frac{\langle 12 \rangle}{\langle 13 \rangle} \tilde{\lambda}_2 + \tilde{\lambda}_3 + \frac{\langle 14 \rangle}{\langle 13 \rangle} \tilde{\lambda}_4\right) \\ &= \langle 13 \rangle^4 \delta^2\left(\langle 13 \rangle \tilde{\lambda}_1 + \langle 23 \rangle \tilde{\lambda}_2 + \langle 43 \rangle \tilde{\lambda}_4\right) \delta^2\left(\langle 12 \rangle \tilde{\lambda}_2 + \langle 13 \rangle \tilde{\lambda}_3 + \langle 14 \rangle \tilde{\lambda}_4\right). \end{aligned} \quad (2.21)$$

The two equations can be obtained from a single momentum conservation equation by contracting with λ_3 and λ_1 respectively, i.e. we have,

$$\delta^4(C \cdot \tilde{\lambda}) = \langle 13 \rangle^2 \delta^4(\lambda_1 \tilde{\lambda}_1 + \lambda_2 \tilde{\lambda}_2 + \lambda_3 \tilde{\lambda}_3 + \lambda_4 \tilde{\lambda}_4) \equiv \langle 13 \rangle^2 \delta^4(P). \quad (2.22)$$

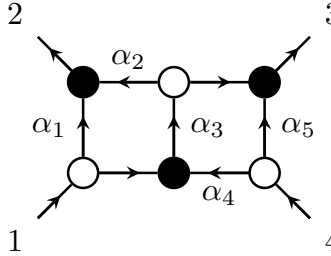
For the last delta-function we get the same thing except for replacing $\tilde{\lambda}_i \rightarrow \tilde{\eta}_i$,

$$\delta^8(C \cdot \tilde{\eta}) = \frac{1}{\langle 13 \rangle^4} \delta^8(\lambda_1 \tilde{\eta}_1 + \lambda_2 \tilde{\eta}_2 + \lambda_3 \tilde{\eta}_3 + \lambda_4 \tilde{\eta}_4) \equiv \frac{1}{\langle 13 \rangle^4} \delta^8(\mathcal{Q}). \quad (2.23)$$

We are now in a position to calculate the on-shell function Ω ,

$$\begin{aligned} \Omega &= \int \frac{d\alpha_1 \dots d\alpha_4 \delta^8(\mathcal{Q}) \delta^4(P)}{\alpha_1 \alpha_2 \alpha_3 \alpha_4 \langle 13 \rangle^4} \delta\left(\alpha_2 - \frac{\langle 12 \rangle}{\langle 13 \rangle}\right) \delta\left(\alpha_1 - \frac{\langle 23 \rangle}{\langle 13 \rangle}\right) \delta\left(\alpha_3 - \frac{\langle 14 \rangle}{\langle 13 \rangle}\right) \delta\left(\alpha_4 - \frac{\langle 43 \rangle}{\langle 13 \rangle}\right) \\ &= \frac{\delta^8(\mathcal{Q}) \delta^4(P)}{\langle 12 \rangle \langle 23 \rangle \langle 34 \rangle \langle 41 \rangle}, \end{aligned} \quad (2.24)$$

which reproduces the on-shell function (2.7) from the previous subsection. The only poles in the on-shell function Ω come from the edge variables being sent to $\alpha_i = 0$ or $\alpha_i = \infty$, which removes an edge and imposes conditions on external kinematics, in complete agreement with our earlier discussion. Note that flipping the orientation of an edge variable also flips $\alpha \leftrightarrow 1/\alpha$ and thus flips the pole at 0 and ∞ . Let us now consider another on-shell diagram,



$$C = \begin{pmatrix} 1 & \alpha_1 + \alpha_2 \alpha_3 & \alpha_3 & 0 \\ 0 & \alpha_2 \alpha_3 \alpha_4 & \alpha_5 + \alpha_3 \alpha_4 & 1 \end{pmatrix}. \quad (2.25)$$

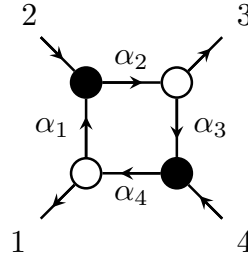
The edge variables α_i 's are given by,

$$\alpha_1 = \frac{\langle 23 \rangle - \alpha_5 \langle 24 \rangle}{\langle 13 \rangle - \alpha_5 \langle 14 \rangle}, \quad \alpha_2 = \frac{\langle 12 \rangle}{\langle 13 \rangle - \alpha_5 \langle 14 \rangle}, \quad \alpha_3 = \frac{\langle 34 \rangle}{\langle 14 \rangle}, \quad \alpha_4 = \frac{\langle 13 \rangle - \alpha_5 \langle 14 \rangle}{\langle 34 \rangle}. \quad (2.26)$$

The Jacobian from solving the δ -functions is $J = \frac{1}{(\langle 13 \rangle - \alpha_5 \langle 14 \rangle) \langle 34 \rangle}$. From (2.18) we get

$$\Omega = \int \frac{d\alpha_5 \delta^4(P) \delta^8(\mathcal{Q})}{\alpha_5 \langle 12 \rangle (\langle 23 \rangle - \alpha_5 \langle 24 \rangle) \langle 34 \rangle \langle 14 \rangle}, \quad (2.27)$$

which we recognize as (2.11) with $\alpha_5 \rightarrow -z$. In some cases the perfect orientation can involve an infinite loop. For example, if we choose the external arrows of the box diagram in the following way:



$$C = \begin{pmatrix} \alpha_2 \alpha_3 \alpha_4 \delta & 1 & \alpha_2 \delta & 0 \\ \alpha_4 \delta & 0 & \alpha_1 \alpha_2 \alpha_3 \delta & 1 \end{pmatrix}. \quad (2.28)$$

The δ that appears here corresponds to a geometric series coming from an infinite loop,

$$\delta = \sum_{j=0}^{\infty} (\alpha_1 \alpha_2 \alpha_3 \alpha_4)^j = \frac{1}{1 - \alpha_1 \alpha_2 \alpha_3 \alpha_4}. \quad (2.29)$$

Solving for edge variables we get

$$\alpha_1 = \frac{\langle 23 \rangle}{\langle 13 \rangle}, \quad \alpha_2 = \frac{\langle 13 \rangle}{\langle 12 \rangle}, \quad \alpha_3 = \frac{\langle 41 \rangle}{\langle 13 \rangle}, \quad \alpha_4 = \frac{\langle 13 \rangle}{\langle 34 \rangle} \quad \text{and also} \quad \delta = \frac{\langle 12 \rangle \langle 34 \rangle}{\langle 13 \rangle \langle 24 \rangle} \quad (2.30)$$

and plugging in (2.18) we get the same formula as in (2.24). Note that in all these cases we considered on-shell diagrams in $\mathcal{N} = 4$ SYM theory which do not depend on the assignment of helicities. Hence, the formulas for diagrams (2.16) and (2.28) gave the same on-shell functions. For $\mathcal{N} < 4$ SYM this is not the case and the helicity assignments are important.

2.3 On-shell diagrams for $\mathcal{N} < 4$ SYM theory

If the theory has less than the maximal supersymmetry, we do need to assign both external and internal helicities to fully specify the on-shell diagram. The same on-shell diagrams with different helicity assignments correspond to the same kinematics (solutions for momenta, edge variables etc) but they are given by different on-shell functions. The on-shell function for the $\mathcal{N} < 4$ SYM on-shell diagram [26] is

$$\Omega = \int \frac{d\alpha_1}{\alpha_1} \frac{d\alpha_2}{\alpha_2} \dots \frac{d\alpha_m}{\alpha_m} \mathcal{J}^{\mathcal{N}-4} \delta(C \cdot Z), \quad (2.31)$$

where the Jacobian \mathcal{J} is given by

$$\mathcal{J} = 1 + \sum_i f_i + \sum_{\substack{\text{disjoint} \\ \text{pairs } i,j}} f_i f_j + \sum_{\substack{\text{disjoint} \\ \text{pairs } i,j,k}} f_i f_j f_k + \dots, \quad (2.32)$$

with f_i denoting the face of a closed cycle, and the sums are over disjoint collections of these closed cycles. We mostly work with edge-variables, and each face f_i can be defined as a clockwise-oriented product of edge-variables. Let us compare the results for two different orientations of the one-loop box diagram. For the diagram with no internal loop (2.16) we have $\mathcal{J} = 1$ and

$$\Omega = \frac{\langle 13 \rangle^{4-\mathcal{N}} \delta^4(P) \delta^{2\mathcal{N}}(\mathcal{Q})}{\langle 12 \rangle \langle 23 \rangle \langle 34 \rangle \langle 41 \rangle}. \quad (2.33)$$

Note that this result is identical up to a trivial helicity factor, $\delta^8(\mathcal{Q}) \rightarrow \langle 13 \rangle^{4-\mathcal{N}} \delta^{2\mathcal{N}}(\mathcal{Q})$, to the $\mathcal{N} = 4$ on-shell function (2.24). The second diagram (2.28) has an internal loop and the Jacobian reads

$$\mathcal{J} = 1 - \alpha_1 \alpha_2 \alpha_3 \alpha_4 = \frac{\langle 13 \rangle \langle 24 \rangle}{\langle 12 \rangle \langle 34 \rangle}. \quad (2.34)$$

The on-shell function is then given by

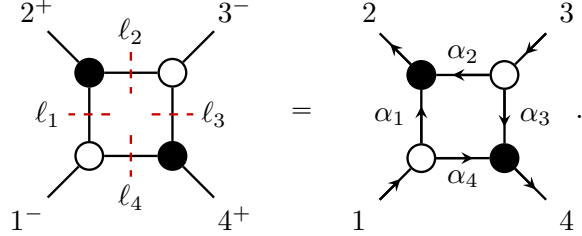
$$\Omega = \frac{\langle 24 \rangle^{4-\mathcal{N}} \delta^4(P) \delta^{2\mathcal{N}}(\mathcal{Q})}{\langle 12 \rangle \langle 23 \rangle \langle 34 \rangle \langle 41 \rangle} \times \left(\frac{\langle 12 \rangle \langle 34 \rangle}{\langle 13 \rangle \langle 24 \rangle} \right)^{4-\mathcal{N}} = \frac{(\langle 12 \rangle \langle 34 \rangle)^{4-\mathcal{N}} \delta^4(P) \delta^{2\mathcal{N}}(\mathcal{Q})}{\langle 12 \rangle \langle 23 \rangle \langle 34 \rangle \langle 41 \rangle \langle 13 \rangle^{4-\mathcal{N}}}. \quad (2.35)$$

Note that the on-shell function (2.35) has a new pole for $\mathcal{N} < 4$ located at $\langle 13 \rangle = 0$. Looking back to (2.6) this sends $\ell_1 \rightarrow \infty$, hence we refer to it as a *pole at infinity* or a *UV pole*. This pole is substantially different from all other poles which correspond to erasing edges in the on-shell diagram – these poles correspond to sending the associated loop momenta to

zero, we will refer to them as *IR poles*. The presence of the Jacobian in (2.31) dramatically changes the pole structure of the on-shell function Ω . We will often divide the form into the bare function Ω^{bare} and the appropriate power of the Jacobian,

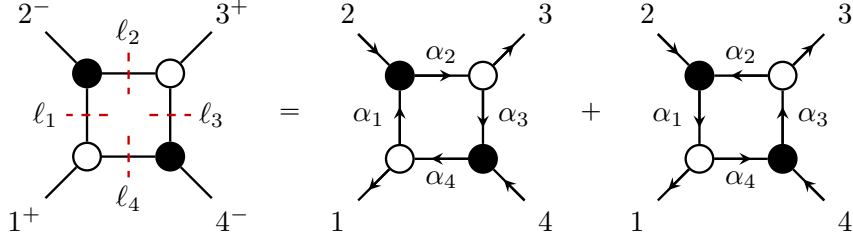
$$\Omega = \Omega^{\text{bare}} \times \mathcal{J}^{\mathcal{N}-4}. \quad (2.36)$$

The IR poles come from Ω^{bare} while the UV poles always come from the Jacobian part. The role of UV poles is the main topic of this paper and we will elaborate on it much more in the next sections. Before diving into this discussion, it is worth noting one important point. For $\mathcal{N}=4$ SYM theory each on-shell diagram directly corresponds to a cut of the loop integrand. For $\mathcal{N}<4$ SYM this is a collection of on-shell diagrams in general: with fixed helicities of external legs we have to sum over all possible orientations of internal legs. For the one-loop example, if legs 1, 3 are incoming there is one orientation and a quadruple cut of the one-loop four-point $\mathcal{N} < 4$ SYM integrand is given by a single diagram,



$$(2.37)$$

For legs 2, 4 incoming there are two possible internal orientations,



$$(2.38)$$

This is exactly the case of on-shell diagrams with internal loops as we always have two different orientations (clockwise and anti-clockwise). While in a cut they only appear in the sum, we can still treat these on-shell diagrams as independent well-defined objects and study their individual properties. For example, in the case of the amplitude $A_4(1^+ 2^- 3^+ 4^-)$ (legs 2, 4 incoming) in $\mathcal{N}=3$ SYM each diagram has a single pole at infinity, located at $\langle 13 \rangle = 0$ while the cut does not have this pole. Plugging (2.31) for $\mathcal{N} = 3$ we get,

$$\text{Cut } A_4(1^+ 2^- 3^+ 4^-) = \frac{\langle 12 \rangle \langle 23 \rangle \delta^4(P) \delta^6(Q)}{\langle 12 \rangle \langle 23 \rangle \langle 34 \rangle \langle 41 \rangle \langle 13 \rangle} + \frac{\langle 23 \rangle \langle 14 \rangle \delta^4(P) \delta^6(Q)}{\langle 12 \rangle \langle 23 \rangle \langle 34 \rangle \langle 41 \rangle \langle 13 \rangle} = \frac{\langle 24 \rangle \delta^4(P) \delta^6(Q)}{\langle 12 \rangle \langle 23 \rangle \langle 34 \rangle \langle 41 \rangle}.$$

This is a general property: cuts of $\mathcal{N}=3$ SYM amplitudes are identical to their $\mathcal{N}=4$ SYM counterparts (up to trivial helicity factors) while $\mathcal{N}=3$ SYM on-shell diagrams are individually different and have poles at infinity. On a $\mathcal{N}=3$ cut we sum over contributing on-shell diagrams and any pole at infinity has to cancel.

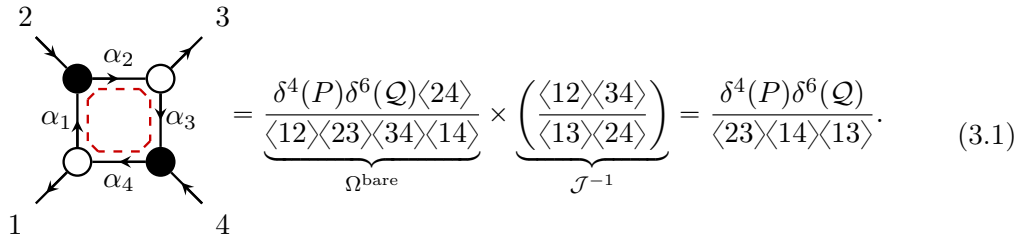
3 UV poles in one-loop graphs

The bare on-shell functions describe the dynamics of scattering amplitudes in the IR sector when the (cut) loop momenta are small. All poles in Ω^{bare} correspond to setting one of these momenta to zero and erasing an edge in the diagram, as a consequence of the perturbative unitarity. In the $\mathcal{N}=4$ SYM theory the on-shell function is given by Ω^{bare} , and hence we only have IR poles. This is true for both planar and non-planar sectors of the theory. In the planar sector, this is also a consequence of the dual conformal symmetry, while the symmetry explanation of the absence of poles at infinity in the non-planar sector is yet-to-be found. Note that the absence of these poles is related, but not identical, to the statement of the UV finiteness of final (integrated) scattering amplitudes in $\mathcal{N}=4$ SYM theory. In fact, the absence of poles at infinity in on-shell diagrams is a stronger property than the UV finiteness of the S-matrix, see [64, 65, 69] for more details.

For $\mathcal{N}<4$ SYM theory, the bare function Ω^{bare} is decorated by a power of the Jacobian \mathcal{J} as outlined in the previous section. The Jacobian changes the pole structure: it removes some of the existing IR poles, and adds new UV poles. Note that the UV poles are not fixed by the (standard) unitarity – unlike IR poles where tree-level factorization or unitarity cuts fully fix corresponding residues. As a result, we can not naively expect that the residue on a UV pole, where the loop momentum goes to infinity, is an operation on an on-shell diagram. In the following, we will show that despite these assumptions the real situation is quite contrary: the UV pole can be understood as a (rather simple) diagrammatic operation, not erasing an edge, but shrinking a corresponding loop (which blows up on the pole) and rejoining internal legs via a “non-planar twist”. As a result, the residue on the UV pole is generally a lower-loop *non-planar* on-shell diagram. In our discussion, we first focus on the $\mathcal{N}=3$ case, where the on-shell function contains only one power of \mathcal{J} , and the pole at infinity in Ω is always a simple pole. For general \mathcal{N} we get higher order poles at infinity and the residues correspond to derivatives of an on-shell function associated with the diagram.

3.1 First $\mathcal{N}=3$ examples

The simplest example is the one-loop box on-shell diagram with an internal loop discussed earlier. The on-shell function is given by,



$$\begin{aligned}
 & \text{Diagram: A box with vertices 1, 2, 3, 4. Internal edges are labeled } \alpha_1, \alpha_2, \alpha_3, \alpha_4. \text{ A dashed red line connects the top and bottom vertices.} \\
 & = \underbrace{\frac{\delta^4(P)\delta^6(Q)\langle 24 \rangle}{\langle 12 \rangle \langle 23 \rangle \langle 34 \rangle \langle 14 \rangle}}_{\Omega^{\text{bare}}} \times \underbrace{\left(\frac{\langle 12 \rangle \langle 34 \rangle}{\langle 13 \rangle \langle 24 \rangle} \right)}_{\mathcal{J}^{-1}} = \frac{\delta^4(P)\delta^6(Q)}{\langle 23 \rangle \langle 14 \rangle \langle 13 \rangle}. \quad (3.1)
 \end{aligned}$$

where the Grassmann variables are η_i^I , $I = 1, 2, 3$, and hence the supermomentum conservation is $\delta^6(Q)$. We can see that the Jacobian \mathcal{J} introduces two new poles, $\langle 13 \rangle$ and $\langle 24 \rangle$ and removes poles $\langle 12 \rangle$ and $\langle 34 \rangle$. The absence of poles $\langle 12 \rangle$ and $\langle 34 \rangle$ is caused by the fact that corresponding edges are no longer removable. For example, removing edge α_2 sends

$\langle 12 \rangle = 0$ which leads to an illegal helicity flow

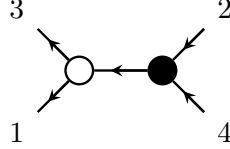


$$(3.2)$$

as we have a wrong number of incoming/outgoing legs in black/white vertices. This pole was perfectly legal pole in the $\mathcal{N}=4$ SYM case but now the Jacobian removes it. Same is true for the pole $\langle 23 \rangle = 0$ and the edge α_4 . Next, the pole $\langle 24 \rangle$ is canceled by the helicity factor in the numerator of Ω and only $\langle 13 \rangle = 0$ stays as a new valid pole. As noted before, this is a pole at infinity as it sends the on-shell loop momentum $\ell_1 \rightarrow \infty$. While this pole does not erase any edge, we can easily see what type of kinematical constraint it imposes:

$$\langle 13 \rangle = 0 \leftrightarrow \lambda_1 \sim \lambda_3, \text{ and by momentum conservation } [24] = 0 \leftrightarrow \tilde{\lambda}_2 \sim \tilde{\lambda}_4. \quad (3.3)$$

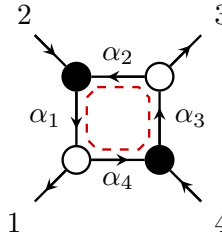
But this is nothing else than the factorization diagram,



$$= \frac{\delta^4(P)\delta^6(Q)\delta(\langle 13 \rangle)}{\langle 23 \rangle \langle 14 \rangle}. \quad (3.4)$$

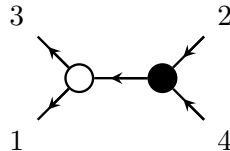
The internal momentum flow is here fixed by the number of incoming/outgoing legs in white/black vertex. Note that our procedure was based solely on the analysis of the kinematical conditions between external legs, i.e. we imposed $\langle 13 \rangle = 0$ and searched for an on-shell diagram which materializes that. But very importantly, the on-shell function for this diagram (3.4) is equal to the residue of the original diagram (3.1) on the pole $\langle 13 \rangle = 0$. In this case it might look a bit trivial as we only replaced $1/\langle 13 \rangle \rightarrow \delta(\langle 13 \rangle)$ but the same procedure is valid for the general case.

Checking the equality of the residue of the original on-shell diagram evaluated on the pole with the new on-shell diagram (with extra delta function imposed) might sometimes be tricky. For example, if we consider the same diagram with the internal loop and the opposite orientation, we get



$$= \underbrace{\frac{\delta^4(P)\delta^6(Q)\langle 24 \rangle}{\langle 12 \rangle \langle 23 \rangle \langle 34 \rangle \langle 14 \rangle}}_{\Omega^{\text{bare}}} \times \underbrace{\left(\frac{\langle 23 \rangle \langle 14 \rangle}{\langle 13 \rangle \langle 24 \rangle} \right)}_{\mathcal{J}^{-1}} = \frac{\delta^4(P)\delta^6(Q)}{\langle 12 \rangle \langle 34 \rangle \langle 13 \rangle}. \quad (3.5)$$

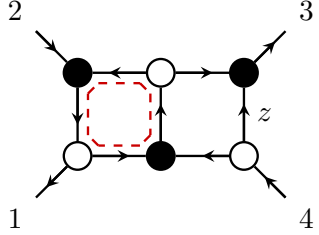
Taking the residue on the pole $\langle 13 \rangle = 0$ we arrive at the same diagram as before,



$$= \frac{\delta^4(P)\delta^6(Q)\delta(\langle 13 \rangle)}{\langle 12 \rangle \langle 34 \rangle}. \quad (3.6)$$

As you can see the on-shell functions look different in (3.4) and (3.6) but they are the same up to a sign, as $\langle 12 \rangle \langle 34 \rangle = \langle 23 \rangle \langle 14 \rangle$ for $\langle 13 \rangle = 0$. In fact, if we sum (3.4) and (3.6) we get zero which is consistent with $\mathcal{N} = 3$ SYM cuts not having any poles at infinity.

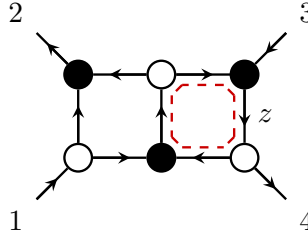
Next, let us consider the four-point double box on-shell diagram we discussed in the previous section. There are multiple different orientations of the same diagram which lead to different structures of poles at infinity. We can see from the parametrization of the loop momenta (2.10) that the left loop blows up for $z = -\langle 13 \rangle / \langle 14 \rangle$, while the right loop momentum goes to infinity for $z = \infty$. The accessibility of these poles depends on a particular orientation and the presence of closed loops. For the following orientation



$$= \int dz \underbrace{\frac{\langle 24 \rangle \delta^4(P) \delta^6(Q)}{z(\langle 23 \rangle + z\langle 24 \rangle) \langle 14 \rangle \langle 34 \rangle \langle 12 \rangle}}_{\Omega^{\text{bare}}} \times \underbrace{\frac{\langle 14 \rangle (\langle 23 \rangle + z\langle 24 \rangle)}{\langle 24 \rangle (\langle 13 \rangle + z\langle 14 \rangle)}}_{\mathcal{J}^{-1}} \quad (3.7)$$

$$= \int dz \frac{\delta^4(P) \delta^6(Q)}{z \langle 34 \rangle \langle 12 \rangle (\langle 13 \rangle + z\langle 14 \rangle)},$$

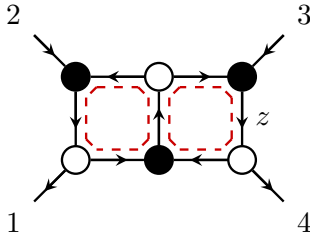
we have a closed cycle in the left loop and the on-shell function has a pole at $z = -\langle 13 \rangle / \langle 14 \rangle$. A different orientation has a closed cycle in the right loop and a pole at $z = \infty$,



$$= \int dz \frac{\langle 13 \rangle \delta^4(P) \delta^6(Q)}{z(\langle 23 \rangle + z\langle 24 \rangle) \langle 14 \rangle \langle 34 \rangle \langle 12 \rangle} \times \frac{z\langle 14 \rangle}{\langle 13 \rangle} \quad (3.8)$$

$$= \int dz \frac{\delta^4(P) \delta^6(Q)}{\langle 12 \rangle \langle 34 \rangle (\langle 23 \rangle + z\langle 24 \rangle)}$$

Finally, we can have an orientation with two internal cycles and both poles in Ω ,



$$= \int dz \frac{\langle 23 \rangle \delta^4(P) \delta^6(Q)}{z(\langle 23 \rangle + z\langle 24 \rangle) \langle 12 \rangle \langle 14 \rangle \langle 34 \rangle} \times \frac{z\langle 14 \rangle (\langle 23 \rangle + z\langle 24 \rangle)}{\langle 23 \rangle (\langle 13 \rangle + z\langle 14 \rangle)} \quad (3.9)$$

$$= \int dz \frac{\delta^4(P) \delta^6(Q)}{\langle 12 \rangle \langle 34 \rangle (\langle 13 \rangle + z\langle 14 \rangle)}$$

Note that in this case there is no IR pole present as erasing any edge would lead to a contradiction with the helicity assignment. As in the previous case, we want to interpret the residue on the pole at infinity as another (now one-loop) on-shell diagram. As both cycles are just one-loop on-shell diagrams, we can treat them locally, see section 4.1 for proof of this. This means that if we blow up the left loop we need to replace the box on-shell diagram with external legs $1, 2, \ell_3, \ell_6$ by the tree-level factorization diagram with

legs 2, ℓ_6 in the black vertex and 1, ℓ_3 in the white vertex,

$$(3.10)$$

Making this replacement in (3.8) we get

$$(3.11)$$

The same expression for the on-shell function can be obtained by taking the residue of (3.7) on the $z = -\langle 13 \rangle / \langle 14 \rangle$ pole. If we blow up the same loop in the third diagram (3.9), we get a one-loop diagram with a closed cycle,

$$(3.12)$$

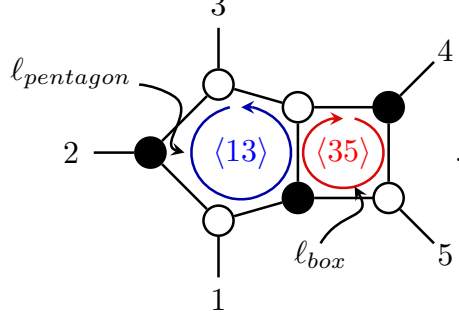
which is precisely equal to the residue of (3.9) on the $z = -\langle 13 \rangle / \langle 14 \rangle$ pole. We can do the same analysis for the $z = \infty$ pole, again finding an agreement between the new on-shell diagram and the residue of the original on-shell function (3.9).

3.2 Two-loop pentabox diagram

Let us now look at a more complicated example: five-point MHV pentabox on-shell diagram. Solving for internal on-shell momenta gives

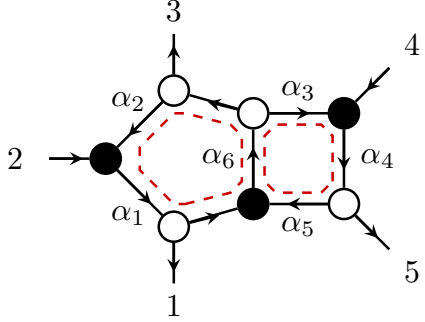
$$(3.13)$$

We see that the left (pentagon) loop has a pole at infinity for $\langle 13 \rangle = 0$, all momenta ℓ_A , ℓ_B , ℓ_C , ℓ_G , ℓ_H blow up, while the right (box) loop has a UV pole for $\langle 35 \rangle = 0$ when ℓ_D , ℓ_E , ℓ_F and ℓ_H go to infinity. The loop momentum ℓ_H contains both poles as it participates in both internal cycles. Note that the assignment of cycles is unique and it critically depends on the *planarity* of the diagram. In particular, we do not consider the external heptagon cycle – there is no pole at infinity associated with it, see Section 6 for elaboration,



$$(3.14)$$

Now we choose a particular orientation where both poles at infinity are present due to helicity assignments and solve for the edge variables,



$$\begin{aligned} \alpha_1 &= \frac{\langle 13 \rangle}{\langle 23 \rangle}, & \alpha_2 &= \frac{\langle 12 \rangle}{\langle 13 \rangle}, & \alpha_3 &= \frac{\langle 45 \rangle}{\langle 35 \rangle}, \\ \alpha_4 &= \frac{\langle 35 \rangle}{\langle 34 \rangle}, & \alpha_5 &= \frac{\langle 13 \rangle}{\langle 35 \rangle}, & \alpha_6 &= \frac{\langle 35 \rangle}{\langle 15 \rangle}. \end{aligned} \quad (3.15)$$

This on-shell diagram is a part of the octacut of the 2-loop 5pt amplitude $A_5(1^+2^-3^+4^-5^+)$. In order to calculate the whole cut we would have to sum over all possible internal helicity assignments (for $\mathcal{N} < 4$ SYM) as discussed earlier, but we can also study this one on-shell diagram individually. For this particular case (3.15) the bare on-shell function (which is identical for any assignment of internal helicities) is,

$$\Omega^{\text{bare}} = \int \frac{d\alpha_1 \dots d\alpha_6 \delta(C \cdot Z)}{\alpha_1 \alpha_2 \alpha_3 \alpha_4 \alpha_5 \alpha_6} = \frac{\langle 24 \rangle \delta^4(P) \delta^6(Q)}{\langle 12 \rangle \langle 23 \rangle \langle 34 \rangle \langle 45 \rangle \langle 51 \rangle} \quad (3.16)$$

and the Jacobian \mathcal{J} consists of two cycles,

$$\mathcal{J} = \frac{1}{1 - \alpha_1 \alpha_2 \alpha_6 - \alpha_3 \alpha_4 \alpha_5 \alpha_6} = \frac{\langle 13 \rangle \langle 24 \rangle \langle 35 \rangle}{\langle 23 \rangle \langle 15 \rangle \langle 34 \rangle} \quad (3.17)$$

The on-shell function Ω is then equal to

$$\Omega = \underbrace{\frac{\langle 24 \rangle \delta^4(P) \delta^6(Q)}{\langle 12 \rangle \langle 23 \rangle \langle 34 \rangle \langle 45 \rangle \langle 51 \rangle}}_{\Omega^{\text{bare}}} \times \underbrace{\left(\frac{\langle 23 \rangle \langle 15 \rangle \langle 34 \rangle}{\langle 13 \rangle \langle 24 \rangle \langle 35 \rangle} \right)}_{\mathcal{J}^{-1}} = \frac{\delta^4(P) \delta^6(Q)}{\langle 12 \rangle \langle 45 \rangle \langle 13 \rangle \langle 35 \rangle} \quad (3.18)$$

We see that three of the IR poles $\langle 23 \rangle$, $\langle 34 \rangle$, $\langle 15 \rangle$ are removed as erasing α_1 , α_4 and α_6 edges would lead to inconsistent helicity flows. On the other hand, both UV poles $\langle 13 \rangle$, $\langle 35 \rangle$ are added. We first blow up the right loop and calculate the residue on the pole $\langle 35 \rangle = 0$. The right loop can be treated as a one-loop box diagram with external legs $C, 4, 5, G$. The residue is a following on-shell diagram,

$$(3.19)$$

Replacing the box by this tree graph in (3.13) we get

$$(3.20)$$

Note that in this diagram the condition $\langle 35 \rangle$ is automatically imposed as evident from legs 3, 5 being connected by a chain of white vertices. We can now assign edge variables

$$\begin{aligned} \alpha_1 &= \frac{\langle 15 \rangle}{\langle 25 \rangle}, & \alpha_2 &= \frac{\langle 12 \rangle}{\langle 13 \rangle}, \\ \alpha_3 &= \frac{\langle 23 \rangle}{\langle 25 \rangle}, & \alpha_4 &= \frac{\langle 15 \rangle}{\langle 14 \rangle}, & \alpha_5 &= \frac{\langle 45 \rangle}{\langle 51 \rangle}. \end{aligned} \quad (3.21)$$

and calculate the on-shell function,

$$\Omega_{UV} = \int \frac{d\alpha_1 \dots d\alpha_5 \delta(C \cdot Z)}{\alpha_1 \alpha_2 \alpha_3 \alpha_4 \alpha_5} \times \frac{1}{1 - \alpha_1 \alpha_2 \alpha_3 \alpha_4 \alpha_5} = \frac{\delta^4(P) \delta^6(Q) \delta(\langle 35 \rangle)}{\langle 12 \rangle \langle 45 \rangle \langle 13 \rangle}, \quad (3.22)$$

which is equal to a residue of (3.18) on $\langle 35 \rangle = 0$ pole. Let us now consider the same pentabox on-shell diagram but calculate the residue on the other pole at infinity $\langle 13 \rangle = 0$ which blows up the left pentagon. As we have already seen, the calculation of UV poles is a local operation and we need to figure out how to do it for the pentagon sub-diagram. As it turns out, the rule is very similar to what we saw for the box. The result is a tree-level on-shell diagram with legs 2, F in the black vertex and legs 1, 3, D connected by a chain of

white vertices,

$$(3.23)$$

where we first merge-expanded the pentagon diagram and then we used the same replacement rule as for the box. In the final tree-level on-shell diagram we merged all legs into one white vertex, which can be interpreted as a 4-point $k = 1$ tree-level amplitude, or alternatively can be further expanded as a chain of regular white three-point vertices,

$$(3.24)$$

The identity between all these diagrams is a consequence of a usual merge-expand rule [26]. Using (3.24) the residue on the $\langle 13 \rangle = 0$ pole is

$$(3.25)$$

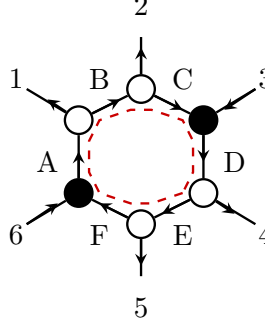
As expected this diagram automatically implements the condition $\langle 13 \rangle = 0$. Note that using other representations of the tree graph (3.24) we would get other one-loop pentagons which differ from (3.25) by the merge-expand move and do not change the on-shell function. It is easy to see that the on-shell function for (3.25) is equal to

$$\Omega_{UV} = \frac{\delta^4(P)\delta^6(Q)\delta(\langle 13 \rangle)}{\langle 12 \rangle \langle 45 \rangle \langle 35 \rangle} \quad (3.26)$$

which is equal to the residue of (3.18) on $\langle 13 \rangle = 0$ pole. Naively, we could access the pole at infinity by solving for one of the edge variables from $\mathcal{J}^{-1} = 0$. However, the meaning of the new edge variables is unclear as they do not correspond to a parametrization of the lower-loop on-shell diagram. Hence we have to work directly in the kinematical space when accessing the poles at infinity.

3.3 MHV one-loop diagrams

As we have already seen, the calculation of the UV pole of an on-shell diagram reduced to the calculation of this pole in the one-loop sub-diagram. The result of this operation was glued into the rest of the graph. Our goal here is to calculate the UV pole for a general one-loop on-shell diagram. This is a direct generalization of what we have already seen for box and pentagon. Let us first look at the MHV hexagon,

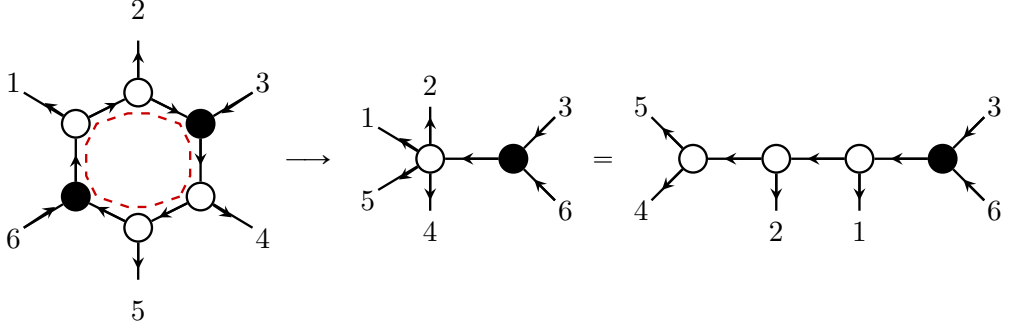


$$\begin{aligned}
 \ell_A &= \frac{[13]}{[36]} \lambda_1 \tilde{\lambda}_6, & \ell_B &= \frac{[16]}{[36]} \lambda_1 \tilde{\lambda}_3, \\
 \ell_C &= \frac{[26]}{[36]} \lambda_2 \tilde{\lambda}_3, & \ell_D &= \frac{[46]}{[36]} \lambda_4 \tilde{\lambda}_3, \\
 \ell_E &= \frac{[34]}{[36]} \lambda_4 \tilde{\lambda}_6, & \ell_F &= \frac{[35]}{[36]} \lambda_5 \tilde{\lambda}_6.
 \end{aligned}
 \tag{3.27}$$

As we can see from the chains of white vertices, the external kinematics is subject to two constraints $\langle 12 \rangle = \langle 45 \rangle = 0$, i.e. $\lambda_2 = \alpha \lambda_1$, $\lambda_5 = \beta \lambda_4$. The pole at infinity is accessed by sending $[36] = 0$ as evident from explicit solutions for internal loop momenta,

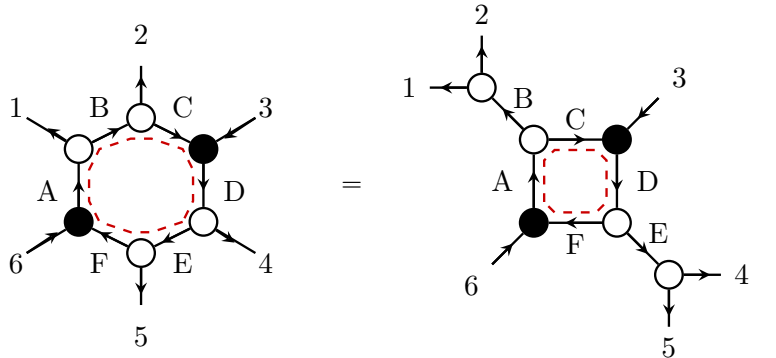
$$0 = s_{36} = s_{1245} = (p_1 + p_2) \cdot (p_4 + p_5) = \langle 14 \rangle ([14] + \alpha [24] + \beta [15] + \alpha \beta [25]) \tag{3.28}$$

Hence $[36] = 0$ implies $\langle 14 \rangle = 0$ on the support of $\langle 12 \rangle = \langle 45 \rangle = 0$. In the end, all λ s of external legs connected to white vertices are collinear, $\lambda_1 \sim \lambda_2 \sim \lambda_4 \sim \lambda_5$, i.e. $\langle ij \rangle = 0$ for $i, j = 1, 2, 4, 5$. This merges legs 1, 2, 4, 5 in the white vertex and 3, 6 into black vertex



$$\tag{3.29}$$

where the five-point white vertex can be again expanded in any way we want. We could obtain the same conclusion if we first merge-expanded the original hexagon,



$$\tag{3.30}$$

By accessing the pole at infinity in the box diagram, we arrive at one particular representation of the resulting tree graph,

$$(3.31)$$

This can be also verified by an explicit calculation. The on-shell function for the hexagon with closed internal loop (3.27) is

$$\Omega = \underbrace{\frac{\langle 36 \rangle \delta^4(P) \delta^6(Q) \delta(\langle 12 \rangle) \delta(\langle 45 \rangle)}{\langle 23 \rangle \langle 34 \rangle \langle 56 \rangle \langle 16 \rangle}}_{\Omega^{\text{bare}}} \times \underbrace{\frac{\langle 23 \rangle \langle 56 \rangle}{\langle 25 \rangle \langle 36 \rangle}}_{\mathcal{J}^{-1}} = \frac{\delta^4(P) \delta^6(Q) \delta(\langle 12 \rangle) \delta(\langle 45 \rangle)}{\langle 34 \rangle \langle 16 \rangle \langle 25 \rangle} \quad (3.32)$$

On the pole at infinity, $\langle 25 \rangle = 0$, and replacing $1/\langle 25 \rangle \rightarrow \delta(\langle 25 \rangle)$ we do get the correct on-shell function for the on-shell diagram (3.31). Note that this is all calculated on a very constrained kinematics so there are many equivalent ways how to write the formula (3.32). It is clear how the calculation of the UV pole generalizes for any one-loop MHV on-shell diagram,

$$(3.33)$$

where we conveniently reduced the n -gon into a “core” box diagram connected to white blobs of external legs. The λ -spinors of all external legs connected to the same white vertex are proportional, so the kinematics are highly constrained. As before, on the pole at infinity $[ij] = 0$ we replace the box diagram by a simple tree-level factorization graph, and all but

legs i, j are now connected to the same white vertex,

$$(3.34)$$

We can expand the white vertex into three-point vertices in an arbitrary way without changing the kinematics or the on-shell function. In the original on-shell diagram many collinearity conditions are already imposed,

$$\lambda_{i+1} \sim \lambda_{i+2} \sim \dots \sim \lambda_{j-1} \quad \text{and} \quad \lambda_{j+1} \sim \lambda_{j+2} \sim \dots \sim \lambda_{i-1} \quad (3.35)$$

The pole at infinity is accessed by $\langle pq \rangle = 0$ where p, q are from two different sets of labels of external legs attached to white vertices, $p \in \{i+1, \dots, j-1\}$ and $q \in \{j+1, \dots, i-1\}$, or alternatively we can access the pole by sending $[ij] = 0$, which are all equivalent conditions.

3.4 Arbitrary n -gons and helicities

Our goal now is to generalize the rule for the UV pole for an n -gon with an arbitrary configuration of white and black vertices, and arbitrary k degree. The first example is a very simple six-point NMHV hexagon

$$(3.36)$$

where we used the merge-expand moves to redraw the diagram. We can see that the core diagram is again a box, hence the rule for the UV pole is the same as before and we have not learnt anything new. This makes it clear that the next qualitatively new case is the hexagon diagram where the white and black vertices are alternating, and the core diagram is a proper hexagon that can not be simplified,

$$(3.37)$$

The kinematics of this on-shell diagram is more involved. There is no chain of black/white vertices and no merge-expand operation can change it. There are two independent kinematical conditions imposed on external momenta but none of these conditions is a simple collinearity of λ or $\tilde{\lambda}$ spinors. Solving for internal momenta we learn that there are three cyclically related kinematical conditions imposed,

$$\langle 1|2+3|4] = \langle 3|4+5|6] = \langle 5|6+1|2] = 0 \quad (3.38)$$

One of these conditions is redundant, i.e. any two of them imply the third one. Looking at the denominator of on-shell loop momenta we can see that the pole at infinity can be approached by setting $\langle 13 \rangle = 0$. On the support of (3.38) this also sends

$$\langle 13 \rangle = \langle 15 \rangle = \langle 35 \rangle = 0 = [24] = [26] = [46] \quad (3.39)$$

In other words, $\lambda_1 \sim \lambda_3 \sim \lambda_5$ and $\tilde{\lambda}_2 \sim \tilde{\lambda}_4 \sim \tilde{\lambda}_6$ on the pole at infinity. The corresponding on-shell diagram is then



and the on-shell function is

$$\Omega_{UV} = \frac{[23]\delta(\langle 13 \rangle)\delta(\langle 35 \rangle)\delta([24])\delta(P)\delta(Q)\delta([56]\tilde{\eta}_4 + [45]\tilde{\eta}_6)}{[34]\langle 12 \rangle \times [25][25][56]^2} \quad (3.41)$$

It is very interesting that the kinematics in (3.37) is already quite constrained (3.38), but it is only after imposing one more condition and approaching the UV pole that it completely factorizes into $\lambda, \tilde{\lambda}$ collinearities (3.39).

We now evaluate the on-shell function for this diagram. The topology allows us to fix the GL(1)s in a symmetric way and choose the edge variables as

$$\begin{aligned} \alpha_1 &= \frac{\langle 23 \rangle}{\langle 13 \rangle}, & \alpha_2 &= \frac{\langle 13 \rangle}{\langle 12 \rangle}, \\ \alpha_3 &= \frac{\langle 45 \rangle}{\langle 35 \rangle}, & \alpha_4 &= \frac{\langle 35 \rangle}{\langle 34 \rangle}, \\ \alpha_5 &= \frac{\langle 16 \rangle}{\langle 15 \rangle}, & \alpha_6 &= \frac{\langle 15 \rangle}{\langle 56 \rangle}. \end{aligned} \quad (3.42)$$

The Jacobian of the diagram is given by

$$\mathcal{J} = 1 - \alpha_1 \alpha_2 \alpha_3 \alpha_4 \alpha_5 \alpha_6 = \frac{\langle 12 \rangle \times [34] \times [56] - \langle 23 \rangle \times [45] \times [16]}{\langle 12 \rangle \times [34] \times [56]} = \frac{\langle 13 \rangle \times [4] \times [3+5|1]}{\langle 12 \rangle \times [34] [12]} \quad (3.43)$$

where in the last equality we used the special kinematics (3.39). The on-shell functions can be then written in many equivalent ways thanks to (3.39), one representation is

$$\Omega = \underbrace{\frac{\langle 4|3+5|1\rangle\langle 34\rangle\langle 15\rangle\delta(\Xi)}{[56]^2[12]\langle 12\rangle\langle 16\rangle\langle 23\rangle\langle 45\rangle\langle 35\rangle}}_{\Omega^{\text{bare}}} \times \underbrace{\frac{\langle 12\rangle\langle 34\rangle[12]}{\langle 13\rangle\langle 4|3+5|1\rangle}}_{\mathcal{J}^{-1}} = \frac{\langle 15\rangle\langle 34\rangle^2\delta(\Xi)}{[56]^2\langle 13\rangle\langle 16\rangle\langle 23\rangle\langle 45\rangle\langle 35\rangle} \quad (3.44)$$

where we denoted all delta functions as

$$\delta(\Xi) \equiv \delta^4(P)\delta^6(\mathcal{Q})\delta(\langle 1|2+3|4\rangle)\delta(\langle 3|4+5|6\rangle)\delta^3([56]\tilde{\eta}_4+[46]\tilde{\eta}_5+[45]\tilde{\eta}_6) \quad (3.45)$$

Looking at the denominator of the inverse Jacobian \mathcal{J}^{-1} we can see two terms: the first is $\langle 4|3+5|1\rangle$ – this is just a helicity factor which is canceled by the numerator of the bare form (and would continue to be canceled also for $\mathcal{N} < 3$), and then the pole at infinity $\langle 13\rangle = 0$. Note that due to the special kinematics, the pole structure of Ω is not very transparent. The singularities, $\langle 23\rangle = 0$, $\langle 45\rangle = 0$, $\langle 16\rangle = 0$, are all physical poles and correspond to erasing edges α_1 , α_3 , α_5 . Pole $[56] = 0$ is not present because it also implies $\langle 34\rangle = 0$ and there is a cancelation between the numerator and the denominator (it also corresponds to non-erasable edge α_4 which is forbidden). We can make manifest an absence of this pole but at the expense of introducing some other spurious pole. This is a general feature of such expressions, because of mass dimension and little group weights any representation has some spurious terms that can be removed by trading them for another spurious object.

Let us look in more detail at the pole at infinity located at $\langle 13\rangle = \langle 15\rangle = \langle 35\rangle = 0$. This pole is not present in Ω^{bare} as the factor $\langle 15\rangle/\langle 35\rangle$ is finite and no singularity is generated. This can be made manifest when choosing a particular parametrization. The Jacobian \mathcal{J}^{-1} does introduce this pole and we can show after some work that the residue on the UV pole is equal to

$$\Omega_{\text{UV}} = \frac{[23]\delta(\langle 13\rangle)\delta(\langle 35\rangle)\delta([24])\delta^4(P)\delta^6(\mathcal{Q})\delta([56]\tilde{\eta}_4+[45]\tilde{\eta}_6)}{[34]\langle 12\rangle\langle 25\rangle[25][56]^2} \quad (3.46)$$

where the delta functions indicate the simple collinearity conditions. The expression (3.46) is equal to (3.41) which proves our conjecture. Note that in (3.46) the kinematics is incredibly constrained (three extra conditions) and there are many equivalent ways how to write it. For arbitrary \mathcal{N} the formula (3.44) is generalized to

$$\Omega = \frac{\langle 4|3+5|1\rangle^{4-\mathcal{N}}\langle 34\rangle\langle 15\rangle\delta(\Xi)}{[56]^2[12]\langle 12\rangle\langle 16\rangle\langle 23\rangle\langle 45\rangle\langle 35\rangle} \times \left(\frac{\langle 12\rangle\langle 34\rangle[12]}{\langle 13\rangle\langle 4|3+5|1\rangle} \right)^{4-\mathcal{N}} \quad (3.47)$$

and while the helicity factor $\langle 4|3+5|1\rangle$ is canceled, we do generate a higher pole at infinity for $\langle 13\rangle = 0$. We will discuss it in more details in the next section.

The next case is an arbitrary NMHV n -gon, with three black and $n-3$ white vertices. We can use the merge-expand moves to redraw this diagram as a core hexagon with three

extra white blobs,

$$(3.48)$$

All the λ spinors in each group are proportional,

$$\lambda_{i+1} \sim \lambda_{i+2} \sim \cdots \sim \lambda_{j-1} \text{ etc.} \quad (3.49)$$

and in addition we have two independent mixed conditions, for example,

$$\langle i-1|P_i|j] = \langle j-1|P_j|k] = 0 \quad (3.50)$$

where $P_i = p_i + p_{i+1} + \cdots + p_{j-1}$ and $P_j = p_j + p_{j+1} + \cdots + p_{k-1}$. The pole at infinity is accessed by a single condition when $\langle pq \rangle = 0$ where p, q are from two different white sectors. This collapses the whole kinematics and all external λ s attached to white vertices are proportional, and all external $\tilde{\lambda}$ s attached to black vertices are proportional. As a result, we get an on-shell diagram

$$(3.51)$$

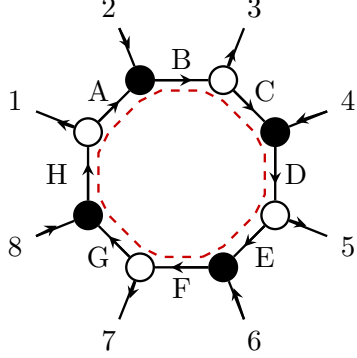
Note that all such tree-level on-shell diagrams are *non-planar* in a sense of the canonical ordering $1, 2, \dots, n$ we started with. The same procedure generalizes to higher k degrees. The “core” N^2 MHV one-loop on-shell diagram is an octagon,

$$(3.52)$$

Here we have four independent kinematical conditions imposed on the external kinematics, for example

$$\langle 1|2+3|4\rangle = \langle 3|1+2|8\rangle = \langle 7|8+1|2\rangle = \langle 5|3+4|2\rangle = 0 \quad (3.53)$$

There are no collinearity conditions between λ s and $\tilde{\lambda}$ s. The four independent constraints (3.53) are quadratic in nature and there is no simplification. The solution for the internal on-shell loop momenta is



$$\begin{aligned} \ell_A &= \frac{\langle 23 \rangle}{\langle 13 \rangle} \lambda_1 \tilde{\lambda}_2, & \ell_B &= \frac{\langle 12 \rangle}{\langle 13 \rangle} \lambda_3 \tilde{\lambda}_2, \\ \ell_C &= \frac{\langle 45 \rangle}{\langle 35 \rangle} \lambda_3 \tilde{\lambda}_4, & \ell_D &= \frac{\langle 34 \rangle}{\langle 35 \rangle} \lambda_5 \tilde{\lambda}_4, \\ \ell_E &= \frac{\langle 67 \rangle}{\langle 57 \rangle} \lambda_5 \tilde{\lambda}_6, & \ell_F &= \frac{\langle 56 \rangle}{\langle 57 \rangle} \lambda_7 \tilde{\lambda}_6, \\ \ell_G &= \frac{\langle 18 \rangle}{\langle 17 \rangle} \lambda_7 \tilde{\lambda}_8, & \ell_H &= \frac{\langle 78 \rangle}{\langle 17 \rangle} \lambda_1 \tilde{\lambda}_8. \end{aligned} \quad (3.54)$$

We see that the pole at infinity is accessed by imposing a simple condition $\langle 13 \rangle = 0$ which again collapses the whole kinematics to two sectors,

$$\lambda_1 \sim \lambda_3 \sim \lambda_5 \sim \lambda_7 \quad \text{and} \quad \tilde{\lambda}_2 \sim \tilde{\lambda}_4 \sim \tilde{\lambda}_6 \sim \tilde{\lambda}_8 \quad (3.55)$$

and the corresponding on-shell diagram is



$$(3.56)$$

We can see that the diagram again does not respect the canonical ordering of the original octagon (3.52). The on-shell function for the octagon is

$$\Omega = \underbrace{\frac{[18][14][23]\langle 56 \rangle^2 \langle 34 \rangle \langle 78 \rangle \langle 4|6+7|8\rangle [17] \delta(\Xi)}{[56]^2 [78]^3 [12]^3 [34] \langle 23 \rangle^3 \langle 45 \rangle \langle 67 \rangle \langle 81 \rangle}}_{\Omega^{\text{bare}}} \times \underbrace{\frac{\langle 12 \rangle \langle 34 \rangle [87] [12]}{\langle 13 \rangle \langle 4|6+7|8\rangle [17]}}_{\mathcal{J}^{-1}} \quad (3.57)$$

where the delta functions are

$$\begin{aligned} \delta(\Xi) &= \delta^4(P) \delta^6(\mathcal{Q}) \delta(\tilde{\eta}_4[56] + \tilde{\eta}_5[46] + \tilde{\eta}_6[45]) \delta(\tilde{\eta}_6[78] + \tilde{\eta}_7[68] + \tilde{\eta}_8[67]) \\ &\quad \times \delta(\langle 3|4+5|6\rangle) \delta(\langle 7|5+6|4\rangle) \delta(\langle 5|6+7|8\rangle) \delta(\langle 1|7+8|6\rangle) \end{aligned} \quad (3.58)$$

The kinematics is incredibly constrained and there are many equivalent ways how to write Ω . Also many of the poles are equivalent, as it is evident from the figure, e.g. setting $\langle 12 \rangle = 0$ (erasing edge B) also sends $[34] = 0$ etc. The pole at infinity is again not present in the bare form – two factors of $\langle 35 \rangle \langle 57 \rangle$ are canceled by $\langle 17 \rangle^2$ in the numerator, and the

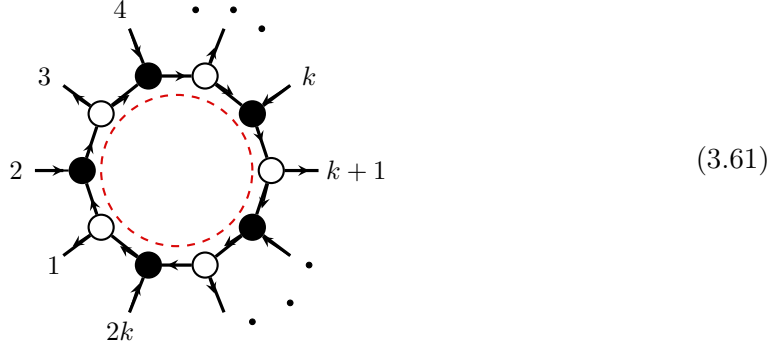
form is regular for (3.55). The UV pole is produced by the inverse Jacobian and the residue on the pole (3.55) gives

$$\Omega_{\text{UV}} = \frac{\langle 34 \rangle \delta(\Xi_a)}{\langle 12 \rangle \langle 23 \rangle \langle 47 \rangle [14]^4 [16] [18]} \quad (3.59)$$

where the delta functions are now denoted

$$\delta(\Xi_a) = \delta^4(P) \delta^6(\mathcal{Q}) \delta(\tilde{\eta}_4[18] + \tilde{\eta}_8[14]) \delta(\tilde{\eta}_4[16] + \tilde{\eta}_6[14]) \delta(\langle 13 \rangle) \delta(\langle 35 \rangle) \delta(\langle 57 \rangle) \delta([46]) \delta([28]) \quad (3.60)$$

which reproduces the on-shell function for the tree on-shell diagram (3.56). Now we are ready to generalize to arbitrary one-loop diagram. It is enough to solve the problem only for a “core diagram” which for $N^{k-2}\text{MHV}$ is a $2k$ -gon with k black and k white alternating vertices.



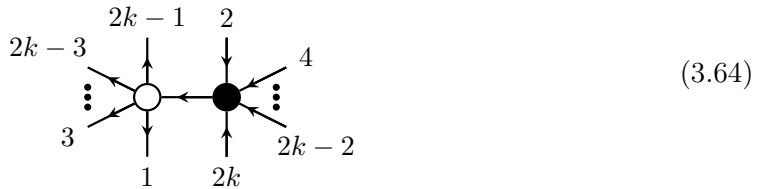
In this diagram $2k - 4$ conditions on external kinematics are imposed. We can characterize them by two cyclic classes

$$\langle j | p_{j+1} + p_{j+2} | j+3 \rangle = \langle j | p_{j-1} + p_{j-2} | j-3 \rangle = 0 \quad (3.62)$$

for all odd $j = 1, 3, \dots, 2k-1$. These are $2k$ conditions, 4 of them are redundant. The pole at infinity is approached by imposing $\langle pq \rangle = 0$ where p, q are attached to two different white vertices (alternatively $[cd] = 0$ where c, d are attached to black vertices). This completely collapses the kinematics into two sectors where all λ , resp. $\tilde{\lambda}$ are proportional,

$$\lambda_1 \sim \lambda_3 \sim \lambda_5 \sim \dots \sim \lambda_{2k-1}, \quad \tilde{\lambda}_2 \sim \tilde{\lambda}_4 \sim \tilde{\lambda}_6 \sim \dots \sim \tilde{\lambda}_{2k} \quad (3.63)$$

and the resulting on-shell diagram is



where all legs originally connected to $\overline{\text{MHV}}$ white vertices in (3.61) are now in the white vertex and all legs originally connected to MHV black vertices are now in the black vertex. For any other n -gon with chains of white and black vertices we can always use merge-expand

moves to identify the core polygon which contains the pole at infinity, and apply the same rule, i.e.

(3.65)

For an arbitrary one-loop on-shell diagram, such as the one above, the residue at infinity corresponds to a tree-level graph where all external legs initially attached to white vertices are now attached together in the same white vertex, and the same applies to black vertices,

(3.66)

and the external momenta are then divided into two sets: in the first set (attached to white vertex) all λ 's are proportional, in the other set (attached to black vertex) all $\tilde{\lambda}$'s are proportional. Note that the cyclic ordering of the original graph is not preserved: the legs connected to black or white vertices are not ordered in any particular way, but the overall canonical ordering is broken. Hence we refer to this operation as a *non-planar twist*. As a result, the residue on the UV pole of a planar on-shell diagram is a lower-loop non-planar on-shell diagram.

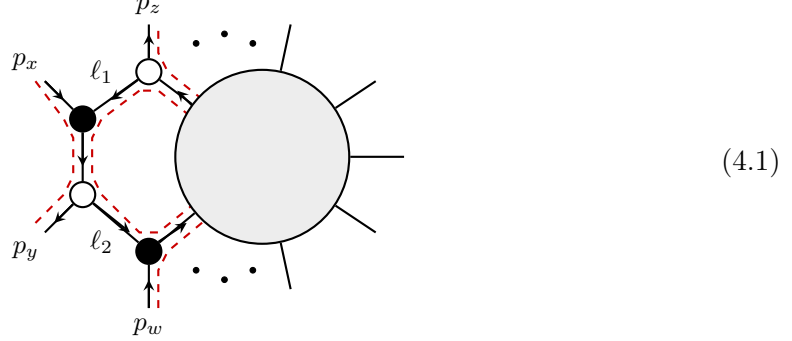
4 All planar diagrams

In the simple examples we discussed earlier, the UV pole was always localized in a one-loop subgraph. We will show that this is a general property of planar on-shell diagrams, and using the rules of the previous section we can then calculate poles at infinity for an arbitrary higher loop planar graph.

4.1 Localization of UV poles in planar diagrams

Let us consider a core n -gon one-loop subdiagram somewhere in the middle of a larger on-shell diagram. As discussed we can always put any one-loop subdiagram in this form by

merge-expand moves. Because the whole on-shell diagram is planar this n -gon is connected to any other one-loop subdiagram through a pair of adjacent legs. If the legs are not adjacent then the diagram is not planar and our proof does not apply.



where the central n -gon has a pole at infinity for $\langle zy \rangle = 0$ which is equivalent to $[xw] = 0$. This n -gon is glued into the rest of the diagram, so all momenta p_x, p_y, p_z, p_w are in general internal momenta. We want to prove that the UV pole does not propagate beyond this one-loop n -gon. In other words, external momenta p_x, p_y, p_z, p_w (from the point of view of the n -gon, otherwise these are internal momenta of the whole diagram) do not blow up for $\langle zy \rangle = [xw] = 0$. We label

$$p_x = \lambda_x \tilde{\lambda}_x, \quad p_y = \lambda_y \tilde{\lambda}_y, \quad p_z = \lambda_z \tilde{\lambda}_z, \quad p_w = \lambda_w \tilde{\lambda}_w \quad (4.2)$$

We focus on p_x, p_y but an analogous argument applies to other loops and we can also prove that p_z, p_w and other momenta attached to our n -gon. Using the kinematical properties of three point vertices we can write internal momenta ℓ_1, ℓ_2 in the following way,

$$\ell_1 = \frac{\alpha}{\langle zy \rangle} \lambda_z \tilde{\lambda}_x, \quad \ell_2 = \frac{\beta}{\langle zy \rangle} \lambda_y \tilde{\lambda}_w \quad (4.3)$$

where α, β are coefficients. We see that both ℓ_1, ℓ_2 blow up for $\langle zy \rangle = 0$ as expected. Note that α, β and spinors $\lambda_y, \lambda_z, \tilde{\lambda}_x, \tilde{\lambda}_w$ do not have a pole in $\langle zy \rangle = 0$. We need to prove that $\lambda_x, \tilde{\lambda}_y$ also do not have this pole, hence p_x, p_y are regular for $\langle zy \rangle = 0$. Using the momentum conservation

$$\ell_1 + p_x = \ell_2 + p_y \quad (4.4)$$

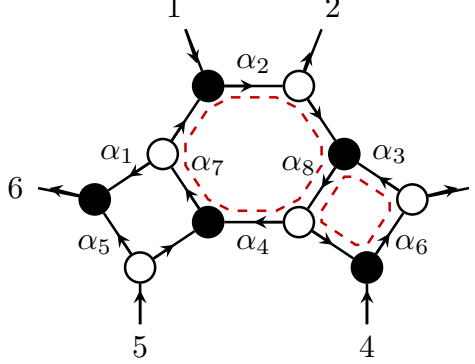
and the expressions (4.2), (4.3) we contract (4.4) with $\tilde{\lambda}_x$, resp. $\tilde{\lambda}_w$ and get

$$[xy] = -\frac{\beta[xw]}{\langle zy \rangle}, \quad \lambda_y[yw] = [xw]\lambda_x + \frac{\alpha[xw]}{\langle zy \rangle} \lambda_z \quad (4.5)$$

The ratio $[xw]/\langle zy \rangle$ is regular for $\langle zy \rangle = 0$ and has no pole. This means that both $[xy]$ and $[yw]$ are free of the UV pole, and hence also $\tilde{\lambda}_y$ and p_y are regular for $\langle zy \rangle = 0$. Very similarly, we can contract (4.4) with λ_y , resp. λ_z and conclude that $\langle xz \rangle$ and $\langle xy \rangle$ have no pole at infinity, hence also λ_x and p_x are free of this pole. This concludes the proof. We can use the same logic and prove that the UV pole $\langle zy \rangle = 0$ does not propagate to any other loop attached to our n -gon, hence this pole is only localized in this one-loop subgraph.

4.2 Three-loop example

We will demonstrate the procedure of calculating poles at infinity on several higher loop examples. First, we take a three-loop six-point NMHV leading singularity on-shell diagram and solve for the edge variables,



$$\begin{aligned}
 \alpha_1 &= -\frac{\langle 2|1+5|6\rangle}{\langle 2|5+6|1\rangle}, & \alpha_2 &= -\frac{\langle 2|5+6|1\rangle}{s_{156}}, \\
 \alpha_3 &= \frac{\langle 2|5+6|1\rangle}{\langle 3|5+6|1\rangle}, & \alpha_5 &= -\frac{\langle 2|1+5|6\rangle}{\langle 2|1+6|5\rangle}, \\
 \alpha_4 &= \frac{\langle 2|1+5|6\rangle\langle 3|5+6|1\rangle}{\langle 34\rangle[56]\langle 2|5+6|1\rangle}, \\
 \alpha_6 &= \frac{\langle 3|5+6|1\rangle}{\langle 4|5+6|1\rangle}, & \alpha_7 &= \frac{[56]}{[16]}, & \alpha_8 &= -\frac{\langle 34\rangle}{\langle 23\rangle}.
 \end{aligned} \tag{4.6}$$

In $\mathcal{N}=4$ SYM the on-shell function associated with this diagram is a famous R -invariant [63, 92] which appears in the context of tree-level recursion relations [92], leading singularities of loop integrands and Grassmannians [93–96], and coefficients of polylogs in the hexagon bootstrap [97–100],

$$\Omega = \int \frac{d\alpha_1 \dots d\alpha_8 \delta(C \cdot Z)}{\alpha_1 \alpha_2 \dots \alpha_8} = \frac{\delta^8(\mathcal{Q})\delta^4(P)\delta([56]\tilde{\eta}_1 + [61]\tilde{\eta}_5 + [15]\tilde{\eta}_6)}{s_{156}\langle 23\rangle\langle 34\rangle\langle 2|3+4|5\rangle\langle 4|5+6|1\rangle[16][56]} \equiv R[4, 5, 6, 1, 2] \tag{4.7}$$

Note that this expression does not depend on any helicity assignments because of the maximal supersymmetry. In the $\mathcal{N}=3$ SYM theory with the helicity assignment (4.6) we get

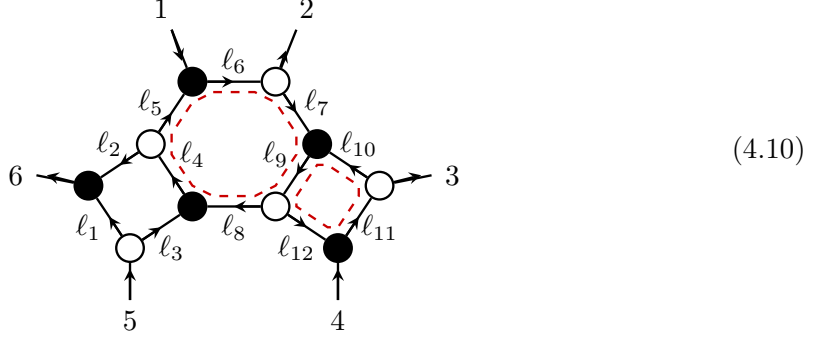
$$\Omega = \int \frac{d\alpha_1 d\alpha_2 \dots d\alpha_8 \delta(C \cdot Z)}{\underbrace{\alpha_1 \alpha_2 \alpha_3 \alpha_4 \alpha_5 \alpha_6 \alpha_7 \alpha_8}_{\Omega^{\text{bare}}}} \times \frac{1}{\underbrace{1 - \alpha_2 \alpha_4 \alpha_7 \alpha_8 - \alpha_3 \alpha_6 \alpha_8}_{\mathcal{J}^{-1}}}. \tag{4.8}$$

which evaluates to

$$\begin{aligned}
 \Omega &= \frac{\langle 4|1+5|6\rangle\delta^6(\mathcal{Q})\delta^4(P)\delta([56]\tilde{\eta}_1 + [61]\tilde{\eta}_5 + [15]\tilde{\eta}_6)}{\underbrace{s_{156}\langle 23\rangle\langle 34\rangle\langle 2|3+4|5\rangle\langle 4|5+6|1\rangle[16][56]}_{\Omega^{\text{bare}}}} \times \frac{s_{156}\langle 23\rangle\langle 4|5+6|1\rangle[16]}{\underbrace{\langle 2|5+6|1\rangle\langle 3|5+6|1\rangle\langle 4|1+5|6\rangle}_{\mathcal{J}^{-1}}} \\
 &= \frac{\delta^6(\mathcal{Q})\delta^4(P)\delta([56]\tilde{\eta}_1 + [61]\tilde{\eta}_5 + [15]\tilde{\eta}_6)}{\langle 34\rangle\langle 2|3+4|1\rangle\langle 3|5+6|1\rangle\langle 2|1+6|5\rangle[56]}
 \end{aligned} \tag{4.9}$$

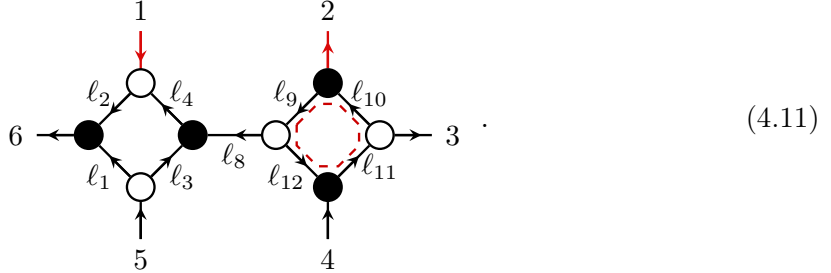
The inverse Jacobian adds two new poles $\langle 2|5+6|1\rangle$ and $\langle 3|5+6|1\rangle$ (the other term $\langle 4|1+5|6\rangle$ is just a helicity factor). These are UV poles and originate from closed cycles in (4.6). In order to see which UV pole corresponds to a hexagon and which one corresponds to a box,

we solve for the internal momenta (where we denoted $Q_{156} = p_1 + p_5 + p_6$ in all formulas),



$$\begin{aligned}
\ell_1 &= \frac{\langle 2|Q_{156}|5\rangle \tilde{\lambda}_6 \lambda_5}{\langle 2|Q_{156}|6\rangle}, & \ell_2 &= \frac{\tilde{\lambda}_6 (\lambda_2 \cdot Q_{34}) \cdot Q_{56}}{\langle 2|Q_{156}|6\rangle}, & \ell_3 &= \frac{[56] \lambda_5 (\lambda_2 \cdot Q_{34})}{\langle 2|Q_{156}|6\rangle} \\
\ell_4 &= \frac{[16] (\lambda_2 \cdot Q_{34}) \cdot Q_{56} (\lambda_2 \cdot Q_{34})}{\langle 2|Q_{156}|6\rangle \langle 2|Q_{156}|1\rangle}, & \ell_5 &= \frac{\tilde{\lambda}_1 (\lambda_2 \cdot Q_{34}) \cdot Q_{56}}{\langle 2|Q_{156}|1\rangle}, & \ell_6 &= \frac{s_{156}}{\langle 2|Q_{156}|1\rangle} \tilde{\lambda}_1 \lambda_2 \\
\ell_7 &= \frac{\lambda_2 (\tilde{\lambda}_1 \cdot Q_{56}) \cdot Q_{34}}{\langle 2|Q_{156}|1\rangle}, & \ell_8 &= \frac{(\lambda_2 \cdot Q_{34}) (\tilde{\lambda}_1 \cdot Q_{56})}{\langle 2|Q_{156}|1\rangle}, & \ell_9 &= \frac{\langle 23 \rangle (\tilde{\lambda}_1 \cdot Q_{56}) \cdot Q_{34} (\tilde{\lambda}_1 \cdot Q_{56})}{\langle 3|Q_{156}|1\rangle \langle 2|Q_{156}|1\rangle} \\
\ell_{10} &= \frac{\lambda_3 (\tilde{\lambda}_1 \cdot Q_{56}) \cdot Q_{34}}{\langle 3|Q_{156}|1\rangle}, & \ell_{11} &= \frac{\langle 4|Q_{156}|1\rangle \tilde{\lambda}_4 \lambda_3}{\langle 3|Q_{156}|1\rangle}, & \ell_{12} &= \frac{\langle 34 \rangle \tilde{\lambda}_4 (\tilde{\lambda}_1 \cdot Q_{56})}{\langle 3|Q_{156}|1\rangle}
\end{aligned}$$

Looking at the denominator of solved on-shell loop momenta we see that $\langle 2|Q_{156}|6\rangle = 0$ is the pole at infinity in the left box diagram, the pole at infinity in the hexagon is $\langle 2|Q_{156}|1\rangle = 0$, and the pole at infinity in the right box is $\langle 3|Q_{156}|1\rangle = 0$. The last two poles are accessible for this orientation as evident from the diagram (presence of both closed cycles) and the poles in the inverse Jacobian \mathcal{J}^{-1} , while the pole $\langle 2|1+5|6\rangle = 0$ can not be reached in this orientation. The inverse Jacobian also removes some of the irremovable edges. For example we can not remove α_2 edge (by sending $\alpha_2 \rightarrow \infty$) forcing $s_{156} = 0$ as it would lead to an illegal diagram,



where we violated the rules about incoming/outgoing legs in black/white vertex.

Going back to the diagram (4.10) we concentrate on the pole at infinity in the hexagon subdiagram. There are two kinematical constraints imposed on the external legs of this hexagon $p_1, p_2, \ell_2, \ell_3, \ell_{10}, \ell_{12}$, while in the context of the whole diagram the last four momenta are internal and the actual external momenta p_1, \dots, p_6 are unconstrained. Using the rules developed in the last section, the residue on the UV pole turns the hexagon into

a tree subdiagram,

$$(4.12)$$

Gluing back into the rest of the diagram we get,

$$(4.13)$$

where we used one particular way to expand the four-point black and white vertices. We can now treat it as a new on-shell diagram and assign edge variables, construct the C matrix and solve for them using delta functions

$$(4.14)$$

$$\alpha_1 = \frac{[56]}{[16]}, \alpha_2 = \frac{[15]}{[16]}, \alpha_3 = \frac{\langle 23 \rangle}{\langle 42 \rangle},$$

$$\alpha_4 = \frac{\langle 43 \rangle}{\langle 23 \rangle}, \alpha_5 = \frac{\langle 2|1+5|6]}{\langle 23 \rangle [16]},$$

$$\alpha_6 = \frac{\langle 3|5+6|1]}{\langle 23 \rangle [16]}, \alpha_7 = \frac{\langle 23 \rangle [16]}{\langle 3|1+5|6]}.$$

Note that in this diagram there is one extra kinematical condition imposed: $\langle 2|5+6|1] = 0$ which was exactly the hexagon UV pole in (4.10). The edge variables in (4.14) are not related in any obvious way with the edge variables in (4.13). Calculating the on-shell function for (4.14) we get

$$\Omega = \int \frac{d\alpha_1 \dots d\alpha_7 \delta(C \cdot Z)}{\alpha_1 \alpha_2 \alpha_3 \alpha_4 \alpha_5 \alpha_6 \alpha_7} \times \frac{1}{1 - \alpha_3 \alpha_4 \alpha_5 \alpha_7}$$

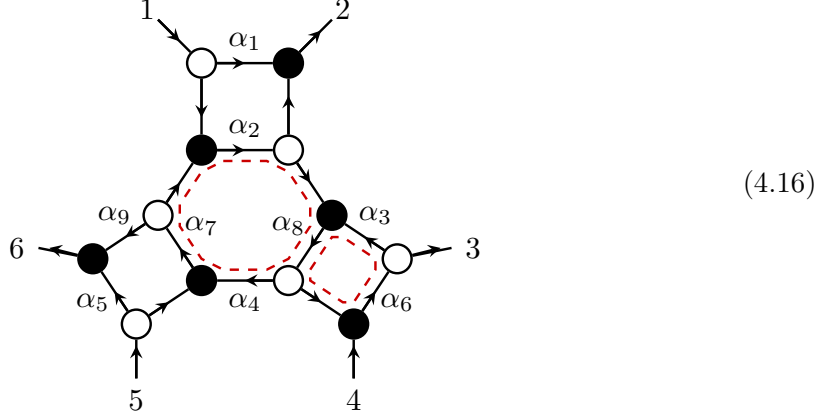
$$= \frac{\langle 4|1+5|6] \delta^4(P) \delta^6(Q) \delta([56] \tilde{\eta}_1 + [61] \tilde{\eta}_5 + [15] \tilde{\eta}_6) \delta(\langle 2|5+6|1])}{s_{156} \langle 24 \rangle \langle 34 \rangle \langle 3|1+5|6] [56] [15]} \times \frac{\langle 24 \rangle \langle 3|1+5|6]}{\langle 23 \rangle \langle 4|1+5|6]} \quad (4.15)$$

$$= \frac{\delta^4(P) \delta^6(Q) \delta([56] \tilde{\eta}_1 + [61] \tilde{\eta}_5 + [15] \tilde{\eta}_6) \delta(\langle 2|5+6|1])}{s_{156} \langle 23 \rangle \langle 34 \rangle [56] [15]}$$

which is the same as the residue of (4.9) on $\langle 2|5+6|1] = 0$ showing explicitly our procedure in action. Note that since we are on special kinematics, $s_{156} \langle 2q \rangle [1p] = \langle 2|1+5+6|p] \langle q|1+5+6|1]$ which is needed to show the equality.

4.3 Non-planarity from the UV pole

The pole at infinity does not preserve the planarity of the original on-shell diagram. We could already see it in our previous example where the original on-shell diagram (4.6) had a canonical ordering of external legs, while the on-shell diagrams we obtained as a result of the UV pole calculation had external legs ordered differently $123456 \rightarrow 134265$. In fact, this was just a special case of a more general phenomenon that the residue on a UV pole of a planar on-shell diagram is a *non-planar on-shell diagram*. Let us consider the following example,



which is an on-shell diagram for a top cell of $G_+(3, 6)$. This is a unique planar 9-dimensional (has 9 independent edge variables α_j) on-shell diagram and all other cells in $G_+(3, 6)$ are associated with descendants of this diagram where one or more edges are removed. See [26] for more details on the stratification. We can also obtain it by adding a BCFW bridge on external legs 1, 2 of the previous on-shell diagram (4.6) – which was an eight-dimensional leading singularity diagram (with no free parameters and generic kinematics). Hence in our diagram there is one unfixed parameter α_1 . The solution for the edge variables is

$$\begin{aligned} \alpha_2 &= -\frac{\langle \hat{2}|5+6|\hat{1} \rangle}{s_{\hat{1}56}}, & \alpha_3 &= \frac{\langle \hat{2}|5+6|\hat{1} \rangle}{\langle 3|5+6|\hat{1} \rangle}, & \alpha_4 &= -\frac{\langle 34 \rangle [56] \langle \hat{2}|5+6|\hat{1} \rangle}{\langle \hat{2}|3+4|6 \rangle \langle 3|5+6|\hat{1} \rangle} \\ \alpha_5 &= -\frac{\langle \hat{2}|3+4|5 \rangle}{\langle \hat{2}|3+4|6 \rangle}, & \alpha_6 &= \frac{\langle 4|5+6|\hat{1} \rangle}{\langle 3|5+6|\hat{1} \rangle}, & \alpha_7 &= \frac{[\hat{1}6]}{[56]}, & \alpha_8 &= -\frac{\langle \hat{2}3 \rangle}{\langle 34 \rangle}, & \alpha_9 &= \frac{\langle \hat{2}|5+6|\hat{1} \rangle}{\langle \hat{2}|3+4|6 \rangle}. \end{aligned} \quad (4.17)$$

where we denoted $\hat{\lambda}_1 = \tilde{\lambda}_1 + \alpha_1 \tilde{\lambda}_2$ and $\hat{\lambda}_2 = \lambda_2 - \alpha_1 \lambda_1$. The on-shell function is

$$\Omega = \int \frac{d\alpha_1 \dots d\alpha_9 \delta(C \cdot \mathcal{Z})}{\alpha_1 \alpha_2 \alpha_3 \alpha_4 \alpha_5 \alpha_6 \alpha_7 \alpha_8 \alpha_9} \times \frac{1}{1 - \alpha_2 \alpha_4 \alpha_7 \alpha_8 - \alpha_3 \alpha_6 \alpha_8} \quad (4.18)$$

Plugging in the edge variables we get,

$$\Omega = \int \underbrace{\frac{d\alpha_1 \langle 4|\hat{1}+5|6 \rangle \delta(\Xi)}{\alpha_1 s_{\hat{1}56} \langle \hat{2}3 \rangle \langle 34 \rangle \langle \hat{2}|3+4|5 \rangle \langle 4|5+6|\hat{1} \rangle [\hat{1}6] [56]}}_{\Omega^{\text{bare}}} \underbrace{\frac{s_{\hat{1}56} \langle \hat{2}3 \rangle \langle 4|5+6|\hat{1} \rangle [\hat{1}6]}{\langle \hat{2}|5+6|\hat{1} \rangle \langle 3|5+6|\hat{1} \rangle (\langle 4|\hat{1}+5|6 \rangle)}}_{\mathcal{J}^{-1}} \quad (4.19)$$

$$= \int \frac{d\alpha_1 \delta(\Xi)}{\alpha_1 \langle 34 \rangle \langle \hat{2}|5+6|\hat{1} \rangle \langle 3|5+6|\hat{1} \rangle \langle \hat{2}|3+4|5 \rangle [56]}, \quad (4.20)$$

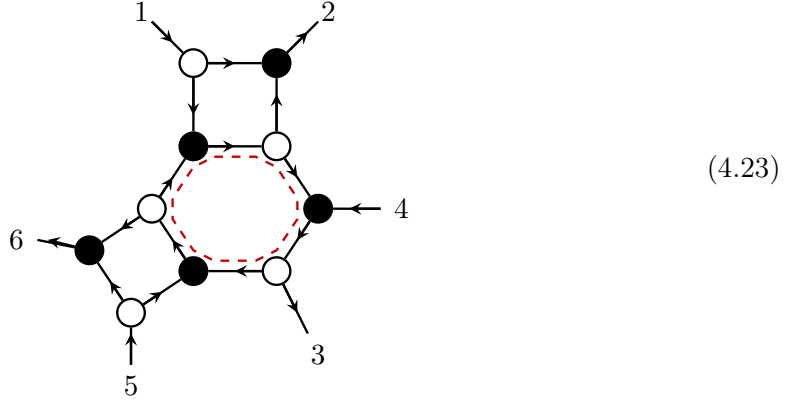
where the delta function

$$\delta(\Xi) \equiv \delta^6(\mathcal{Q}) \delta^4(P) \delta([56]\tilde{\eta}_1 + \alpha_1[56]\tilde{\eta}_2 + [\hat{6}\hat{1}]\tilde{\eta}_5 + [\hat{1}5]\tilde{\eta}_6). \quad (4.21)$$

We can recognize the usual BCFW shift for $\tilde{\eta}_1$ in the super delta function. Note that the $\alpha_1 = 0$ pole erases a corresponding edge and we reproduce the diagram already encountered (4.6). In $\mathcal{N}=4$ SYM theory there are six erasable edges which do not impose constraints on external kinematics (poles in α_1 in the Ω^{bare}). They correspond to six co-dimension-1 (i.e. eight-dimensional) cells of $G_+(3,6)$ and their on-shell functions are the six R -invariants. For our orientation (4.16) in $\mathcal{N}<3$ SYM we have three IR poles and two UV poles from the inverse Jacobian. The UV pole in the box is accessed by $\langle 3|5+6|\hat{1}\rangle = 0$, the residue is

$$\text{Res}_{\alpha_1 = -\frac{\langle 3|5+6|1\rangle}{\langle 3|5+6|2\rangle}} [\Omega] = \frac{\delta^6(\mathcal{Q}) \delta^4(P) \delta([24]\tilde{\eta}_1 + [14]\tilde{\eta}_2 + [12]\tilde{\eta}_4)}{\langle 56\rangle[12]\langle 3|5+6|1\rangle\langle 3|1+2|4\rangle\langle 6|1+2|4\rangle} \quad (4.22)$$

Based on our diagrammatic rule this UV pole corresponds to an on-shell diagram,



Calculating the on-shell function we get

$$\begin{aligned} \Omega_{\text{UV}} &= \underbrace{\frac{\langle 5|1+4|2\rangle \delta^6(\mathcal{Q}) \delta^4(P) \delta([24]\tilde{\eta}_1 + [14]\tilde{\eta}_2 + [12]\tilde{\eta}_4)}{s_{124}\langle 35\rangle\langle 56\rangle\langle 3|2+4|1\rangle\langle 6|1+2|4\rangle[12][24]}}_{\Omega^{\text{bare}}} \times \underbrace{\frac{s_{124}\langle 35\rangle[24]}{\langle 3|1+2|4\rangle\langle 5|1+4|2\rangle}}_{\mathcal{J}^{-1}} \\ &= \frac{\delta^6(\mathcal{Q}) \delta^4(P) \delta([24]\tilde{\eta}_1 + [14]\tilde{\eta}_2 + [12]\tilde{\eta}_4)}{\langle 56\rangle[12]\langle 3|5+6|1\rangle\langle 3|1+2|4\rangle\langle 6|1+2|4\rangle} \end{aligned} \quad (4.24)$$

which agrees with (4.22). The UV pole in the hexagon subdiagram corresponds to $\langle \hat{2}|5+6|\hat{1}\rangle = 0$ which is a quadratic condition in α_1 ,

$$\langle 2|5+6|1\rangle - \alpha_1\langle 1|5+6|1\rangle + \alpha_1^2\langle 2|5+6|2\rangle + \alpha_1^2\langle 1|5+6|2\rangle = 0 \quad (4.25)$$

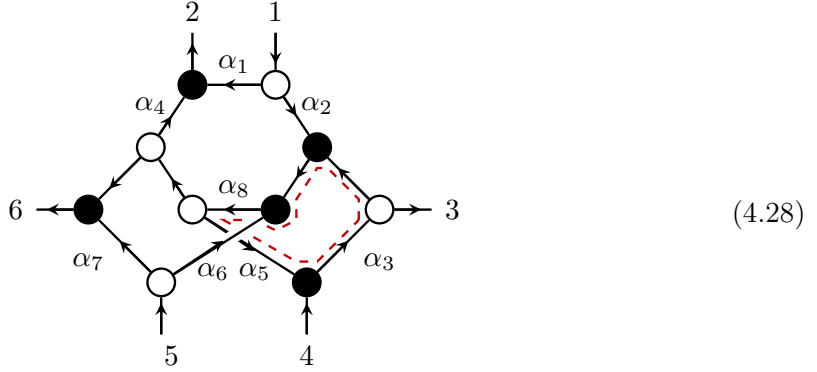
and leads to two solutions,

$$\alpha_1^\pm = \frac{(\langle 2|5+6|2\rangle - \langle 1|5+6|1\rangle) \pm \sqrt{(\langle 1|5+6|1\rangle + \langle 2|5+6|2\rangle)^2 - 4s_{12}s_{56}}}{2\langle 1|5+6|2\rangle}. \quad (4.26)$$

Plugging back into the form for the top cell (4.20) using $\langle \hat{2}|5+6|\hat{1}\rangle = \langle 1|5+6|2\rangle(\alpha_1 - \alpha_1^+)(\alpha_1 - \alpha_1^-)$, we get an on-shell function which contains square-roots of kinematical variables.

$$\Omega = \int \frac{d\alpha_1 \delta^6(\mathcal{Q}) \delta^4(P) \delta([56]\tilde{\eta}_1 + \alpha_1[56]\tilde{\eta}_2 + [6\hat{1}]\tilde{\eta}_5 + [\hat{1}5]\tilde{\eta}_6)}{\alpha_1 \langle 34 \rangle \langle 1|5+6|2\rangle (\alpha_1 - \alpha_1^+) (\alpha_1 - \alpha_1^-) (\langle 3|5+6|1\rangle + \alpha_1 \langle 3|5+6|2\rangle) (\langle 2|3+4|5\rangle - \alpha_1 \langle 1|3+4|5\rangle) [56]}. \quad (4.27)$$

The quadratic (or higher order) equation for a parameter we localize and the presence of roots is not something unusual. For example, it also happens for the four-mass-box leading singularity, and in general we get very complicated structures. The UV pole in (4.6) can be again calculated diagrammatically using our operation: replacing the hexagon with the tree diagram (3.40). But now, something new happens: as a result, we get a *non-planar on-shell diagram*



The expression for the on-shell diagram using edge variables is the same as in the planar case and we can evaluate

$$\Omega_{\text{UV}} = \pm \frac{\delta^6(\mathcal{Q}) \delta^4(P) \delta([56]\tilde{\eta}_1 + \alpha_1^\pm [56]\tilde{\eta}_2 + [6\hat{1}]\tilde{\eta}_5 + [\hat{1}5]\tilde{\eta}_6)}{\alpha_1^\pm \langle 34 \rangle \langle 1|5+6|2\rangle (\alpha_1^- - \alpha_1^+) s_{\hat{1}56} \langle \hat{2}3 \rangle [\hat{1}5] [56]} \quad (4.29)$$

where $\hat{1}$ and $\hat{2}$ are defined by the same convention as (4.17) and α_1^\pm is:

$$\alpha_1^\pm = \frac{(\langle 2|5+6|2\rangle - \langle 1|5+6|1\rangle) \pm \sqrt{(\langle 1|5+6|1\rangle + \langle 2|5+6|2\rangle)^2 - 4s_{12}s_{56}}}{2\langle 1|5+6|2\rangle}. \quad (4.30)$$

which agrees with the residue on either the plus or minus pole of (4.27). This six-point NMHV non-planar diagram corresponds to one of the eight dimensional cells in $G(3,6)$ (not the positive part). All these cells for $G(3,6)$ were classified in [33], and the subset of them relevant for BCFW recursion relations (for higher k and n) in [39].

4.4 UV poles and modified GRTs

One of the most important features of on-shell functions Ω for leading singularity on-shell diagrams is that they satisfy Global Residue Theorems (GRTs). The leading singularity on-shell diagram has a dimensionality $2n-4$ and the on-shell function has neither free parameters, nor are there any constraints imposed on external kinematics (other than momentum conservation). For the on-shell diagram of dimensionality $2n-3$, the on-shell function

(after solving for edge variables) has one free parameter z , i.e. $\Omega(z)$. We can write Cauchy's integral theorem for this function,

$$\oint dz \Omega(z) = 0. \quad (4.31)$$

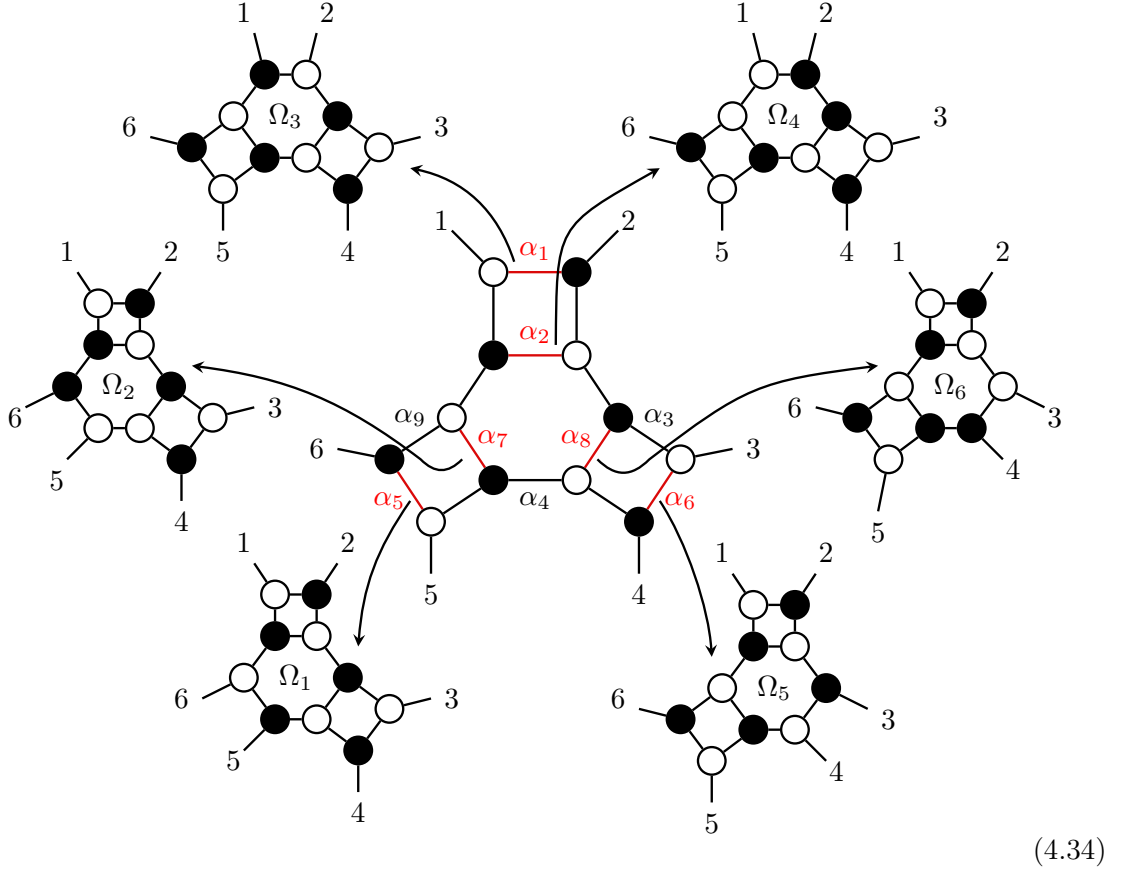
If the on-shell diagram has no pole at infinity, then all poles in z come from erasable edges and we can write

$$\text{GRT} = \sum_j \Omega_j = 0 \quad \text{where} \quad \Omega_j = \text{Res}_{z=z_j} \Omega(z) \quad (4.32)$$

Let us look at the most famous example which is our diagram (4.16). In $\mathcal{N}=4$ SYM theory the on-shell form is given by $\Omega = \Omega^{\text{bare}}$,

$$\Omega = \int \frac{d\alpha_1 \dots d\alpha_9 \delta(C \cdot Z)}{\alpha_1 \alpha_2 \dots \alpha_9} = \int \frac{d\alpha_1 \delta(\Xi)}{\alpha_1 s_{\widehat{1}56} \langle \widehat{2}3 \rangle \times 34 \times \widehat{2} | 3+4 | 5 \rangle \langle 4 | 5+6 | \widehat{1} \rangle [\widehat{1}6] [56]}. \quad (4.33)$$

There are six poles in this on-shell function corresponding to erasing edges $\alpha_1, \alpha_2, \alpha_5, \alpha_6, \alpha_7, \alpha_8$. Going to each of these six boundaries can be illustrated as follows,



where each arrow starts at the edge that is being erased, and all erasable edges are shown in red. This leads to the GRT in the form

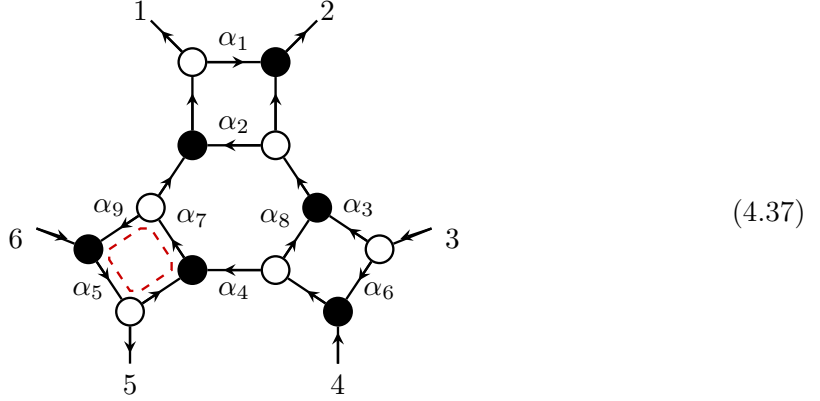
$$\sum_{i=1}^6 \Omega_i = 0, \quad \text{with} \quad \Omega_1 = \frac{\delta^4(P) \delta^8(\mathcal{Q}) \delta([34] \tilde{\eta}_5 + [45] \tilde{\eta}_3 + [53] \tilde{\eta}_4)}{s_{345} [34] [45] \langle 16 \rangle \times 12 \times \langle 2 | 3+4 | 5 \rangle \langle 6 | 1+2 | 3 \rangle} \quad (4.35)$$

where $\Omega_1 = R[23456]$ is a famous R -invariant, and all other Ω_j are related by cyclic shifts. The BCFW recursion relations for two different shifts represent the six-point NMHV tree-level as

$$\mathcal{A}_{6,3}^{\text{tree}} = \Omega_1 + \Omega_3 + \Omega_5 = -\Omega_2 - \Omega_4 - \Omega_6 \quad (4.36)$$

where the equality of two representations is guaranteed by the GRT (4.35). All these relations were crucial in the early discovery of momentum twistor polytopes [101, 102], on-shell diagrams and positive Grassmannians [26, 91, 93, 94] and later the Amplituhedron construction [40, 42].

For $\mathcal{N} < 4$ SYM the Global Residue Theorems change dramatically. The Jacobian removes some of the poles in $\Omega(z)$ but also adds poles at infinity. The on-shell functions associated with IR poles also change as they are corrected by the Jacobian. We work in the context of $\mathcal{N} = 3$ SYM theory and consider the same on-shell diagram for the top cell $G_+(3, 6)$. At first, we choose the orientation with one pole at infinity,



Solving for edge variables and plugging in the formula we get for the on-shell function,

$$\begin{aligned} \Omega &= \int \frac{d\alpha_1 \langle 34 \rangle [\hat{1}5] \delta(\Xi)}{\underbrace{\alpha_1 s_{\hat{1}56} \langle \hat{2}3 \rangle \times 34 \times \langle \hat{2} | 3+4 | 5 \rangle \langle 4 | 5+6 | \hat{1} \rangle [\hat{1}6] [56]}_{\Omega^{\text{bare}}}} \underbrace{\frac{\langle \hat{2} | 3+4 | 5 \rangle [\hat{1}6]}{\langle \hat{2} | 3+4 | 6 \rangle [\hat{1}5]}}_{\mathcal{J}^{-1}} \\ &= \int \frac{d\alpha_1 \delta(\Xi)}{\alpha_1 s_{\hat{1}56} \langle \hat{2}3 \rangle \times 4 | 5+6 | \hat{1} \rangle \langle \hat{2} | 3+4 | 6 \rangle [56]}, \end{aligned} \quad (4.38)$$

where, again, $\delta(\Xi) \equiv \delta^6(\mathcal{Q}) \delta^4(P) \delta([56] \tilde{\eta}_1 + \alpha_1 [56] \tilde{\eta}_2 + [6\hat{1}] \tilde{\eta}_5 + [\hat{1}5] \tilde{\eta}_6)$. Taking the residue on the UV pole $\alpha_1 = \frac{\langle \hat{2} | 3+4 | 6 \rangle}{\langle \hat{1} | 3+4 | 6 \rangle}$ one obtains

$$\Omega_{\text{UV}} = \frac{\delta^6(\mathcal{Q}) \delta^4(P) \delta([46] \tilde{\eta}_3 + [36] \tilde{\eta}_4 + [34] \tilde{\eta}_6)}{\langle 15 \rangle \times 12 \times \langle 2 | 3+4 | 6 \rangle \langle 5 | 2+4 | 3 \rangle [34] [46]}, \quad (4.39)$$

which matches the form obtained by collapsing the box into a tree as per the prescription. We can use this to define a modified global residue theorem (GRT):

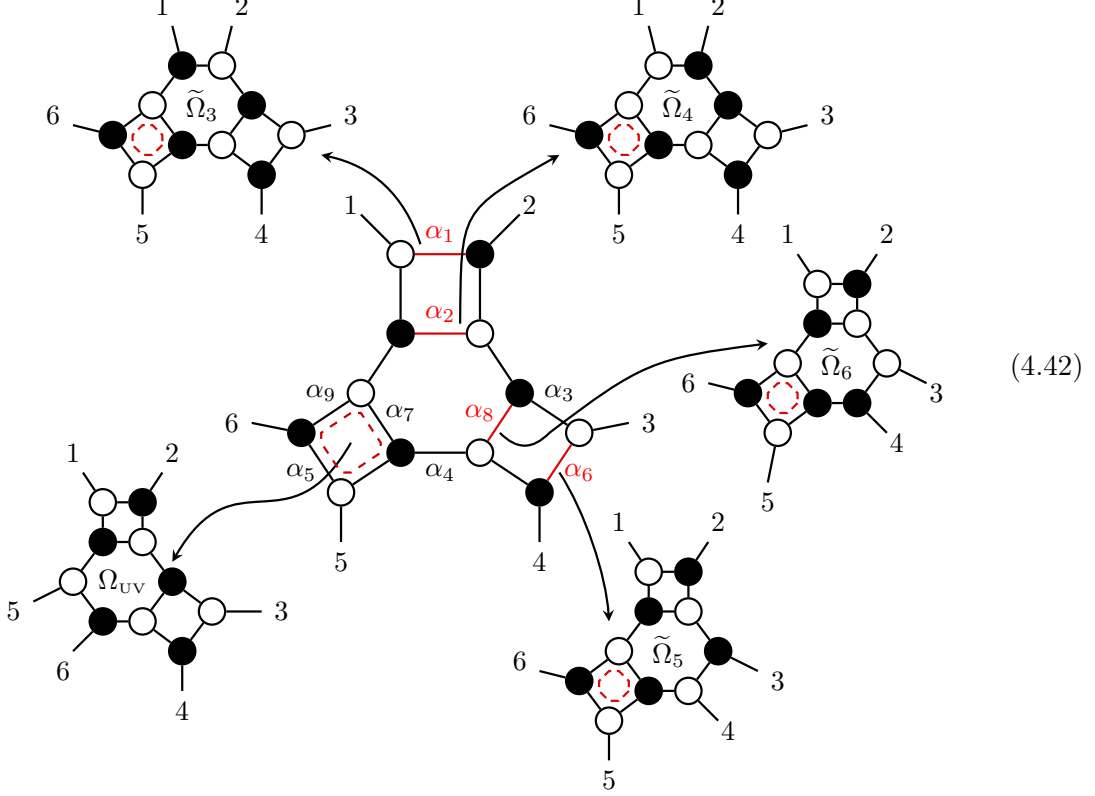
$$\text{GRT} = \tilde{\Omega}_3 + \tilde{\Omega}_4 + \tilde{\Omega}_5 + \tilde{\Omega}_6 + \Omega_{\text{UV}} = 0 \quad (4.40)$$

with the IR poles given by

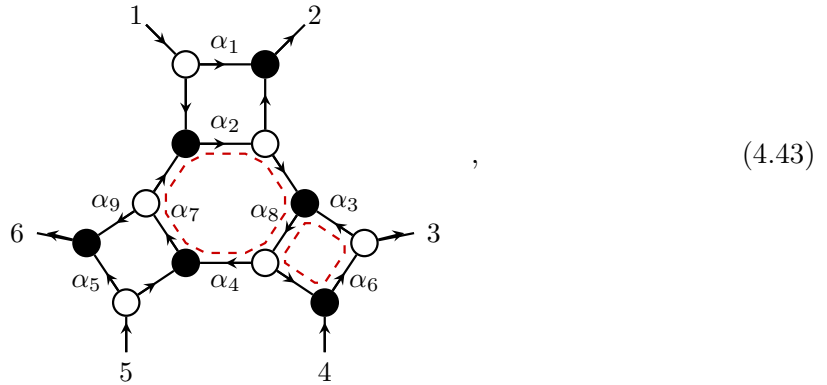
$$\tilde{\Omega}_3 = \frac{\delta^6(\mathcal{Q}) \delta^4(P) \delta([56] \tilde{\eta}_1 + [16] \tilde{\eta}_5 + [15] \tilde{\eta}_6)}{s_{156} \langle 23 \rangle \times 4 | 5+6 | 1 \rangle \langle 2 | 3+4 | 6 \rangle [56]}, \quad \tilde{\Omega}_4 = \frac{\delta^6(\mathcal{Q}) \delta^4(P) \delta([23] \tilde{\eta}_2 + [24] \tilde{\eta}_3 + [23] \tilde{\eta}_4)}{s_{156} \langle 1 | 5+6 | 4 \rangle [23] [34] \langle 15 \rangle \times 56},$$

$$\tilde{\Omega}_5 = \frac{\delta^6(\mathcal{Q})\delta^4(P)\delta([23]\tilde{\eta}_1+[13]\tilde{\eta}_2+[12]\tilde{\eta}_3)}{s_{123}\langle 56\rangle\langle 5|1+2|3\rangle\langle 4|5+6|2\rangle[[13][12]]}, \quad \tilde{\Omega}_6 = \frac{\delta^6(\mathcal{Q})\delta^4(P)\delta([56]\tilde{\eta}_4+[46]\tilde{\eta}_5+[45]\tilde{\eta}_6)}{s_{456}\langle 23\rangle\langle 12\rangle\langle 1|5+6|4\rangle[[56][46]]}. \quad (4.41)$$

We can illustrate the GRT as before,



where each arrow starts at the edge that is being erased, and all erasable edges are shown in red, while the accesible UV pole is shown using the dashed internal cycle. Notice, how α_5 and α_7 now no longer are removable compared to the normal GRT in (4.34). Also note that the on-shell functions $\tilde{\Omega}$ contain Jacobians from the internal cycle in the box. This is a new type of GRT that relates the on-shell function for the UV pole to IR poles. Note that in this case all diagrams are planar, but the on-shell diagram for the UV pole does not respect the original canonical ordering with $5 \leftrightarrow 6$. Now we consider a more complicated case of the same diagram with the orientation discussed in the previous subsection,



where the pole at infinity in the hexagon subdiagram is also accessible. In that case the Jacobian removes the IR poles for edges $\alpha_2, \alpha_6, \alpha_7, \alpha_8$ leaving only two IR poles $\alpha_5 = \langle \hat{2}|3+4|5 \rangle = 0$ and $\alpha_1 = 0$. On the other hand we add 3 UV poles – a pair of poles from the hexagon loop for $\langle \hat{2}|5+6|\hat{1} \rangle = 0$ and one UV pole from the right box subdiagram $\langle 3|5+6|\hat{1} \rangle = 0$ as before. The global residue theorem in this case can be written as

$$\text{GRT} = \tilde{\Omega}_1 + \tilde{\Omega}_3 + \Omega_{UV_1}^+ + \Omega_{UV_1}^- + \Omega_{UV_2} = 0 \quad (4.44)$$

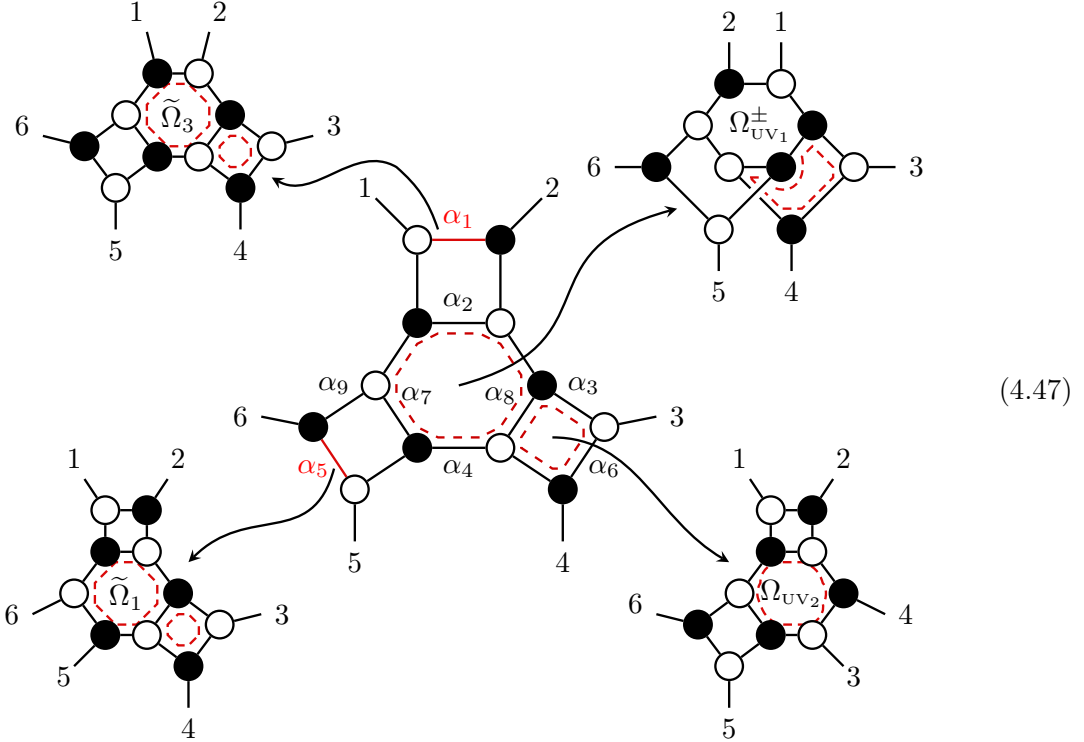
where

$$\begin{aligned} \tilde{\Omega}_1 &= \frac{\delta^4(P)\delta^6(Q)\delta([45]\tilde{\eta}_3 + [35]\tilde{\eta}_4 + [34]\tilde{\eta}_5)}{[34]\langle 12 \rangle \langle 6|3+5|4 \rangle \langle 2|3+4|5 \rangle \langle 6|3+4|5 \rangle}, \quad \tilde{\Omega}_3 = \frac{\delta^6(Q)\delta^4(P)\delta([56]\tilde{\eta}_1 + [61]\tilde{\eta}_5 + [15]\tilde{\eta}_6)}{\langle 34 \rangle \langle 2|5+6|1 \rangle \langle 3|5+6|1 \rangle \langle 2|1+6|5 \rangle [56]} \\ \Omega_{UV_1}^\pm &= \pm \frac{\delta^6(Q)\delta^4(P)\delta([56]\tilde{\eta}_1 + \alpha_1^\pm [56]\tilde{\eta}_2 + [6\hat{1}]\tilde{\eta}_5 + [\hat{1}5]\tilde{\eta}_6)}{\langle 1|5+6|2 \rangle (\alpha_1^- - \alpha_1^+) s_{\hat{1}56} \langle \hat{2}3 \rangle \langle 34 \rangle [56] [\hat{1}5] \alpha_1^\pm} \\ \Omega_{UV_2} &= \frac{\delta^6(Q)\delta^4(P)\delta([24]\tilde{\eta}_1 + [14]\tilde{\eta}_2 + [12]\tilde{\eta}_4)}{\langle 56 \rangle [12] \langle 3|5+6|1 \rangle \langle 3|1+2|4 \rangle \langle 6|1+2|4 \rangle}, \end{aligned} \quad (4.45)$$

with

$$\alpha_1^\pm = \frac{(\langle 2|5+6|2 \rangle + \langle 1|5+6|1 \rangle) \pm \sqrt{(\langle 1|5+6|1 \rangle + \langle 2|5+6|2 \rangle)^2 - 4s_{12}s_{56}}}{2\langle 1|5+6|2 \rangle}. \quad (4.46)$$

This is a new type of residue theorem for on-shell functions for two IR poles (modified R -invariants) and two UV poles – one is a planar R -invariant for a different ordering and the other is a pair of non-planar on-shell functions. Note that while each on-shell function $\Omega_{UV_1}^\pm$ contains square-roots, they do cancel in the sum as evident from the GRT (4.44). Once again we can illustrate the GRT in this case,



from which it is clear that the only two removable edges left are α_5 and α_1 .

In $\mathcal{N}=4$ SYM theory we do not have any poles at infinity whatsoever, so we can never generate non-planar diagrams from planar diagrams. However, even in $\mathcal{N}=4$ SYM theory we can just directly consider non-planar on-shell diagrams, but with no orientations and internal cycles. The on-shell functions in $\mathcal{N}=4$ SYM for the same diagrams are then

$$4 = \frac{\delta^4(P)\delta^8(\mathcal{Q})\delta([24]\tilde{\eta}_1 + [14]\tilde{\eta}_2 + [12]\tilde{\eta}_4)}{s_{124}\langle 35\rangle\langle 56\rangle\langle 3|5+6|1]\langle 6|1+2|4][12][24]} \quad (4.48)$$

$$3 = \pm \frac{\delta^4(P)\delta^8(\mathcal{Q})\delta([56]\tilde{\eta}_1 + \alpha_1^\pm[56]\tilde{\eta}_2 + [\hat{6}1]\tilde{\eta}_5 + [\hat{1}5]\tilde{\eta}_6)}{(\alpha_1^- - \alpha_1^+)s_{\hat{1}56}\langle \hat{2}4\rangle\langle 34\rangle\langle 1|5+6|2]\langle 3|\hat{1}+5|6][56][\hat{1}5]\alpha_1^\pm} \quad (4.49)$$

where the first on-shell function is just a regular R-invariant with $5 \leftrightarrow 6$ from canonical ordering, as also evident from the on-shell diagram. The on-shell function for the second, genuine non-planar, on-shell diagram is of a new type and is not related to an R-invariant as also evident from the presence of square-roots. It would be interesting to identify this form with the items in the list of appendix B of [33].

Having thoroughly gone through the procedure of taking UV poles of general n -gons and how to incorporate this into larger on-shell diagrams in $\mathcal{N}=3$ we are ready to tackle the higher order poles at infinity that arise in $\mathcal{N}<3$ in the next section.

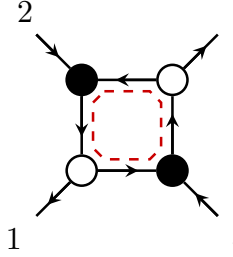
5 Higher order poles at infinity

So far we have studied the minimal version of the problem of UV poles in the context of $\mathcal{N}=3$ SYM theory where all poles at infinity are simple poles. We want to generalize it to gauge theories with lower supersymmetries, including pure Yang-Mills theory. As explained in previous sections, there are two parts of the story: (i) locations of poles at infinity and the kinematics of on-shell diagrams which are produced on these poles; and (ii) the actual residues at infinity, i.e. on-shell functions associated with on-shell diagrams. The first part

of the story is general and not specific to any theory, hence our discussion is valid for all relevant QFTs (with fundamental 3-point vertices) including gravity. The second part, the on-shell function, is specific to a particular theory and here, indeed, we solved only the case of $\mathcal{N} = 3$ SYM and need to find a generalization to other theories.

5.1 UV pole as a residue

Let us consider $\mathcal{N} = 2$ SYM theory, the case of general \mathcal{N} is just a trivial generalization. The main challenge is to figure out how to deal with higher poles at infinity which come from the inverse Jacobian \mathcal{J}^{-1} . For $\mathcal{N} = 2$ these are double poles. First, we redo the box on-shell diagram (3.1) and get



$$= \frac{\delta^4(P)\delta^4(Q)\langle 24 \rangle^2}{\langle 12 \rangle \langle 23 \rangle \langle 34 \rangle \langle 14 \rangle} \times \left(\frac{\langle 23 \rangle \langle 14 \rangle}{\langle 13 \rangle \langle 24 \rangle} \right)^2 = \frac{\langle 23 \rangle \langle 14 \rangle \delta^4(P)\delta^4(Q)}{\langle 12 \rangle \langle 34 \rangle \langle 13 \rangle^2} \quad (5.1)$$

where the supermomentum delta function has the same form, but now in η_i^I , $I = 1, 2$. Our goal is to calculate the residue on the UV pole $\langle 13 \rangle = 0$. Just based on the little group weights and the mass dimension, the resulting expression must be

$$\text{Res}_{\langle 13 \rangle = 0} \frac{\langle 23 \rangle \langle 14 \rangle \delta^4(P)\delta^4(Q)}{\langle 12 \rangle \langle 34 \rangle \langle 13 \rangle^2} \sim \frac{\langle 24 \rangle \delta^4(P)\delta^4(Q)\delta(\langle 13 \rangle)}{\langle 12 \rangle \langle 34 \rangle} \quad (5.2)$$

Note that on the support of $\langle 13 \rangle = 0$ we have a relation $\langle 12 \rangle \langle 34 \rangle = \langle 23 \rangle \langle 14 \rangle$. We want to derive this result by taking the residue of (5.1).

The first issue is to find a good parametrization that allows us to approach the pole in a nice way. One approach is to write $\langle 13 \rangle = \lambda_1^{(1)} \lambda_3^{(2)} - \lambda_1^{(2)} \lambda_3^{(1)}$, fix three of the components and then solve for the last one, e.g. $\lambda_3^{(2)}$, making sure that $\langle 13 \rangle = 0$. However, we need to have in mind that through momentum conservation this parameter also appears in other momenta, which makes this approach less clean. Therefore, it is simplest to shift the external kinematics, e.g. using a BCFW shift $\lambda_3 \rightarrow \lambda_3 + z\lambda_4$, $\tilde{\lambda}_4 \rightarrow \tilde{\lambda}_4 - z\tilde{\lambda}_3$, we get $\Omega(z)$ but with an extra $\delta(z)$ ensuring we preserve the same kinematics. Then we take a residue on $\langle 13 \rangle \rightarrow \langle 13 \rangle + z\langle 14 \rangle = 0$ using the formula (5.4),

$$\Omega_{\text{UV}} = \text{Res}_{z = -\frac{\langle 13 \rangle}{\langle 14 \rangle}} \frac{\langle 14 \rangle (\langle 23 \rangle + z\langle 24 \rangle) \delta^4(P)\delta^4(Q)\delta(z)}{\langle 12 \rangle \langle 34 \rangle (\langle 13 \rangle + z\langle 14 \rangle)^2} = \frac{\langle 24 \rangle \delta^4(P)\delta^4(Q)\delta(\langle 13 \rangle)}{\langle 12 \rangle \langle 34 \rangle} \quad (5.3)$$

where we used $\delta\left(-\frac{\langle 13 \rangle}{\langle 14 \rangle}\right) = -\frac{\delta(\langle 13 \rangle)}{\langle 14 \rangle}$ and for the calculation of the residue on the higher pole we used the definition

$$\text{Res}_{x=x_0} f(x) = \frac{1}{(m-1)!} \lim_{x \rightarrow x_0} \frac{d^{m-1}}{dx^{m-1}} ((x-x_0)^m f(x)) \quad (5.4)$$

Same result is obtained using the shift $\lambda_3 \rightarrow \lambda_3 + z\lambda_2$, $\tilde{\lambda}_2 \rightarrow \tilde{\lambda}_2 - z\tilde{\lambda}_3$,

$$\Omega_{UV} = \text{Res}_{z=-\frac{\langle 13 \rangle}{\langle 12 \rangle}} \frac{\langle 14 \rangle \langle 23 \rangle \delta^4(P) \delta^4(Q) \delta(z)}{\langle 12 \rangle (\langle 34 \rangle + z \langle 24 \rangle) (\langle 13 \rangle + z \langle 12 \rangle)^2} = \frac{\langle 24 \rangle \delta^4(P) \delta^4(Q) \delta(\langle 13 \rangle)}{\langle 23 \rangle \langle 14 \rangle} \quad (5.5)$$

which is the same as (5.3) using $\langle 12 \rangle \langle 34 \rangle = \langle 14 \rangle \langle 23 \rangle$ on the support of $\delta(\langle 13 \rangle)$. We can show that the result is independent of the shift. For general $\mathcal{N} < 4$ we can repeat the same exercise and get,

$$\Omega_{UV} = \frac{\langle 24 \rangle^{3-\mathcal{N}} \delta^4(P) \delta^{2\mathcal{N}}(Q) \delta(\langle 13 \rangle)}{\langle 12 \rangle \langle 34 \rangle} \quad (5.6)$$

Note that m-shell function for the on-shell diagram (3.6) with additional helicity factor for $\mathcal{N} < 3$ supersymmetry. Therefore, our diagrammatic rule works perfectly here for any \mathcal{N} for this case. Let us look at the double box on-shell diagram in $\mathcal{N} = 2$ SYM,

$$= \int dz \frac{\langle 24 \rangle^2 \delta^4(P) \delta^4(Q)}{z(\langle 23 \rangle + z \langle 24 \rangle) \langle 14 \rangle \langle 34 \rangle \langle 12 \rangle} \times \left(\frac{\langle 14 \rangle (\langle 23 \rangle + z \langle 24 \rangle)}{\langle 24 \rangle (\langle 13 \rangle + z \langle 14 \rangle)} \right)^2$$

$$= \int dz \frac{\langle 14 \rangle (\langle 23 \rangle + z \langle 24 \rangle) \delta^4(P) \delta^4(Q)}{z \langle 12 \rangle \langle 34 \rangle (\langle 13 \rangle + z \langle 14 \rangle)^2}$$

(5.7)

This on-shell diagram has only two poles: IR pole for $z = 0$ (deleting the far right edge) and the double UV pole which blows up the left loop. The residue on the IR pole is

$$\Omega_{IR} = \text{Res}_{z=0} \Omega(z) = \frac{\delta^4(P) \delta^4(Q) \langle 14 \rangle \langle 23 \rangle}{\langle 12 \rangle \langle 34 \rangle \langle 13 \rangle^2} \quad (5.8)$$

which is a box with an internal loop (5.1) as expected. The residue on the UV pole is

$$\Omega_{UV} = \text{Res}_{z=-\frac{\langle 13 \rangle}{\langle 14 \rangle}} \Omega(z) = -\frac{\delta^4(P) \delta^4(Q) \langle 14 \rangle \langle 23 \rangle}{\langle 12 \rangle \langle 34 \rangle \langle 13 \rangle^2} \quad (5.9)$$

and the sum $\Omega_{IR} + \Omega_{UV} = 0$ as dictated by the GRT for Ω . Note that the on-shell diagram associated with the UV pole (based on our rule) should be just a box without an internal loop and an ordering (1342). However, the on-shell function obtained in (5.9) is not an on-shell function for this diagram,

(5.10)

But rather, is its given by

$$\Omega_{UV} = \underbrace{\frac{\langle 24 \rangle^2 \delta^4(P) \delta^4(Q)}{\langle 13 \rangle \langle 34 \rangle \langle 42 \rangle \langle 21 \rangle}}_{\Omega_D} \times \underbrace{\frac{\langle 14 \rangle \langle 23 \rangle}{\langle 13 \rangle \langle 24 \rangle}}_{\mathcal{K}} \quad (5.11)$$

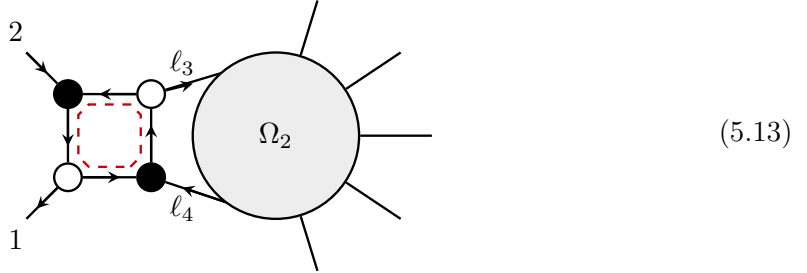
where Ω_D is the on-shell function associated with the diagram and \mathcal{K} is some prefactor. This formula generalizes to arbitrary \mathcal{N} ,

$$\Omega_{UV} = \frac{\delta^4(P)\delta^{2\mathcal{N}}(\mathcal{Q})\langle 24 \rangle^{4-\mathcal{N}}}{\langle 13 \rangle \langle 34 \rangle \langle 42 \rangle \langle 21 \rangle} \times \left(\frac{\langle 14 \rangle \langle 23 \rangle}{\langle 13 \rangle \langle 24 \rangle} \right)^{3-\mathcal{N}} = \frac{(\langle 14 \rangle \langle 23 \rangle)^{3-\mathcal{N}} \delta^4(P) \delta^{2\mathcal{N}}(\mathcal{Q})}{\langle 13 \rangle^{4-\mathcal{N}} \langle 34 \rangle \langle 42 \rangle \langle 21 \rangle} \quad (5.12)$$

We can see that the situation is not as simple as in the $\mathcal{N}=3$ SYM case, the on-shell function is now corrected by some prefactor. This prefactor does not add any new poles, it only increases the degree of some of the poles. We will see shortly that it is generated by a derivative operator acting on this on-shell diagram.

5.2 Infinity operator

To start with, let us consider a generalization of the two-loop double box on-shell diagram,



where the one-loop box on-shell diagram with an internal loop is glued to an arbitrary other on-shell diagram through two on-shell internal legs ℓ_3, ℓ_4 . The on-shell function for the diagram for $\mathcal{N} = 2$ SYM can be then written as

$$\Omega = \int d^2 \tilde{\eta}_{\ell_3} d^2 \tilde{\eta}_{\ell_4} \int \frac{d^2 \lambda_{\ell_3} d^2 \tilde{\lambda}_{\ell_3}}{\text{GL}(1)} \int \frac{d^2 \lambda_{\ell_4} d^2 \tilde{\lambda}_{\ell_4}}{\text{GL}(1)} \{ \Omega_1 \times \Omega_2 \} \quad (5.14)$$

The on-shell functions for left and right parts of the diagram are:

$$\Omega_1 = \frac{\langle 2\ell_4 \rangle^2 \delta^4(P_1) \delta^4(Q_1)}{\langle 12 \rangle \langle 2\ell_3 \rangle \langle \ell_3 \ell_4 \rangle \langle \ell_4 1 \rangle} \left(\frac{\langle 1\ell_4 \rangle \langle 2\ell_3 \rangle}{\langle 2\ell_4 \rangle \langle 1\ell_3 \rangle} \right)^2 = \frac{\langle 2\ell_3 \rangle \langle 1\ell_4 \rangle \delta^4(P_1) \delta^4(Q_1)}{\langle 12 \rangle \langle \ell_3 \ell_4 \rangle \langle 1\ell_3 \rangle^2} \quad (5.15)$$

$$\Omega_2 = \delta^4(P_2) \delta^4(Q_2) \omega_2 \quad (5.16)$$

where P_1, P_2 are momentum conservation and Q_1, Q_2 are supermomentum conservation for each part of the diagram. ω_2 for the right part of the diagram is arbitrary, and while it can contain additional delta functions or extra parameters, it does not depend on legs 1, 2 (only through ℓ_3, ℓ_4). Now we want to calculate the residue on the pole at infinity $\langle 1\ell_3 \rangle = 0$ of the box diagram. In order to do that we have to take λ_{ℓ_3} to be collinear with λ_1 . However, due to momentum conservation any changes in λ_{ℓ_3} also propagate into other momenta, and it is relevant when we calculate the derivative of the function in (5.4). We can remove this dependence by integrating over ℓ_4 , then ℓ_3 becomes independent,

$$\Omega = \int d^2 \tilde{\eta}_{\ell_3} \int \frac{d^2 \lambda_{\ell_3} d^2 \tilde{\lambda}_{\ell_3}}{\text{GL}(1)} \left\{ \frac{\langle 12 \rangle}{\langle 1\ell_3 \rangle^2} \times \underbrace{\int d^2 \tilde{\eta}_{\ell_4} \int \frac{d^2 \lambda_{\ell_4} d^2 \tilde{\lambda}_{\ell_4}}{\text{GL}(1)} \frac{\langle 2\ell_3 \rangle \langle 1\ell_4 \rangle \delta^4(P_1) \delta^4(Q_1)}{\langle 12 \rangle^2 \langle \ell_3 \ell_4 \rangle}}_{\omega} \times \Omega_2 \right\} \quad (5.17)$$

where we defined an on-shell function ω which automatically implements the momentum conservation between ℓ_3 , ℓ_4 and external legs, and the momentum ℓ_3 is now independent and not subject to any constraints. In this form we can take a residue on the pole $\langle 1\ell_3 \rangle = 0$. In order to approach the pole we parametrize

$$\lambda_{\ell_3} = \alpha\lambda_1 + \beta\lambda_2 \quad (5.18)$$

and rewrite

$$\Omega = \int d^2\tilde{\eta}_{\ell_3} \int \frac{d\alpha d\beta d^2\tilde{\lambda}_{\ell_3}}{\text{GL}(1)} \left\{ \frac{1}{\beta^2} \times \omega \right\} \quad (5.19)$$

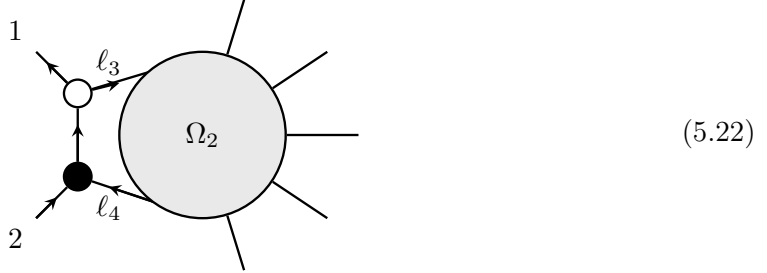
The UV pole is then given by the residue on $\beta = 0$,

$$\Omega_{\text{UV}} = \int d^2\tilde{\eta}_{\ell_3} \int \frac{d\alpha d^2\tilde{\lambda}_{\ell_3}}{\text{GL}(1)} \left\{ \frac{d\omega}{d\beta} \Big|_{\beta=0} \right\} \quad (5.20)$$

We can also undo the parametrization (5.18) and rewrite the result in a more invariant way,

$$\Omega_{\text{UV}} = \int d^2\tilde{\eta}_{\ell_3} \int \frac{d^2\lambda_{\ell_3} d^2\tilde{\lambda}_{\ell_3}}{\text{GL}(1)} \left\{ \delta(\langle 1\ell_3 \rangle) \left\langle \lambda_2 \frac{d\omega}{d\lambda_{\ell_3}} \right\rangle \right\} \quad (5.21)$$

In the angle bracket we take the derivative of ω with respect to λ_{ℓ_3} and then contract with λ_2 . This is the on-shell function associated with the pole at infinity in (5.13). Now we need to compare (5.21) with the on-shell diagram for the collapsed box diagram,



The on-shell function for this diagram is

$$\Omega_{\text{UV}}^{\text{bare}} = \int d^2\tilde{\eta}_{\ell_3} \int \frac{d^2\lambda_{\ell_3} d^2\tilde{\lambda}_{\ell_3}}{\text{GL}(1)} \left\{ \delta(\langle 1\ell_3 \rangle) \underbrace{\int d^2\tilde{\eta}_{\ell_4} \int \frac{d^2\lambda_{\ell_4} d^2\tilde{\lambda}_{\ell_4}}{\text{GL}(1)} \frac{\langle 2\ell_4 \rangle \delta^4(P_1) \delta^4(Q_1)}{\langle 12 \rangle \langle \ell_3 \ell_4 \rangle}}_{\omega^{\text{bare}}} \times \Omega_2 \right\} \quad (5.23)$$

where we again eliminated ℓ_4 . Comparing (5.21) and (5.23) we find the relation

$$\left\langle \lambda_2 \frac{d\omega}{d\lambda_{\ell_3}} \right\rangle = \frac{\langle 2\ell_3 \rangle [2\ell_3]}{\langle 12 \rangle [1\ell_3]} \left\langle \lambda_2 \frac{d\omega^{\text{bare}}}{d\lambda_{\ell_3}} \right\rangle \quad (5.24)$$

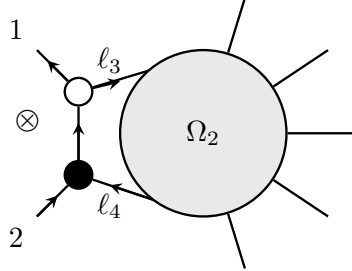
Plugging back we get

$$\Omega_{\text{UV}} = \int d^2\tilde{\eta}_{\ell_3} \int \frac{d^2\lambda_{\ell_3} d^2\tilde{\lambda}_{\ell_3}}{\text{GL}(1)} \left\{ \delta(\langle 1\ell_3 \rangle) \frac{\langle 2\ell_3 \rangle [2\ell_3]}{\langle 12 \rangle [1\ell_3]} \left\langle \lambda_2 \frac{d\omega^{\text{bare}}}{d\lambda_{\ell_3}} \right\rangle \right\} \quad (5.25)$$

We can then interpret the result in the following way: the pole at infinity of the original on-shell diagram (5.13) for $\mathcal{N} = 2$ SYM is equal to the “infinity operator”

$$\mathcal{O} = \frac{\langle 2\ell_3 \rangle [2\ell_3]}{\langle 12 \rangle [1\ell_3]} \left\langle \lambda_2 \frac{d}{d\lambda_{\ell_3}} \right\rangle \quad (5.26)$$

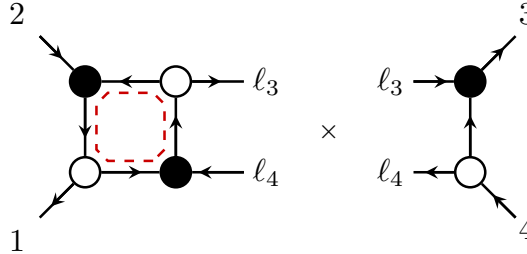
acting on the bare on-shell function

$$\Omega_{\text{UV}} = \frac{\langle 2\ell_3 \rangle [2\ell_3]}{\langle 12 \rangle [1\ell_3]} \left\langle \lambda_2 \frac{d}{d\lambda_{\ell_3}} \right\rangle \otimes \Omega_2 \quad (5.27)$$


or, more schematically $\Omega_{\text{UV}} = \mathcal{O} \otimes \Omega_{\text{UV}}^{\text{bare}}$ in the sense of the formulas (5.23) and (5.24). Note that for $\mathcal{N} = 3$ SYM the operator $\mathcal{O} = \mathbb{I}$ and the residue of Ω on the pole at infinity is equal to $\Omega_{\text{UV}} = \Omega_{\text{UV}}^{\text{bare}}$. This relation is very easy to generalize for arbitrary $\mathcal{N} < 4$. In that case the operator \mathcal{O} is given by

$$\mathcal{O}^{\mathcal{N}} = \frac{1}{(3-\mathcal{N})!} \left(\frac{\langle 2\ell_3 \rangle [2\ell_3]}{\langle 12 \rangle [1\ell_3]} \left\langle \lambda_2 \frac{d}{d\lambda_{\ell_3}} \right\rangle \right)^{3-\mathcal{N}} \quad (5.28)$$

Note that the derivative commutes with the prefactor. As an example of our procedure, we look at the double box on-shell diagram studied in the previous section. We interpret the diagram in the context of (5.13) as a one-loop box with legs 1, 2, ℓ_3 , ℓ_4 glued to the tree-level diagram with legs 3, 4, ℓ_3 , ℓ_4 ,



$$\quad (5.29)$$

The on-shell function Ω_2 is now

$$\Omega_2 = \frac{\langle \ell_3 4 \rangle^2 \delta^4(P_2) \delta^4(Q_2) \delta(\langle 4\ell_4 \rangle)}{\langle \ell_3 3 \rangle \langle 3 4 \rangle \langle \ell_3 \ell_4 \rangle} = \frac{\langle \ell_3 4 \rangle [3\ell_4] \delta^4(P_2) \delta^4(Q_2) \delta([3\ell_3])}{\langle \ell_3 3 \rangle \langle 3 4 \rangle \langle \ell_3 \ell_4 \rangle} \quad (5.30)$$

where we rewrote the delta function on the support of the momentum conservation,

$$\delta(\langle 4\ell_4 \rangle) = [\ell_4 3] \delta(\langle 4|\ell_4|3 \rangle) = -[\ell_4 3] \delta(\langle 4|\ell_3|3 \rangle) = \frac{[3\ell_4]}{\langle \ell_3 4 \rangle} \delta([3\ell_3]) \quad (5.31)$$

where the function ω , further integrated over $\tilde{\eta}_{\ell_3}$ and $\tilde{\lambda}_{\ell_3}$ for simplicity (this does not interfere with λ_{ℓ_3} derivative) is equal to

$$\int d^2 \tilde{\eta}_{\ell_3} \int \frac{d^2 \tilde{\lambda}_{\ell_3}}{\text{GL}(1)} \omega =$$

$$\begin{aligned}
&= \int d^2 \tilde{\eta}_{\ell_3} d^2 \tilde{\eta}_{\ell_4} \int \frac{d^2 \tilde{\lambda}_{\ell_3}}{\text{GL}(1)} \int \frac{d^2 \lambda_{\ell_4} d^2 \tilde{\lambda}_{\ell_4}}{\text{GL}(1)} \frac{\langle 1\ell_4 \rangle [\ell_4 3] \langle 2\ell_3 \rangle \langle 4\ell_3 \rangle \delta^4(P_1) \delta^4(Q_1) \delta^4(P_2) \delta^4(Q_2) \delta([3\ell_3])}{\langle 12 \rangle^2 \langle 34 \rangle \langle 3\ell_3 \rangle \langle \ell_3 \ell_4 \rangle^2} \\
&= \int \frac{d^2 \tilde{\lambda}_{\ell_3}}{\text{GL}(1)} \frac{(\langle 1\ell_3 \rangle [\ell_3 3] + \langle 14 \rangle [34]) \langle 2\ell_3 \rangle \langle 4\ell_3 \rangle \delta^4(P) \delta^4(Q) \delta((p_3+p_4-\ell_3)^2) \delta([3\ell_3])}{\langle 12 \rangle^2 \langle 34 \rangle \langle 3\ell_3 \rangle} \quad (5.32)
\end{aligned}$$

where the integration over $\tilde{\eta}_{\ell_3}$, $\tilde{\eta}_{\ell_4}$ reproduced an overall supermomentum conservation $\delta^4(Q)$ and an extra factor $\langle \ell_3 \ell_4 \rangle^2$ while the integral over ℓ_4 lead to an overall momentum conservation $\delta^4(P)$ and an extra delta function $\delta((p_3+p_4-\ell_3)^2)$. We can also integrate over $\tilde{\lambda}_{\ell_3}$ which fixes $\tilde{\lambda}_{\ell_3} = \tilde{\lambda}_3$ and factorizes the delta function

$$\delta((p_3+p_4-\ell_3)^2) = \frac{1}{[34]} \delta(\langle 34 \rangle - \langle 4\ell_3 \rangle) \quad (5.33)$$

Plugging back we get

$$\int d^2 \tilde{\eta}_{\ell_3} \int \frac{d^2 \tilde{\lambda}_{\ell_3}}{\text{GL}(1)} \omega = \frac{\langle 14 \rangle \langle 2\ell_3 \rangle \langle 4\ell_3 \rangle \delta^4(P) \delta^4(Q) \delta(\langle 34 \rangle - \langle 4\ell_3 \rangle)}{\langle 12 \rangle^2 \langle 34 \rangle \langle 3\ell_3 \rangle} \quad (5.34)$$

Now we calculate the derivative with respect to λ_{ℓ_3} and contract with λ_2 ,

$$\int d^2 \tilde{\eta}_{\ell_3} \int \frac{d^2 \tilde{\lambda}_{\ell_3}}{\text{GL}(1)} \left\langle \lambda_2 \frac{d\omega}{d\lambda_{\ell_3}} \right\rangle = \frac{\langle 14 \rangle \langle 2\ell_3 \rangle (\langle 2\ell_3 \rangle \langle 34 \rangle^2 + \langle 23 \rangle \langle 4\ell_3 \rangle^2) \delta^4(P) \delta^4(Q) \delta((\langle 34 \rangle - \langle 4\ell_3 \rangle)^2)}{\langle 12 \rangle^2 \langle 34 \rangle \langle 3\ell_3 \rangle^2} \quad (5.35)$$

where all delta functions are here considered in the context of contour integrals and residues, i.e. under the integral $\delta(z) \sim \frac{1}{z}$. This is important since the derivative also acts on the delta function. Plugging back into (5.21) and integrating over λ_{ℓ_3} we get

$$\Omega_{\text{UV}} = \delta^4(P) \delta^4(Q) \int d^2 \lambda_{\ell_3} \frac{\langle 14 \rangle \langle 2\ell_3 \rangle (\langle 2\ell_3 \rangle \langle 34 \rangle^2 + \langle 23 \rangle \langle 4\ell_3 \rangle^2) \delta^4(P) \delta^4(Q) \delta((\langle 34 \rangle - \langle 4\ell_3 \rangle)^2) \delta(\langle 1\ell_3 \rangle)}{\langle 12 \rangle^2 \langle 34 \rangle \langle 3\ell_3 \rangle^2} \quad (5.36)$$

In order to make the integration easier, we can expand ℓ_3 using (5.18),

$$\begin{aligned}
\Omega_{\text{UV}} &= \frac{\langle 14 \rangle}{\langle 12 \rangle \langle 34 \rangle} \delta^4(P) \delta^4(Q) \oint d\alpha d\beta \frac{\alpha^2 \langle 12 \rangle \langle 34 \rangle^2 + \alpha \langle 23 \rangle (\alpha \langle 14 \rangle + \beta \langle 24 \rangle)^2}{\beta (\langle 34 \rangle + \alpha \langle 14 \rangle + \beta \langle 24 \rangle)^2 (\alpha \langle 13 \rangle + \beta \langle 23 \rangle)^2} \\
&= - \frac{\langle 14 \rangle \langle 23 \rangle \delta^4(P) \delta^4(Q)}{\langle 12 \rangle \langle 34 \rangle \langle 13 \rangle^2} \quad (5.37)
\end{aligned}$$

where the integral was evaluated on the contour given by the delta functions, $\beta = 0$ and $\alpha = -\langle 34 \rangle / \langle 14 \rangle$ (this was a double pole). Now we compare (5.37) with the infinity operator (5.26) acting on the on-shell diagram

$$(5.38)$$

which is obtained by collapsing the left box with the UV pole in (5.29). The on-shell function ω^{bare} for Ω_2 for the diagram (5.38), again integrated over $\tilde{\eta}_{\ell_3}$ and $\tilde{\lambda}_{\ell_3}$ is

$$\int d^2 \tilde{\eta}_{\ell_3} \int \frac{d^2 \tilde{\lambda}_{\ell_3}}{\text{GL}(1)} \omega^{\text{bare}} = \quad (5.39)$$

$$\begin{aligned} &= \int d^2 \tilde{\eta}_{\ell_3} d^2 \tilde{\eta}_{\ell_4} \int \frac{d^2 \tilde{\lambda}_{\ell_3}}{\text{GL}(1)} \int \frac{d^2 \lambda_{\ell_4} d^2 \tilde{\lambda}_{\ell_4}}{\text{GL}(1)} \frac{\langle 2\ell_4 \rangle \langle 4\ell_3 \rangle [3\ell_4] \delta^4(P_1) \delta^4(Q_1) \delta^4(P_2) \delta^4(Q_2) \delta([3\ell_3])}{\langle 12 \rangle \langle 34 \rangle \langle \ell_3 \ell_4 \rangle^2 \langle 3\ell_3 \rangle} \\ &= \frac{\langle 24 \rangle \langle 4\ell_3 \rangle \delta^4(P) \delta^4(Q) \delta(\langle 34 \rangle - \langle 4\ell_3 \rangle)}{\langle 12 \rangle \langle 34 \rangle \langle 3\ell_3 \rangle} \end{aligned} \quad (5.40)$$

If we now integrated over λ_{ℓ_3} we would just recover the ordinary on-shell function for the box on-shell diagram (5.38),

$$\Omega^{\text{bare}} = \int d^2 \lambda_{\ell_3} \frac{\langle 24 \rangle \langle 4\ell_3 \rangle \delta^4(P) \delta^4(Q) \delta(\langle 34 \rangle - \langle 4\ell_3 \rangle) \delta(\langle 1\ell_3 \rangle)}{\langle 12 \rangle \langle 34 \rangle \langle 3\ell_3 \rangle} = \frac{\langle 24 \rangle \delta^4(P) \delta^4(Q)}{\langle 12 \rangle \langle 13 \rangle \langle 34 \rangle} \quad (5.41)$$

where the contour integral over the delta functions fixed $\lambda_{\ell_3} = \frac{\langle 34 \rangle}{\langle 14 \rangle} \lambda_1$. But instead of that we have to calculate the derivative,

$$\begin{aligned} &\int d^2 \tilde{\eta}_{\ell_3} \int \frac{d^2 \tilde{\lambda}_{\ell_3}}{\text{GL}(1)} \frac{\langle 2\ell_3 \rangle [2\ell_3]}{\langle 12 \rangle [1\ell_3]} \left\langle \lambda_2 \frac{d\omega^{\text{bare}}}{d\lambda_{\ell_3}} \right\rangle \\ &= \frac{[23] \langle 24 \rangle \langle 2\ell_3 \rangle (\langle 34 \rangle^2 \langle 2\ell_3 \rangle + \langle 23 \rangle \langle 4\ell_3 \rangle^2) \delta^4(P) \delta^4(Q) \delta((\langle 34 \rangle - \langle 4\ell_3 \rangle)^2)}{[13] \langle 12 \rangle^2 \langle 34 \rangle \langle 3\ell_3 \rangle^2} \end{aligned} \quad (5.42)$$

and then integrate over λ_{ℓ_3} ,

$$\begin{aligned} \Omega_{\text{UV}} &= \int d^2 \lambda_{\ell_3} \frac{[23] \langle 24 \rangle \langle 2\ell_3 \rangle (\langle 34 \rangle^2 \langle 2\ell_3 \rangle + \langle 23 \rangle \langle 4\ell_3 \rangle^2) \delta^4(P) \delta^4(Q) \delta((\langle 34 \rangle - \langle 4\ell_3 \rangle)^2) \delta(\langle 1\ell_3 \rangle)}{[13] \langle 12 \rangle^2 \langle 34 \rangle \langle 3\ell_3 \rangle^2} \\ &= - \frac{\langle 14 \rangle \langle 23 \rangle \delta^4(P) \delta^4(Q)}{\langle 12 \rangle \langle 34 \rangle \langle 13 \rangle^2} \end{aligned} \quad (5.43)$$

with a perfect agreement with (5.37). In pure Yang-Mills theory ($\mathcal{N}=0$) we act with the operator \mathcal{O} three times, and get

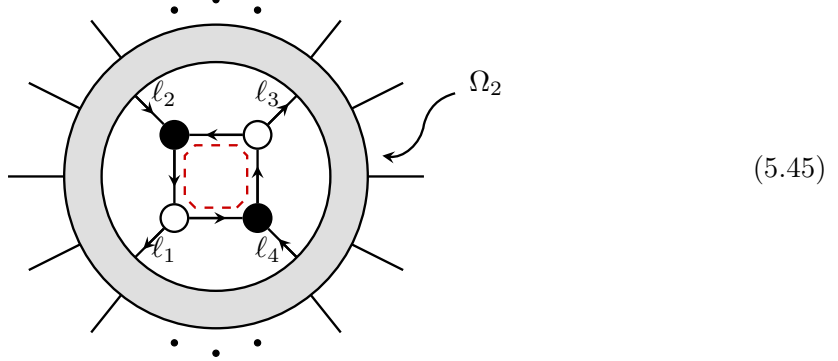
$$\begin{aligned} \Omega_{\text{UV}} &= \frac{1}{6} \int d^2 \tilde{\eta}_{\ell_3} \int \frac{d^2 \lambda_{\ell_3} d^2 \tilde{\lambda}_{\ell_3}}{\text{GL}(1)} \left(\frac{\langle 2\ell_3 \rangle [2\ell_3]}{\langle 12 \rangle [1\ell_3]} \right)^3 \left\langle \lambda_2 \frac{d}{d\lambda_{\ell_3}} \left\langle \lambda_2 \frac{d}{d\lambda_{\ell_3}} \left\langle \lambda_2 \frac{d\omega^{\text{bare}}}{d\lambda_{\ell_3}} \right\rangle \right\rangle \right\rangle \\ &= - \frac{\langle 14 \rangle^3 \langle 23 \rangle^3 \delta^4(P)}{\langle 12 \rangle \langle 34 \rangle \langle 13 \rangle^4} \end{aligned} \quad (5.44)$$

where ω^{bare} is the same as before up to an extra $\langle 24 \rangle^2$ helicity factor and supermomentum delta function. Finally, let us summarize the procedure of the calculation of the UV pole:

- Calculate the bare on-shell function ω^{bare} of a lower-loop on-shell diagram obtained by diagrammatic rules: a collapse of the loop and a non-planar twist. This includes an integration over the internal leg ℓ_4 which eliminates the dependencies from the momentum conservation.
- Take the appropriate number of derivatives with respect to λ_{ℓ_3} and plug into (5.44). This is the value of the original on-shell diagram on the UV pole.

5.3 General on-shell diagram

We are now ready to solve a more general problem where the box diagram with the UV pole is inside an arbitrary on-shell diagram,



The on-shell function for the diagram is

$$\Omega = \int d^2\tilde{\eta}_{\ell_1} \dots d^2\tilde{\eta}_{\ell_4} \int \frac{d^2\lambda_{\ell_1} d^2\tilde{\lambda}_{\ell_1}}{\text{GL}(1)} \dots \int \frac{d^2\lambda_{\ell_4} d^2\tilde{\lambda}_{\ell_4}}{\text{GL}(1)} \left\{ \Omega_1 \times \Omega_2 \right\} \quad (5.46)$$

where on-shell functions for the internal box and the rest of the diagram are

$$\Omega_1 = \frac{\langle \ell_2 \ell_4 \rangle^2 \delta^4(P_1) \delta^4(Q_1)}{\langle \ell_1 \ell_2 \rangle \langle \ell_2 \ell_3 \rangle \langle \ell_3 \ell_4 \rangle \langle \ell_4 \ell_1 \rangle} \left(\frac{\langle \ell_1 \ell_4 \rangle \langle \ell_2 \ell_3 \rangle}{\langle \ell_2 \ell_4 \rangle \langle \ell_1 \ell_3 \rangle} \right)^2, \quad \Omega_2 = \delta^4(P_2) \delta^4(Q_2) \omega_2 \quad (5.47)$$

We rewrite this expression as

$$\Omega = \int d^2\tilde{\eta}_{\ell_1} \dots d^2\tilde{\eta}_{\ell_3} \int \frac{d^2\lambda_{\ell_1} d^2\tilde{\lambda}_{\ell_1}}{\text{GL}(1)} \dots \int \frac{d^2\lambda_{\ell_3} d^2\tilde{\lambda}_{\ell_3}}{\text{GL}(1)} \left\{ \frac{\langle \ell_1 \ell_2 \rangle}{\langle \ell_1 \ell_3 \rangle^2} \times \omega \right\} \quad (5.48)$$

where the function ω is defined as

$$\omega = \int d^2\tilde{\eta}_{\ell_4} \int \frac{d^2\lambda_{\ell_4} d^2\tilde{\lambda}_{\ell_4}}{\text{GL}(1)} \left\{ \frac{\langle \ell_2 \ell_3 \rangle \langle \ell_1 \ell_4 \rangle \delta^4(P_1) \delta^4(Q_1)}{\langle \ell_1 \ell_2 \rangle^2 \langle \ell_3 \ell_4 \rangle} \times \Omega_2 \right\} \quad (5.49)$$

This is a straight generalization of the case discussed in the last subsection. We included the integration over internal particle ℓ_4 in the definition of ω in order to eliminate the momentum conservation on four internal legs, such that we can then take a derivative of the expression without any ambiguities. But this is just one choice, we can obviously choose another internal leg to be eliminated in this way. The residue on the pole at infinity $\langle \ell_1 \ell_3 \rangle = 0$ is then given by

$$\Omega_{\text{UV}} = \mathcal{O} \otimes \Omega_{\text{UV}}^{\text{bare}} \quad \text{where} \quad \Omega_{\text{UV}}^{\text{bare}} = \text{Diagram} \quad (5.50)$$

where the operator \mathcal{O} is given by

$$\mathcal{O} = \left(\frac{\langle \ell_2 \ell_3 \rangle [\ell_2 \ell_3]}{\langle \ell_1 \ell_2 \rangle [\ell_1 \ell_3]} \right) \left\langle \lambda_{\ell_2} \frac{d}{d\lambda_{\ell_3}} \right\rangle \quad (5.51)$$

and the action on the (bare) on-shell function in (5.27) is given by the analogous formula to (5.34),

$$\Omega_{\text{UV}} = \int d^2 \tilde{\eta}_{\ell_1} \dots d^2 \tilde{\eta}_{\ell_3} \int \frac{d^2 \lambda_{\ell_1} d^2 \tilde{\lambda}_{\ell_1}}{\text{GL}(1)} \dots \int \frac{d^2 \lambda_{\ell_3} d^2 \tilde{\lambda}_{\ell_3}}{\text{GL}(1)} \left\{ \delta(\langle \ell_1 \ell_3 \rangle) \frac{\langle \ell_2 \ell_3 \rangle [\ell_2 \ell_3]}{\langle \ell_1 \ell_2 \rangle [\ell_1 \ell_3]} \left\langle \lambda_{\ell_2} \frac{d\omega^{\text{bare}}}{d\lambda_{\ell_3}} \right\rangle \right\} \quad (5.52)$$

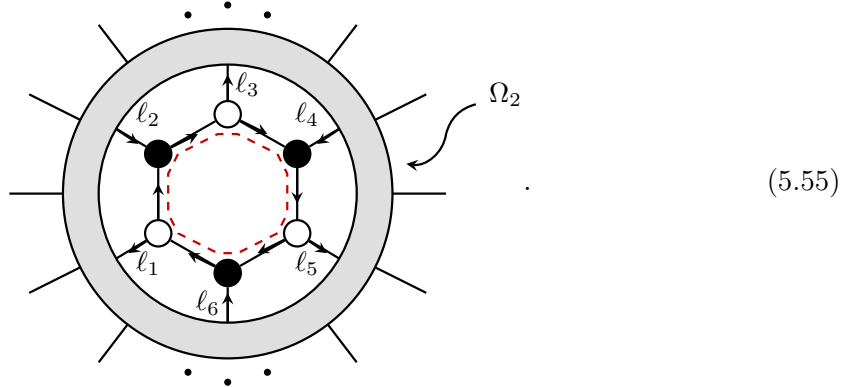
where the bare on-shell function ω^{bare} for (5.50) is

$$\omega^{\text{bare}} = \int d^2 \tilde{\eta}_{\ell_4} \int \frac{d^2 \lambda_{\ell_4} d^2 \tilde{\lambda}_{\ell_4}}{\text{GL}(1)} \left\{ \frac{\langle \ell_2 \ell_4 \rangle \delta^4(P_1) \delta^4(Q_1)}{\langle \ell_1 \ell_2 \rangle \langle \ell_3 \ell_4 \rangle} \times \Omega_2 \right\} \quad (5.53)$$

which is just a straightforward generalization of our discussion before. Note that the only limitation is that we required that the leg ℓ_4 is an internal leg. In case it is an external leg, and we do not integrate over it (hence we do not resolve the momentum conservation), we just have to choose another leg to integrate over first. The generalization to an arbitrary number of supersymmetries is again straightforward, we just act with $3-\mathcal{N}$ copies of \mathcal{O} , i.e.

$$\Omega_{\text{UV}} = \mathcal{O}^{3-\mathcal{N}} \otimes \Omega_{\text{UV}}^{\text{bare}} \quad (5.54)$$

We are now ready to generalize this procedure to higher n -gons. Let us now consider the NMHV hexagon subdiagram,



The on-shell function for $\mathcal{N} = 2$ SYM is

$$\Omega = \int d^2 \tilde{\eta}_{\ell_1} \dots d^2 \tilde{\eta}_{\ell_6} \int \frac{d^2 \lambda_{\ell_1} d^2 \tilde{\lambda}_{\ell_1}}{\text{GL}(1)} \dots \int \frac{d^2 \lambda_{\ell_6} d^2 \tilde{\lambda}_{\ell_6}}{\text{GL}(1)} \left\{ \Omega_1 \times \Omega_2 \right\}, \quad (5.56)$$

where the on-shell function for the hexagon can be written as

$$\begin{aligned} \Omega_1 &= \frac{\langle \ell_4 | \ell_3 + \ell_5 | \ell_1 \rangle^2 \langle \ell_3 \ell_4 \rangle \langle \ell_1 \ell_5 \rangle \delta(\Xi)}{[\ell_5 \ell_6]^2 [\ell_1 \ell_2] \langle \ell_1 \ell_2 \rangle \langle \ell_1 \ell_6 \rangle \langle \ell_2 \ell_3 \rangle \langle \ell_4 \ell_5 \rangle \langle \ell_3 \ell_5 \rangle} \times \left(\frac{\langle \ell_1 \ell_2 \rangle \langle \ell_3 \ell_4 \rangle [\ell_1 \ell_2]}{\langle \ell_1 \ell_3 \rangle \langle \ell_4 | \ell_3 + \ell_5 | \ell_1 \rangle} \right)^2 \\ &= \frac{\langle \ell_3 \ell_4 \rangle^3 \langle \ell_1 \ell_5 \rangle \langle \ell_1 \ell_2 \rangle [\ell_1 \ell_2] \delta(\Xi)}{[\ell_5 \ell_6]^2 \langle \ell_1 \ell_6 \rangle \langle \ell_2 \ell_3 \rangle \langle \ell_4 \ell_5 \rangle \langle \ell_3 \ell_5 \rangle \langle \ell_1 \ell_3 \rangle^2} \end{aligned} \quad (5.57)$$

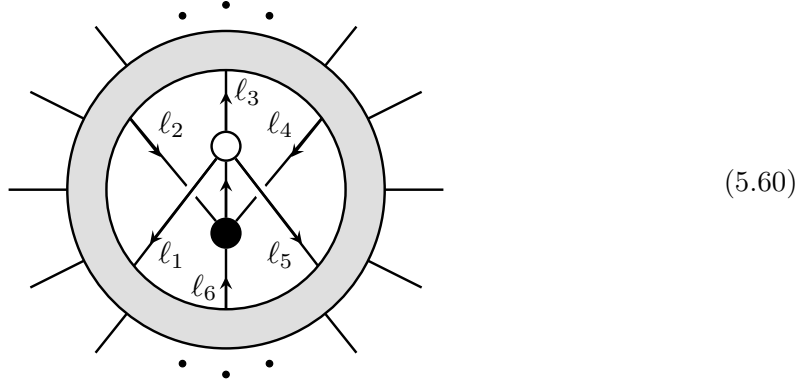
where the delta functions are

$$\delta(\Xi_1) \equiv \delta^4(P_1) \delta^4(Q_1) \delta(\langle \ell_1 | \ell_2 + \ell_3 | \ell_4 \rangle) \delta(\langle \ell_3 | \ell_4 + \ell_5 | \ell_6 \rangle) \delta([\ell_5 \ell_6] \tilde{\eta}_{\ell_4} + [\ell_6 \ell_4] \tilde{\eta}_{\ell_5} + [\ell_4 \ell_5] \tilde{\eta}_{\ell_6}) \quad (5.58)$$

The residue on the pole at infinity $\langle \ell_1 \ell_3 \rangle = 0$ is then given by

$$\Omega_{\text{UV}} = \int d^2 \tilde{\eta}_{\ell_1} \dots d^2 \tilde{\eta}_{\ell_5} \int \frac{d^2 \lambda_{\ell_1} d^2 \tilde{\lambda}_{\ell_1}}{\text{GL}(1)} \dots \int \frac{d^2 \lambda_{\ell_5} d^2 \tilde{\lambda}_{\ell_5}}{\text{GL}(1)} \left\{ \delta(\langle \ell_1 \ell_3 \rangle) \left(\frac{\langle \ell_2 \ell_3 \rangle [\ell_2 \ell_3]}{\langle \ell_1 \ell_2 \rangle [\ell_1 \ell_3]} \right) \left\langle \lambda_{\ell_2} \frac{d\omega^{\text{bare}}}{d\lambda_{\ell_3}} \right\rangle \right\} \quad (5.59)$$

where ω^{bare} is now the on-shell function associated with the graph



before we integrate over momenta ℓ_1, \dots, ℓ_5 (in fact, we can integrate over all momenta except λ_{ℓ_3} in which we take the derivative). This straightforwardly generalizes to any one-loop n -gon, and also to any number of supersymmetries – we again act $(3-\mathcal{N})$ times with the operator \mathcal{O} .

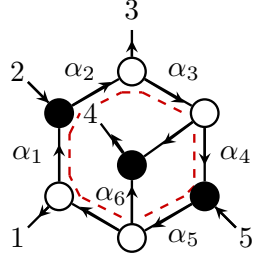
It is worth noting that in our procedure of approaching and calculating the higher pole at infinity we made a certain choice: we parametrized $\lambda_{\ell_3} = \alpha \lambda_{\ell_1} + \beta \lambda_{\ell_2}$ and calculated the pole for $\beta = 0$ which then transformed into a certain form of the \mathcal{O} . Note that the final result does not depend on this choice (the calculation of the residue is independent on the parametrization). One assumption we made in our calculation was that the leg ℓ_3 was internal (as we integrated over it and removed any dependencies between ℓ_j through momentum conservation). If this was an external leg we would have to approach the pole via another leg. For the general on-shell diagram with $L > 1$ at least one of the legs of the n -gon (which UV pole we approach) is internal and we can use it in our procedure. The only exception is the one-loop n -gon itself as an on-shell diagram, in this case we can just attach a BCFW bridge as we did for the box diagram in the previous section. The result for the UV pole does not depend on the particular procedure used to approach that pole.

6 Non-planar diagrams

The non-planar on-shell diagrams have been extensively studied in the past. Based on the principles of generalized unitarity they represent the cuts of non-planar loop integrands. In the dual description, the on-shell function is reproduced by the simple dlog form in $\mathcal{N} = 4$ SYM theory while in the lower SUSY Yang-Mills theories we have to include the Jacobians

[26], and the formula is the same as for the planar diagrams. Unlike in the planar case not much is known about the connection of non-planar on-shell diagrams to the Grassmannian geometry, permutations, stratifications, identity moves etc. Some interesting observations were made for MHV on-shell diagrams in the context of $\mathcal{N} = 4$ SYM theory [28] where the on-shell function for each diagram was written as a special linear combination of Parke-Taylor factors. A more systematic study was performed in [30] and the classification of all on-shell diagrams for 6 point NMHV amplitudes was performed in [33]. The first attempts to associate NMHV on-shell diagrams with Grassmannian geometries were provided in [39] in the context of non-adjacent BCFW recursion relations.

In our discussion of UV poles in on-shell diagrams, we restricted only to planar diagrams and also our proof of the localization of UV poles in one loop subdiagrams required the planarity of the whole diagram. We will show that indeed the same argument does not hold for non-planar on-shell diagrams and the poles at infinity propagate beyond just a one-loop subgraph. We explore one particular five-point non-planar diagram,

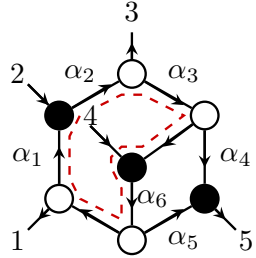


$$\begin{aligned} \alpha_1 &= \frac{\langle 32 \rangle}{\langle 13 \rangle}, & \alpha_2 &= \frac{\langle 13 \rangle}{\langle 12 \rangle}, \\ \alpha_3 &= \frac{\langle 14 \rangle}{\langle 13 \rangle}, & \alpha_4 &= \frac{\langle 51 \rangle}{\langle 14 \rangle}, \\ \alpha_5 &= \frac{\langle 13 \rangle}{\langle 53 \rangle}, & \alpha_6 &= \frac{\langle 43 \rangle}{\langle 13 \rangle}. \end{aligned} \tag{6.1}$$

The Jacobian from the cycle is

$$\mathcal{J} = 1 - \alpha_1 \alpha_2 \alpha_3 \alpha_4 \alpha_5 = \frac{\langle 13 \rangle \langle 25 \rangle}{\langle 12 \rangle \langle 35 \rangle}, \tag{6.2}$$

where we can identify the UV pole as $\langle 13 \rangle \rightarrow 0$, while $\langle 25 \rangle$ is the helicity factor. We could instead have picked an orientation with a different internal cycle as follows,



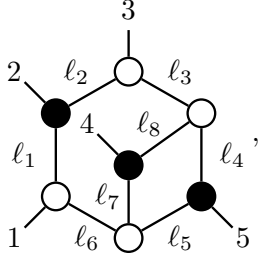
$$\begin{aligned} \alpha_1 &= \frac{\langle 32 \rangle}{\langle 13 \rangle}, & \alpha_2 &= \frac{\langle 13 \rangle}{\langle 12 \rangle}, \\ \alpha_3 &= \frac{\langle 14 \rangle}{\langle 13 \rangle}, & \alpha_4 &= \frac{\langle 51 \rangle}{\langle 14 \rangle}, \\ \alpha_5 &= \frac{\langle 35 \rangle}{\langle 13 \rangle}, & \alpha_6 &= \frac{\langle 13 \rangle}{\langle 34 \rangle}. \end{aligned} \tag{6.3}$$

Here the Jacobian from the cycle is

$$\mathcal{J} = 1 - \alpha_1 \alpha_2 \alpha_3 \alpha_6 = \frac{\langle 13 \rangle \langle 24 \rangle}{\langle 12 \rangle \langle 34 \rangle}. \tag{6.4}$$

We find once again that the pole at infinity is at $\langle 13 \rangle \rightarrow 0$, even though we are looking at

different loop. We can uncover the same problem by solving for internal momenta,

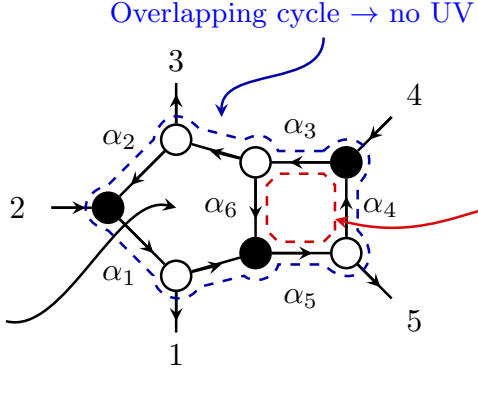


$$\begin{aligned}
\ell_1 &= \frac{\langle 23 \rangle}{\langle 13 \rangle} \lambda_1 \tilde{\lambda}_2, & \ell_2 &= \frac{\langle 12 \rangle}{\langle 13 \rangle} \lambda_3 \tilde{\lambda}_2, & \ell_3 &= \frac{(Q_{23} \cdot \lambda_1)}{\langle 13 \rangle} \lambda_3, \\
\ell_4 &= \frac{\langle 15 \rangle}{\langle 13 \rangle} \lambda_3 \tilde{\lambda}_5, & \ell_5 &= \frac{\langle 35 \rangle}{\langle 13 \rangle} \lambda_1 \tilde{\lambda}_5, & \ell_6 &= \frac{(Q_{12} \cdot \lambda_3)}{\langle 13 \rangle} \lambda_1, \\
\ell_7 &= \frac{\langle 34 \rangle}{\langle 13 \rangle} \lambda_1 \tilde{\lambda}_4, & \ell_8 &= \frac{\langle 14 \rangle}{\langle 13 \rangle} \lambda_3 \tilde{\lambda}_4.
\end{aligned}
\tag{6.5}$$

and we see that the UV pole $\langle 13 \rangle$ is present in multiple loops rather than only one-loop subgraph. There is a purely graph theoretic reason for these subtleties: we can not invariantly talk about “fundamental” and “overlapping” internal loops. In the planar case, the first type corresponds to poles at infinity, while the second type does not. Take e.g. the pentabox (3.14) with the orientation in the box flipped. Schematically we can show the pole and cycle structure as,

No cycle \rightarrow no UV pole

$\ell_{\text{pentagon}} \sim \frac{1}{\langle 13 \rangle}$



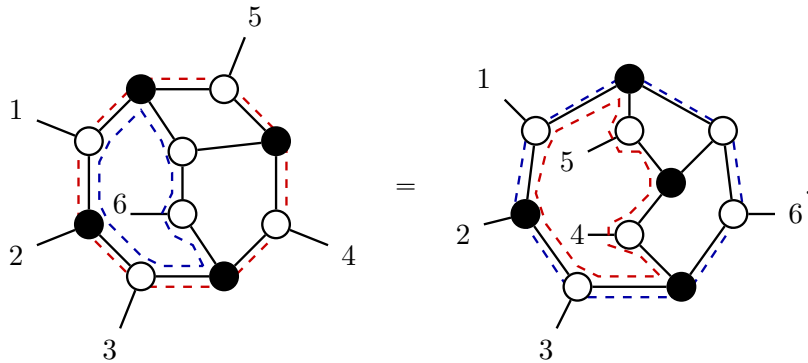
Overlapping cycle \rightarrow no UV pole

Inner cycle \rightarrow UV pole

$\ell_{\text{box}} \sim \frac{1}{\langle 35 \rangle}$

(6.6)

Even with the overlapping cycle, the Jacobian still only introduces the UV pole of the box $\langle 35 \rangle$. For the non-planar graphs there is no difference between these two types of cycles, and we can always redraw a diagram in a way which turns one type into the other,



(6.7)

This makes it clear that we need to generalize our rule to capture the UV poles in non-planar diagrams where multiple loops blow up at the same time. This also concerns the gravity on-shell diagrams [34–37] which are intrinsically non-planar.

7 Conclusion and Outlook

In this paper we studied the poles at infinity in on-shell diagrams for $\mathcal{N}<4$ SYM theory. We showed that for planar diagrams the poles at infinity are located in one-loop subgraphs and the kinematical condition on the pole reduces the graph to a simpler on-shell diagram with a *non-planar twist*, hence the diagram is generally non-planar. The on-shell function on the UV pole is then given by a certain derivative operator acting on the on-shell function for a new non-planar on-shell diagram. This comes naturally from the definition of the residue on a higher pole as a derivative. We also showed that for non-planar on-shell diagrams the situation is more complicated as the poles at infinity are not localized in one-loop subgraphs and a different procedure is needed.

Our work is a direct attempt to systematically study the poles at infinity in scattering amplitudes. While the residues of tree-level amplitudes and loop integrands in the deep IR are governed by principles of unitarity and lead to factorizations and unitarity cuts, the poles in the UV are naively not constrained by similar principles. We do not face this problem directly in the context of scattering amplitudes, but we chose simpler on-shell gauge-invariant objects – on-shell diagrams, and solve the problem here. Note that tree-level amplitudes (and in special cases also loop integrands) can be expressed as sums of on-shell diagrams, so it is suggestive that our results would be relevant to amplitudes problem as well. The two main lessons from our analysis are: (i) the kinematics of UV poles correspond to non-planar objects, in this case non-planar on-shell diagrams, (ii) on-shell functions are given by derivatives of the bare on-shell diagrams. In future work, we want to use this insight to address this problem directly in the context of tree-level amplitudes and loop integrands.

The further goal is to formulate the general prescription for the calculation of poles at infinity for arbitrary tree-level amplitudes, and loop integrands – similar to rules of factorizations and cuts. This would have major implications on our ability to calculate amplitudes using recursion relations, and possibly search for positive geometries that could capture amplitudes in theories with non-trivial UV physics.

Acknowledgments

We thank Nima Arkani-Hamed, Enrico Herrmann and Shruti Paranjape for useful discussions and comments. This work is supported by a DOE grant No. SC0009999, GACR 21-26574S and the funds of the University of California.

References

- [1] H. Elvang and Y.-t. Huang, *Scattering Amplitudes*, [1308.1697](#).
- [2] L. J. Dixon, *A brief introduction to modern amplitude methods*, in *Theoretical Advanced Study Institute in Elementary Particle Physics : Particle Physics: The Higgs Boson and Beyond*, pp. 31–67, 2014, [1310.5353](#), DOI.
- [3] J. M. Henn and J. C. Plefka, *Scattering Amplitudes in Gauge Theories*, vol. 883. Springer, Berlin, 2014, [10.1007/978-3-642-54022-6](#).

- [4] C. Cheung, *TASI Lectures on Scattering Amplitudes*, pp. 571–623. 2018. [1708.03872](#). [10.1142/9789813233348_0008](#).
- [5] G. Travaglini et al., *The SAGEX review on scattering amplitudes**, *J. Phys. A* **55** (2022) [443001](#) [[2203.13011](#)].
- [6] Z. Bern and J. Trnka, *Snowmass TF04 Report: Scattering Amplitudes and their Applications*, [2210.03146](#).
- [7] R. Britto, F. Cachazo and B. Feng, *New recursion relations for tree amplitudes of gluons*, *Nucl. Phys. B* **715** (2005) 499 [[hep-th/0412308](#)].
- [8] R. Britto, F. Cachazo, B. Feng and E. Witten, *Direct proof of tree-level recursion relation in Yang-Mills theory*, *Phys. Rev. Lett.* **94** (2005) 181602 [[hep-th/0501052](#)].
- [9] T. Cohen, H. Elvang and M. Kiermaier, *On-shell constructibility of tree amplitudes in general field theories*, *JHEP* **04** (2011) 053 [[1010.0257](#)].
- [10] C. Cheung, *On-Shell Recursion Relations for Generic Theories*, *JHEP* **03** (2010) 098 [[0808.0504](#)].
- [11] C. Cheung, C.-H. Shen and J. Trnka, *Simple Recursion Relations for General Field Theories*, *JHEP* **06** (2015) 118 [[1502.05057](#)].
- [12] C. Cheung, K. Kampf, J. Novotny, C.-H. Shen and J. Trnka, *On-Shell Recursion Relations for Effective Field Theories*, *Phys. Rev. Lett.* **116** (2016) 041601 [[1509.03309](#)].
- [13] H. Luo and C. Wen, *Recursion relations from soft theorems*, *JHEP* **03** (2016) 088 [[1512.06801](#)].
- [14] H. Elvang, M. Haddjantonis, C. R. T. Jones and S. Paranjape, *Soft Bootstrap and Supersymmetry*, *JHEP* **01** (2019) 195 [[1806.06079](#)].
- [15] C. Cheung, K. Kampf, J. Novotny, C.-H. Shen, J. Trnka and C. Wen, *Vector Effective Field Theories from Soft Limits*, *Phys. Rev. Lett.* **120** (2018) 261602 [[1801.01496](#)].
- [16] Z. Bern, L. J. Dixon, D. C. Dunbar and D. A. Kosower, *One loop n point gauge theory amplitudes, unitarity and collinear limits*, *Nucl. Phys. B* **425** (1994) 217 [[hep-ph/9403226](#)].
- [17] Z. Bern, L. J. Dixon, D. C. Dunbar and D. A. Kosower, *Fusing gauge theory tree amplitudes into loop amplitudes*, *Nucl. Phys. B* **435** (1995) 59 [[hep-ph/9409265](#)].
- [18] Z. Bern, L. J. Dixon and V. A. Smirnov, *Iteration of planar amplitudes in maximally supersymmetric Yang-Mills theory at three loops and beyond*, *Phys. Rev. D* **72** (2005) [085001](#) [[hep-th/0505205](#)].
- [19] Z. Bern, J. J. Carrasco, L. J. Dixon, H. Johansson and R. Roiban, *The Ultraviolet Behavior of $N=8$ Supergravity at Four Loops*, *Phys. Rev. Lett.* **103** (2009) 081301 [[0905.2326](#)].
- [20] Z. Bern, L. J. Dixon, D. A. Kosower, R. Roiban, M. Spradlin, C. Vergu et al., *The Two-Loop Six-Gluon MHV Amplitude in Maximally Supersymmetric Yang-Mills Theory*, *Phys. Rev. D* **78** (2008) 045007 [[0803.1465](#)].
- [21] Z. Bern, J. J. M. Carrasco, H. Johansson and R. Roiban, *The Five-Loop Four-Point Amplitude of $N=4$ super-Yang-Mills Theory*, *Phys. Rev. Lett.* **109** (2012) 241602 [[1207.6666](#)].
- [22] Z. Bern, J. J. Carrasco, W.-M. Chen, A. Edison, H. Johansson, J. Parra-Martinez et al., *Ultraviolet Properties of $\mathcal{N} = 8$ Supergravity at Five Loops*, *Phys. Rev. D* **98** (2018) 086021 [[1804.09311](#)].

- [23] J. J. M. Carrasco, A. Edison and H. Johansson, *Maximal Super-Yang-Mills at Six Loops via Novel Integrand Bootstrap*, [2112.05178](#).
- [24] J. L. Bourjaily, P. Heslop and V.-V. Tran, *Amplitudes and Correlators to Ten Loops Using Simple, Graphical Bootstraps*, *JHEP* **11** (2016) 125 [[1609.00007](#)].
- [25] J. L. Bourjaily, E. Herrmann and J. Trnka, *Prescriptive Unitarity*, *JHEP* **06** (2017) 059 [[1704.05460](#)].
- [26] N. Arkani-Hamed, J. L. Bourjaily, F. Cachazo, A. B. Goncharov, A. Postnikov and J. Trnka, *Grassmannian Geometry of Scattering Amplitudes*. Cambridge University Press, 4, 2016, [10.1017/CBO9781316091548](#), [[1212.5605](#)].
- [27] S. Franco, D. Galloni and A. Mariotti, *The Geometry of On-Shell Diagrams*, *JHEP* **08** (2014) 038 [[1310.3820](#)].
- [28] N. Arkani-Hamed, J. L. Bourjaily, F. Cachazo, A. Postnikov and J. Trnka, *On-Shell Structures of MHV Amplitudes Beyond the Planar Limit*, *JHEP* **06** (2015) 179 [[1412.8475](#)].
- [29] Y. Bai and S. He, *The Amplituhedron from Momentum Twistor Diagrams*, *JHEP* **02** (2015) 065 [[1408.2459](#)].
- [30] S. Franco, D. Galloni, B. Penante and C. Wen, *Non-Planar On-Shell Diagrams*, *JHEP* **06** (2015) 199 [[1502.02034](#)].
- [31] P. Benincasa, *On-shell diagrammatics and the perturbative structure of planar gauge theories*, [1510.03642](#).
- [32] P. Benincasa and D. Gordo, *On-shell diagrams and the geometry of planar $\mathcal{N} < 4$ SYM theories*, *JHEP* **11** (2017) 192 [[1609.01923](#)].
- [33] J. L. Bourjaily, S. Franco, D. Galloni and C. Wen, *Stratifying On-Shell Cluster Varieties: the Geometry of Non-Planar On-Shell Diagrams*, *JHEP* **10** (2016) 003 [[1607.01781](#)].
- [34] P. Heslop and A. E. Lipstein, *On-shell diagrams for $\mathcal{N} = 8$ supergravity amplitudes*, *JHEP* **06** (2016) 069 [[1604.03046](#)].
- [35] E. Herrmann and J. Trnka, *Gravity On-shell Diagrams*, *JHEP* **11** (2016) 136 [[1604.03479](#)].
- [36] J. A. Farrow and A. E. Lipstein, *From 4d Ambitwistor Strings to On Shell Diagrams and Back*, *JHEP* **07** (2017) 114 [[1705.07087](#)].
- [37] C. Armstrong, J. A. Farrow and A. E. Lipstein, *$\mathcal{N} = 7$ On-shell diagrams and supergravity amplitudes in momentum twistor space*, *JHEP* **01** (2021) 181 [[2010.11813](#)].
- [38] F. Cachazo, N. Early, A. Guevara and S. Mizera, *Δ -algebra and scattering amplitudes*, *JHEP* **02** (2019) 005 [[1812.01168](#)].
- [39] S. Paranjape, J. Trnka and M. Zheng, *Non-planar BCFW Grassmannian Geometries*, [2208.02262](#).
- [40] N. Arkani-Hamed and J. Trnka, *The Amplituhedron*, *JHEP* **10** (2014) 030 [[1312.2007](#)].
- [41] N. Arkani-Hamed and J. Trnka, *Into the Amplituhedron*, *JHEP* **12** (2014) 182 [[1312.7878](#)].
- [42] N. Arkani-Hamed, H. Thomas and J. Trnka, *Unwinding the Amplituhedron in Binary*, *JHEP* **01** (2018) 016 [[1704.05069](#)].
- [43] D. Damgaard, L. Ferro, T. Lukowski and M. Parisi, *The Momentum Amplituhedron*, *JHEP* **08** (2019) 042 [[1905.04216](#)].

- [44] L. Ferro and T. Lukowski, *Amplituhedra, and beyond*, *J. Phys. A* **54** (2021) 033001 [[2007.04342](#)].
- [45] L. Ferro and T. Lukowski, *The Loop Momentum Amplituhedron*, [2210.01127](#).
- [46] E. Herrmann and J. Trnka, *Chapter 7: Positive geometry of scattering amplitudes*, *J. Phys. A* **55** (2022) 443008 [[2203.13018](#)].
- [47] S. Franco, D. Galloni, A. Mariotti and J. Trnka, *Anatomy of the Amplituhedron*, *JHEP* **03** (2015) 128 [[1408.3410](#)].
- [48] L. Ferro, T. Łukowski, A. Orta and M. Parisi, *Yangian symmetry for the tree amplituhedron*, *J. Phys. A* **50** (2017) 294005 [[1612.04378](#)].
- [49] L. Ferro, T. Lukowski, A. Orta and M. Parisi, *Towards the Amplituhedron Volume*, *JHEP* **03** (2016) 014 [[1512.04954](#)].
- [50] L. Ferro, T. Lukowski, A. Orta and M. Parisi, *Tree-level scattering amplitudes from the amplituhedron*, *J. Phys. Conf. Ser.* **841** (2017) 012037 [[1612.06276](#)].
- [51] L. Ferro, T. Łukowski and M. Parisi, *Amplituhedron meets Jeffrey–Kirwan residue*, *J. Phys. A* **52** (2019) 045201 [[1805.01301](#)].
- [52] L. Ferro, T. Łukowski and R. Moerman, *From momentum amplituhedron boundaries to amplitude singularities and back*, *JHEP* **07** (2020) 201 [[2003.13704](#)].
- [53] E. Herrmann, C. Langer, J. Trnka and M. Zheng, *Positive Geometries for One-Loop Chiral Octagons*, [2007.12191](#).
- [54] E. Herrmann, C. Langer, J. Trnka and M. Zheng, *Positive geometry, local triangulations, and the dual of the Amplituhedron*, *JHEP* **01** (2021) 035 [[2009.05607](#)].
- [55] R. Kojima and C. Langer, *Sign Flip Triangulations of the Amplituhedron*, *JHEP* **05** (2020) 121 [[2001.06473](#)].
- [56] N. Arkani-Hamed, J. Henn and J. Trnka, *Nonperturbative negative geometries: amplitudes at strong coupling and the amplituhedron*, *JHEP* **03** (2022) 108 [[2112.06956](#)].
- [57] J. Rao, *All-loop Mondrian Reduction of 4-particle Amplituhedron at Positive Infinity*, *Nucl. Phys. B* **957** (2020) 115086 [[1910.14612](#)].
- [58] R. Kojima and J. Rao, *Triangulation-free Trivialization of 2-loop MHV Amplituhedron*, *JHEP* **10** (2020) 140 [[2007.15650](#)].
- [59] G. Dian and P. Heslop, *Amplituhedron-like geometries*, *JHEP* **11** (2021) 074 [[2106.09372](#)].
- [60] G. Dian, P. Heslop and A. Stewart, *Internal boundaries of the loop amplituhedron*, [2207.12464](#).
- [61] A. Postnikov, *Total positivity, Grassmannians, and networks*, [math/0609764](#).
- [62] J. M. Drummond, J. Henn, V. A. Smirnov and E. Sokatchev, *Magic identities for conformal four-point integrals*, *JHEP* **01** (2007) 064 [[hep-th/0607160](#)].
- [63] J. M. Drummond, J. Henn, G. P. Korchemsky and E. Sokatchev, *Dual superconformal symmetry of scattering amplitudes in $N=4$ super-Yang-Mills theory*, *Nucl. Phys. B* **828** (2010) 317 [[0807.1095](#)].
- [64] N. Arkani-Hamed, J. L. Bourjaily, F. Cachazo and J. Trnka, *Singularity Structure of Maximally Supersymmetric Scattering Amplitudes*, *Phys. Rev. Lett.* **113** (2014) 261603 [[1410.0354](#)].

- [65] Z. Bern, E. Herrmann, S. Litsey, J. Stankowicz and J. Trnka, *Logarithmic Singularities and Maximally Supersymmetric Amplitudes*, *JHEP* **06** (2015) 202 [[1412.8584](#)].
- [66] Z. Bern, E. Herrmann, S. Litsey, J. Stankowicz and J. Trnka, *Evidence for a Nonplanar Amplituhedron*, *JHEP* **06** (2016) 098 [[1512.08591](#)].
- [67] Z. Bern, M. Enciso, H. Ita and M. Zeng, *Dual Conformal Symmetry, Integration-by-Parts Reduction, Differential Equations and the Nonplanar Sector*, *Phys. Rev. D* **96** (2017) 096017 [[1709.06055](#)].
- [68] Z. Bern, M. Enciso, C.-H. Shen and M. Zeng, *Dual Conformal Structure Beyond the Planar Limit*, *Phys. Rev. Lett.* **121** (2018) 121603 [[1806.06509](#)].
- [69] J. L. Bourjaily, E. Herrmann and J. Trnka, *Maximally supersymmetric amplitudes at infinite loop momentum*, *Phys. Rev. D* **99** (2019) 066006 [[1812.11185](#)].
- [70] D. Chicherin, J. M. Henn and E. Sokatchev, *Implications of nonplanar dual conformal symmetry*, *JHEP* **09** (2018) 012 [[1807.06321](#)].
- [71] J. L. Bourjaily, E. Herrmann, C. Langer, A. J. McLeod and J. Trnka, *All-Multiplicity Nonplanar Amplitude Integrands in Maximally Supersymmetric Yang-Mills Theory at Two Loops*, *Phys. Rev. Lett.* **124** (2020) 111603 [[1911.09106](#)].
- [72] F. Cachazo and P. Svrcek, *Tree level recursion relations in general relativity*, [hep-th/0502160](#).
- [73] J. Bedford, A. Brandhuber, B. J. Spence and G. Travaglini, *A Recursion relation for gravity amplitudes*, *Nucl. Phys. B* **721** (2005) 98 [[hep-th/0502146](#)].
- [74] N. Arkani-Hamed and J. Kaplan, *On Tree Amplitudes in Gauge Theory and Gravity*, *JHEP* **04** (2008) 076 [[0801.2385](#)].
- [75] E. Herrmann and J. Trnka, *UV cancellations in gravity loop integrands*, *JHEP* **02** (2019) 084 [[1808.10446](#)].
- [76] A. Edison, E. Herrmann, J. Parra-Martinez and J. Trnka, *Gravity loop integrands from the ultraviolet*, *SciPost Phys.* **10** (2021) 016 [[1909.02003](#)].
- [77] Z. Bern, S. Davies, T. Dennen and Y.-t. Huang, *Ultraviolet Cancellations in Half-Maximal Supergravity as a Consequence of the Double-Copy Structure*, *Phys. Rev. D* **86** (2012) 105014 [[1209.2472](#)].
- [78] Z. Bern, S. Davies and T. Dennen, *Enhanced ultraviolet cancellations in $\mathcal{N} = 5$ supergravity at four loops*, *Phys. Rev. D* **90** (2014) 105011 [[1409.3089](#)].
- [79] Z. Bern, M. Enciso, J. Parra-Martinez and M. Zeng, *Manifesting enhanced cancellations in supergravity: integrands versus integrals*, *JHEP* **05** (2017) 137 [[1703.08927](#)].
- [80] Z. Bern, L. J. Dixon, M. Perelstein and J. S. Rozowsky, *Multileg one loop gravity amplitudes from gauge theory*, *Nucl. Phys. B* **546** (1999) 423 [[hep-th/9811140](#)].
- [81] H. Elvang and D. Z. Freedman, *Note on graviton MHV amplitudes*, *JHEP* **05** (2008) 096 [[0710.1270](#)].
- [82] J. M. Drummond, M. Spradlin, A. Volovich and C. Wen, *Tree-Level Amplitudes in $\mathcal{N}=8$ Supergravity*, *Phys. Rev. D* **79** (2009) 105018 [[0901.2363](#)].
- [83] L. J. Mason and D. Skinner, *Gravity, Twistors and the MHV Formalism*, *Commun. Math. Phys.* **294** (2010) 827 [[0808.3907](#)].

- [84] D. Nguyen, M. Spradlin, A. Volovich and C. Wen, *The Tree Formula for MHV Graviton Amplitudes*, *JHEP* **07** (2010) 045 [[0907.2276](#)].
- [85] A. Hodges, *New expressions for gravitational scattering amplitudes*, *JHEP* **07** (2013) 075 [[1108.2227](#)].
- [86] A. Hodges, *A simple formula for gravitational MHV amplitudes*, [1204.1930](#).
- [87] J. Trnka, *Towards the Gravituhedron: New Expressions for NMHV Gravity Amplitudes*, *JHEP* **04** (2021) 253 [[2012.15780](#)].
- [88] Z. Bern, J. J. M. Carrasco and H. Johansson, *New Relations for Gauge-Theory Amplitudes*, *Phys. Rev. D* **78** (2008) 085011 [[0805.3993](#)].
- [89] Z. Bern, J. J. M. Carrasco and H. Johansson, *Perturbative Quantum Gravity as a Double Copy of Gauge Theory*, *Phys. Rev. Lett.* **105** (2010) 061602 [[1004.0476](#)].
- [90] Z. Bern, J. J. Carrasco, M. Chiodaroli, H. Johansson and R. Roiban, *The Duality Between Color and Kinematics and its Applications*, [1909.01358](#).
- [91] N. Arkani-Hamed, F. Cachazo, C. Cheung and J. Kaplan, *A Duality For The S Matrix*, *JHEP* **03** (2010) 020 [[0907.5418](#)].
- [92] J. M. Drummond and J. M. Henn, *All tree-level amplitudes in $N=4$ SYM*, *JHEP* **04** (2009) 018 [[0808.2475](#)].
- [93] L. J. Mason and D. Skinner, *Dual Superconformal Invariance, Momentum Twistors and Grassmannians*, *JHEP* **11** (2009) 045 [[0909.0250](#)].
- [94] N. Arkani-Hamed, F. Cachazo and C. Cheung, *The Grassmannian Origin Of Dual Superconformal Invariance*, *JHEP* **03** (2010) 036 [[0909.0483](#)].
- [95] N. Arkani-Hamed, J. L. Bourjaily, F. Cachazo, S. Caron-Huot and J. Trnka, *The All-Loop Integrand For Scattering Amplitudes in Planar $N=4$ SYM*, *JHEP* **01** (2011) 041 [[1008.2958](#)].
- [96] N. Arkani-Hamed, J. L. Bourjaily, F. Cachazo and J. Trnka, *Local Integrals for Planar Scattering Amplitudes*, *JHEP* **06** (2012) 125 [[1012.6032](#)].
- [97] L. J. Dixon, J. M. Drummond and J. M. Henn, *Analytic result for the two-loop six-point NMHV amplitude in $N=4$ super Yang-Mills theory*, *JHEP* **01** (2012) 024 [[1111.1704](#)].
- [98] L. J. Dixon, M. von Hippel and A. J. McLeod, *The four-loop six-gluon NMHV ratio function*, *JHEP* **01** (2016) 053 [[1509.08127](#)].
- [99] L. J. Dixon, M. von Hippel, A. J. McLeod and J. Trnka, *Multi-loop positivity of the planar $\mathcal{N} = 4$ SYM six-point amplitude*, *JHEP* **02** (2017) 112 [[1611.08325](#)].
- [100] S. Caron-Huot, L. J. Dixon, F. Dulat, M. von Hippel, A. J. McLeod and G. Papathanasiou, *Six-Gluon amplitudes in planar $\mathcal{N} = 4$ super-Yang-Mills theory at six and seven loops*, *JHEP* **08** (2019) 016 [[1903.10890](#)].
- [101] A. Hodges, *Eliminating spurious poles from gauge-theoretic amplitudes*, *JHEP* **05** (2013) 135 [[0905.1473](#)].
- [102] N. Arkani-Hamed, J. L. Bourjaily, F. Cachazo, A. Hodges and J. Trnka, *A Note on Polytopes for Scattering Amplitudes*, *JHEP* **04** (2012) 081 [[1012.6030](#)].